ABSTRACT

ABDELSAMAD, AHMED MOHAMED SAAD. Microgrid Strategic Planning based on a Stochastic Reliability Assessment. (Under the direction of David Lubkeman.)

Power grids have been historically centralized systems where bulk power is generated and transported through long distances to end-users. However, the generation is recently shifting to distributed systems following the energy industry interest to decentralize the system. Microgrids (MG) are groups of distributed energy resources (DER), operating to meet local power demands. Developers and service providers aim to provide cost-effective and flexible designs to meet customers' objectives. Microgrids with islanding capabilities have great potential to provide green and reliable solutions. In this research, a microgrid planning methodology is developed to consider reliability and penetration targets.

A time-series analysis approach is presented to simulate and analyze hybrid distributed systems. System reliability is evaluated using a long-term assessment based on sequential Monte Carlo simulation (SMCS). System operation is simulated while considering load demands and renewable resources historical data. The battery cycling is simulated to meet the demand with the maximum renewable utilization. The system and the components' constraints are implemented to simulate a regular operation while randomly generating outage events based on component failure. At each simulation trial, the Energy Not Served (ENS) and Loss of Load Duration (LLD) are aggregated to estimate the annual Loss of Energy Expectation and the Loss of Load Expectation indices in kWh/year and hour/year respectively. When the simulation achieves convergence, other performance metrics are calculated to evaluate the sustainability of the system.

The research presents a new methodology to support MG design and planning. A combined optimization strategy is used to find the best system configuration while considering reliability and renewable performance as problem constraints. The developed reliability assessment is used to calculate reliability and renewable indices, in addition to fuel-fired system performance metrics such as the annual fuel consumption and hours of operation. A life cycle cost analysis (LCC) is performed to evaluate the cost-effectiveness of the system. Particle swarm optimization (PSO) algorithm is developed to search for the best system configuration. PSO is found to be suitable for problems when the linearization of the constraints is not possible. The algorithm achieved highly accurate results with a reasonable computational effort for commercial microgrid case studies.

Finally, a predictive maintenance approach is developed based on reinforcement learning (RL). The q-learning algorithm was able to structure a maintenance plan that reduces the number of failures and outage duration by 28% and 21% compared to a reactive maintenance strategy.

Microgrid Strategic Planning based on a Stochastic Reliability Assessment

by
Ahmed Mohamed Saad Abdelsamad

A dissertation submitted to the Graduate Faculty of
North Carolina State University
in partial fulfillment of the
requirements for the Degree of
Doctor of Philosophy

Electrical Engineering

Raleigh, North Carolina

2020

APPROVED BY:

Ning Lu	Srdjan Lukic
Joseph DeCarolis	David Lubkeman Chair of Advisory Committee

DEDICATION

To my parents and my sisters.

BIOGRAPHY

Ahmed was born in the year 1987 in Cairo, Egypt. In 2010, He graduated with a bachelor's degree in Electrical Power and Machines Engineering from Cairo University. Aiming to gain field experience, he worked as an Electrical Engineer in the construction for four years.

In pursuit of his passion to renewable energy engineering, Ahmed completed a master's double degree at Instituto Superio de Tecnico in Portugal and Ecole Polytechnique in France. The master's focused on energy management for renewable resources and energy storage. In 2016, he joined the Energy Management System team at Total. He is currently a Ph.D. candidate at North Carolina State University. His main areas of interest are energy economics, electricity market and distributed energy resources planning.

ACKNOWLEDGEMENTS

May I thank my advisor, Dr. David Lubkeman, for the dedicated guidance, support and advice he has been providing since the beginning of this doctoral program. It has been possible to tackle the research challenges only with his constant care and availability. I am very grateful to Dr. Ning Lu for her continuous support to maintain an adequate research environment for me. I also thank Dr. Srdjan Lukic and Dr. Joseph DeCarolis for serving on the committee and taking the time to review my work. Finally, I would like thank Dr. Yunan Liu for his interest and advice for my research work.

I would like express my gratitude to the EMS team at Total for granting me the opportunity to study at one of the top engineering programs. Last but not the least, I would like to thank FREEDM center for supplying all the necessary tools and facilities to execute the research work.

TABLE OF CONTENTS

LIST OF TABLES

LIST OF FIGURES

CHAPTER

1 INTRODUCTION

1.1 Background

A distributed energy system is usually planned based on economic and reliability requirements. Besides, renewable penetration has been recently considered in the planning problem. While optimizing economics as the primary objective function, the non-linear nature of the reliability and accuracy constraints need to be considered. The cost of generation is expected to vary significantly between different high reliability and renewable levels. There are other various factors expected to influence the planning results. Electrical system operators have been investigating methods and techniques to improve the maintenance element in the planning. Preventive maintenance (PM) is scheduled maintenance actions created to reduce the occurrence of failures. Technology has facilitated the monitoring and storing of measurements and data from the field. Thus, the abundance of information is used to utilize a predictive maintenance approach.

Risk in power systems is derived from the probabilistic behavior of the system components. Reliability is a very general term and is associated with several definitions. It is essential to recognize the generality of the term and use it to describe a general concept of the overall ability of a system to execute its function [1]. Random Failures of the system are usually outside the control of the system operators. Besides, the uncertainty of load demand makes it harder to expect the exact load forecast. The integration of intermittent renewable resources also increases the uncertainty of the power system. Smart grid technologies and applications have increased the level of controllability and data availability. However, the system complexity and the numerous system components have increased the risk in a power system. Power failure ranges from a momentary interruption to a blackout. Failures have substantial economic impacts, not only due to the loss of revenue but also the cost of slowing down society's activities and needs.

Power risk assessment can be looked at from several points of view, such as quantitative risk evaluation, probabilistic security assessment, risk assessments of renewable energy systems, and reliability-centered maintenance [2]. Reliability analysis of MG components considers each component operation and maintenance nature. In reliability engineering, historical field maintenance and factory testing records are vital elements in the reliability estimation process. Therefore, acquiring MG components maintenance history is essential to predict and simulate the system behavior in a MG setup. State transition sampling techniques are often used to evaluate power system reliability. Monte Carlo simulation is often used to perform state transition sampling as in [3–5].

In the assessment of system performance and reliability, it is essential to find the best methodology that can achieve accurate results with a reasonable computational time. Analytical approaches are minimal when it comes to complex system analysis. Markov chains and analytical methods such as contingency enumeration are suitable for a small number of components. In contrast, state sampling methods such as Monte Carlo simulation are generally more flexible when a complex system operation exists. Monte Carlo methods take into account composite system considerations such as states, chronology, operation rules, bus load uncertainty, and weather effects [6]. Estimates can be obtained for a given system by random sampling by using this class of simulations.

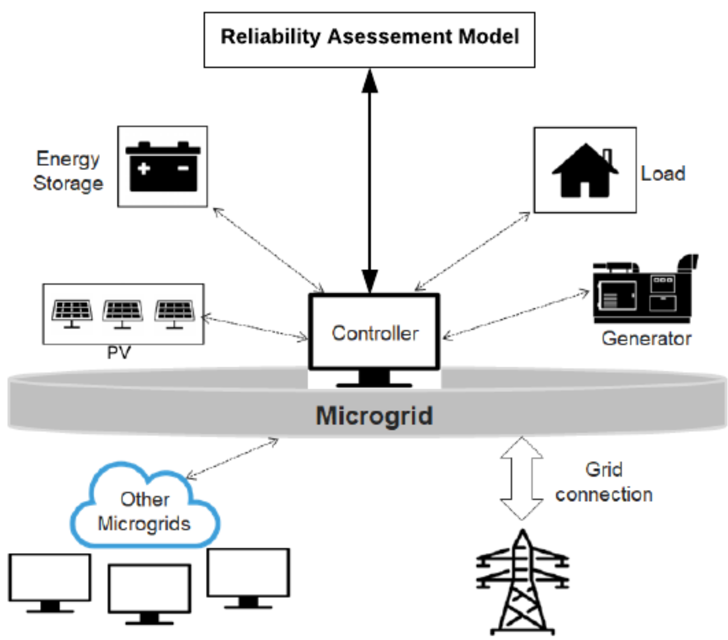

Figure 1.1 A microgrid system example

1.2 Objective

This thesis presents a distributed systems assessment methodology based on sequential Monte Carlo. By using components failure history, reliability and renewable penetration metrics are estimated. The reliability assessment is used in an optimization framework to consider several targets while searching for the system's optimal configuration. Finally, a predictive maintenance algorithm is presented to improve the number of outages and duration. The main objective of the thesis is to develop a microgrid planning framework that can support the decision-making process during the system design phase, as shown in Fig. 1.2.

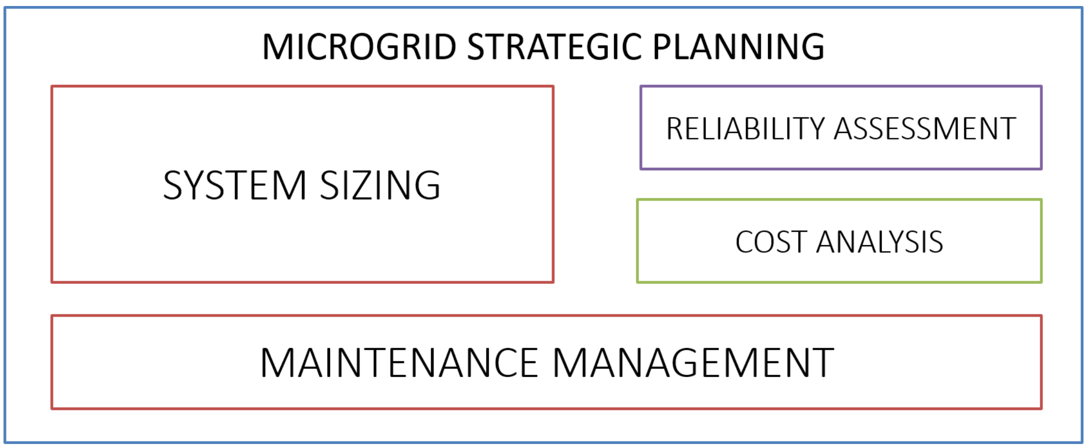

Figure 1.2 Microgrid planning methodology

1.3 Thesis structure

The thesis chapters are organized in three parts as shown in Fig. 1.3. Chapter 2 and 3 are focused on composite reliability introduction and reliability function estimation for microgrid systems. Chapter 4 and 5 provide random sampling and sequential techniques for reliability assessment. Chapter 6 presents the optimal sizing methodology. Chapter 7 focuses on the reinforcement learning algorithm developed to implement predictive maintenance.

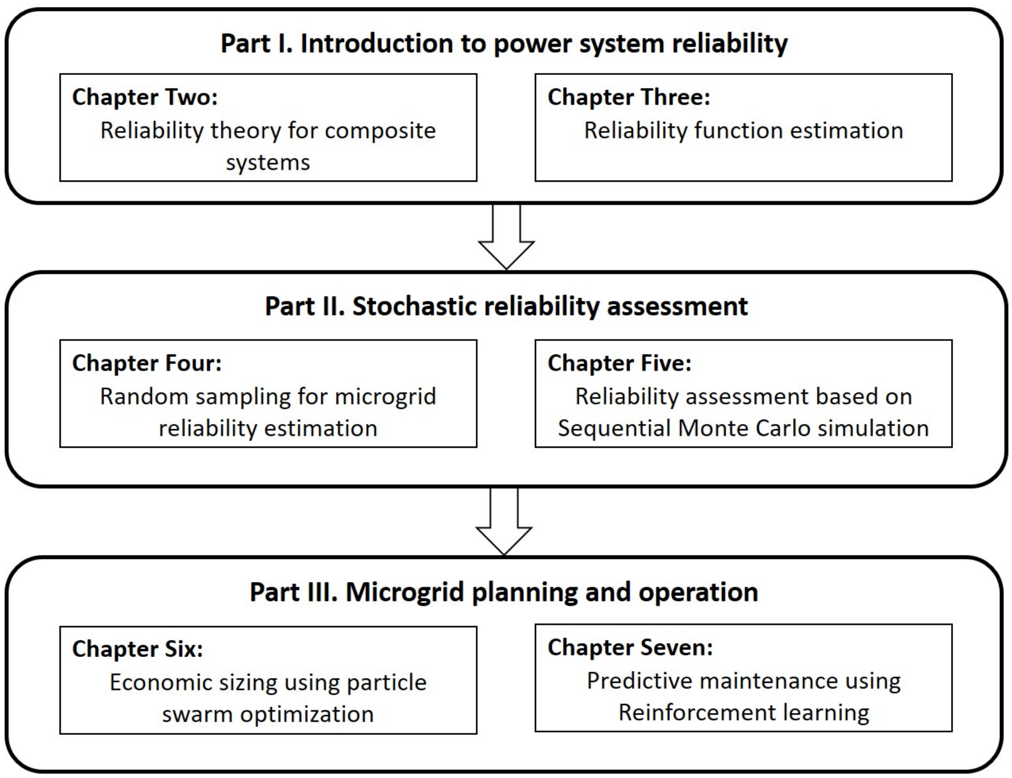

Figure 1.3 Thesis structure

CHAPTER

2

RELIABILITY THEORY FOR COMPOSITE SYSTEMS

This chapter introduces the reliability theory model of microgrid system components. Microgrid system consists of distributed generation components; fuel-based systems such as diesel generators, renewable energy systems like PV power, or wind turbines. Intermittent resources are managed by energy storage systems such as lithium-ion batteries. These components are very versatile in terms of operation dynamics and associated possible failures. Therefore, the essential measures for studying component reliability have to be discussed. The categories of failure models are classified, as shown in Section 2.7. Lastly, as the initial step for the following chapters, the pathways taken to improve microgrid reliability is illustrated in Section 2.8.

2.1 Time to failure, *TTF* and time to repair, *TTR*

Failure of a component is mostly a probabilistic process. One of the essential metrics to evaluate the reliability function of a component or a system is time to failure (ttf or TTF). TTF is the time between the starting time of a component and the instant it fails. In a testing setup, each time the component fails, the TTF is reset to zero. Collecting data of TTF is used to estimate reliability through a probability distribution or a non-parametric function. Consequently, the time to repair (ttr or TTR) is the time it takes the system to be back online after a failure event. The general hypothesis is that each component in the system goes through time cycles consists of functioning and non-functioning periods that are separated by a random failure event.

In Fig. 2.1, a generic example for the mentioned cycles is given. In the first cycle, the time to

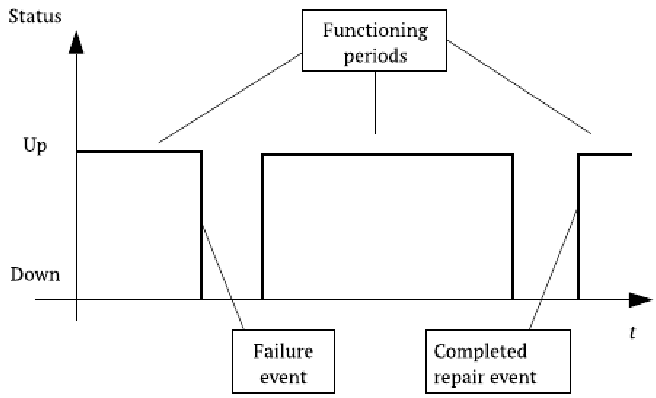

Figure 2.1 Component failure and repair events

failure is the time since the component last started its operation, in this case, at t=0, until it failed for the first time since it started. On the other hand, the time to repair in the same cycle is the time since it had this failure event until the repair process is completed, and the system was brought online once again. TTF and TTR, as shown, are information about the history of the component. They represent failure and repair events occurring during component lifetime or in a testing setup. The data-driven analysis performed in this work is initially based on acquiring this part of the component's history.

2.2 Failure probability distribution function, *f(t)*

The random events of failure can be represented by a probability distribution that expresses the values of those events and the probability of them happening. All possible results must be covered, and the probability of those results must add up to 1. A failure probability distribution can be presented as a probability density function. $f(x)$ is the function representing this probability density, where a time interval presents this time-based value. This random variable X in this case is the *ttf* or *ttr*.

$$\begin{aligned} P(a \leq ttf \leq b) &= \int_a^b f(x)\mathrm{d}x \\ P(t \leq \mathrm{ttf} \leq t+\Delta t) &= \int_t^{t+\Delta t} f(t)\mathrm{d}t. \end{aligned} \tag{2.1}$$

The probability distribution is presented by a density function if and only if it has a continuous cumulative distribution function *cdf*. Therefore, to describe failure probability distribution function *pdf* in the form of the cumulative distribution function, we get

$$F(T) = P(ttf \leq T) = \int_{-\infty}^{T} f(x)\mathrm{d}x, \tag{2.2}$$

where T is a specific period of time which can be called the *Mission time*. It is the time interval during which the failure probability is analyzed. Given this time interval, the $F(T)$ can be expressed as

$$\begin{aligned} F(T) &= \int_{t_1}^{t_2} f(t)dt \\ &= \int_{-\infty}^{t_2} f(t)dt - \int_{-\infty}^{t_1} f(t)dt \\ &= F(t_2) - F(t_1). \end{aligned} \tag{2.3}$$

2.3 Hazard rate, *h(t)*

Failure rate function $\lambda(t)$ is a momentary rate of failure. This conditional probability expressing a moment in time t, given that the component is functioning at the initial time $t0$. This function can be expressed in terms of failure distribution function as

$$\begin{aligned} \lambda(t)\Delta t = P(t &\leq \mathrm{ttf} \leq t + \Delta t / \\ &\textit{given that the component} \\ &\textit{is operating before time t}) \\ &= P(t \leq \mathrm{ttf} \leq t + \Delta t / \mathrm{ttf} \geq t) \end{aligned} \tag{2.4}$$

Figure 2.2 represents the bathtub curve for the component life cycle. Failure rate starts at time $t = 0$ with a high value and decreases, usually exponentially, through *infant mortality* period. During the *service life* period, the failure rate is steady at the expected lifetime of the component, and it is assumed to be constant throughout this phase. Finally, failure rate function increases proportionally to the degradation acceleration during the *end-of-life* period.

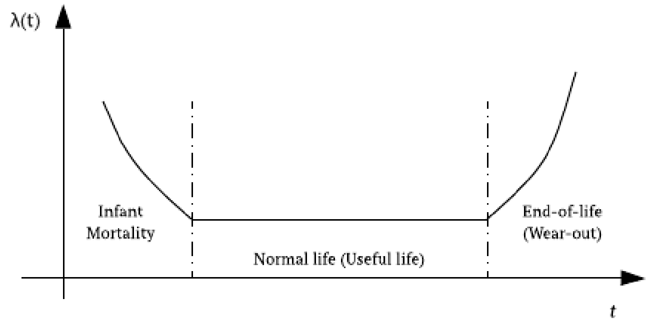

Figure 2.2 Bathtub curve for the failure rate function

2.4 Reliability function, *R(t)*

The reliability engineering field has been developing for decades to estimate systems reliability. Metrics have been designed to achieve relevant estimation models. Reliability metrics distinguishes repairable from non-repairable components. Non-repairable components are illustrated generally in Fig. 2.3, where it is not possible to bring them back online after a failure event. In the incident where the component goes from in-service status to out of order, they would require a replacement.

In contrast, repairable components can be brought back to service after a fault takes place. Different measures are used to evaluate the reliability of repairable and non-repairable components. Reliability R(t) and Availability A(t) functions are used to model the reliability of non-repairable and repairable components and systems, respectively.

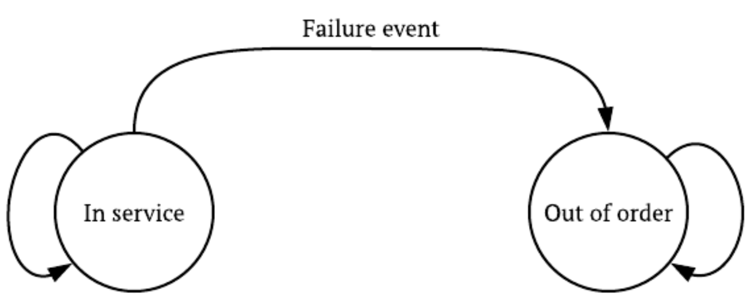

Figure 2.3 Two state diagram for a non-repairable component

TTF is a random variable and due to the lack of controllability. In the case previously stated, where a continuous function expresses these random values, and their distribution is represented by a density function, fitting the values with statistical distributions can be helpful. The cumulative function of the random variable *ttf* can be expressed as shown in Eq. 2.2 where *f(t)* is the probability density function or the non-conditional failure rate. It means that the failure rate is analyzed with an assumption that the component is functioning at the start of the mission time $t = 0$. Presenting the probability of the component to fail by time *t*, F(T) can be expressed as

$$F(t) = P(t \leq T) \quad t \geq 0. \tag{2.5}$$

The *reliability* function R(T) defines the capability of the component to perform the required functions for a specific period of time[7]. Reliability can be used to measure the system's success to perform its function properly. Therefore this metric represents a quality measure. Mathematically, R(t) is the probability function of the system to operate correctly in an interval from time 0 to time *t*. Hence, time is an essential parameter to express the reliability of a system.

$$R(t) = P(ttf > T) = \int_{T}^{\infty} f(t)\mathrm{d}t \quad t \geq 0 \tag{2.6}$$

where *ttf* is a random variable expressing time-to-failure.

The components are assumed to be new and in-service at time 0. The system becomes more likely to fail as the period increases, which indicates that the reliability function starts with R(t) = 1 and ends with R(t) = 0 at t = ∞. Hence, a statement such as system reliability is 0.95 is incomplete since the time interval is undeclared, where the reliability of the system is 0.95 at time $t = 4000h$ is a valid statement. Reliability function is the complimentary of the *Unreliability* or Failure cumulative function, F(T), previously presented in Section 2.2.

$$R(T) = 1 - F(T). \tag{2.7}$$

2.5 Mean time to failure, *MTTF*

The expected value of failure time at which the component manages to operate successfully is defined as the meantime to failure (MTTF). It is the statistical mean value of the previously defined random variable ttf. MTTF and the variance are one of the essential reliability analysis parameters.

$$\begin{aligned} \mathrm{MTTF} &= \int_{-\infty}^{\infty} t f(t)\mathrm{d}t = \int_{0}^{\infty} t f(t)\mathrm{d}t \\ &= -\int_{0}^{\infty} t \frac{\mathrm{d}R(t)}{\mathrm{d}t}\mathrm{d}t \end{aligned} \tag{2.8}$$

By integrating the MTTF equation, we get

$$\begin{cases} \text{MTTF} &= |-tR(t)|_0^\infty + \int_0^\infty R(t)\mathrm{d}t \\ &= \int_0^\infty R(t)\mathrm{d}t \\ & \text{since} \\ \lim_{t\to\infty}[tR(t)] = \lim_{t\to\infty}\left[t\exp\left(-\int_0^t \lambda(x)\mathrm{d}x\right)\right] = 0 \end{cases} \tag{2.9}$$

MTTF and variance can be estimated from a historical time to failure data sample of n number of data points by

$$M\hat{T}TF = \sum_{i=1}^{n} \frac{t_i}{n} \tag{2.10}$$

and

$$\sigma^2 = \sum_{i=1}^{n} \frac{\left(t_i - M\hat{T}TF^2\right)}{n-1} = \frac{\sum_{i=1}^{n} t_i^2 - n\left(M\hat{T}TF\right)^2}{n-1}, \tag{2.11}$$

where $M\hat{T}TF$ is the mean time to failure estimated value.

Confidence interval (CI) is an estimated range of values for a parameter with a stated confidence level that the interval contains the true value of this parameter. This estimated interval is calculated from a set of sample data [8]. If n in Eq. 2.10 is large enough, the central limit theorem can be applied, and the MTTF confidence interval following the t distribution will be

$$\sigma^2 = \sum_{i=1}^{n} \frac{\left(t_i - M\hat{T}TF^2\right)}{n-1} = \frac{\sum_{i=1}^{n} t_i^2 - n\left(M\hat{T}TF\right)^2}{n-1}, \tag{2.12}$$

In case where the failure rate $\lambda(t)$ is defined as a constant, during service life, mean time to failure can be estimated as

$$100(1-\alpha)\%\ \text{CI for}\ MTTF = M\hat{T}TF \pm t_{\alpha/2,n-1}\frac{\sigma}{\sqrt{n}}, \tag{2.13}$$

where α is the level of confidence and $t_{\alpha/2,n-1}$ is parameters obtained from the t distribution tables.

MTTF can be misinterpreted as the minimum life time or the expected failure time for half of the mission time. MTTF is an incomplete information without the failure time probability distribution. Since MTTF is one of the most used measures for reliability assessment, it is important to be defined correctly.

The ttf data in Table 2.1 has an estimated failure time average of 3550 hours. Even though a component failed after 830 hours, the expected mean time to failure is still a larger value, 3550 hours. Hence, it is important to understand that MTTF alone only expresses the expected mean value of failure time.

Table 2.1 A generic example of ttf dataset for a life duration test

i	**Time to failure (hour)**
1	3310
2	3258
3	2202
4	2684
5	830
6	2850
7	4037
8	5552
9	3541
10	4339
11	6447
12	5821
13	3674
14	2027
15	2784

2.6 Availability

Reliability is previously defined as a metric that involves a system success throughout a period, mission time. In other words, the repair process is not adopted. Unlike the reliability function, availability allows the system to be repaired when a failure occurs. Availability is a useful metric to measure the degree of a component to be operating at any given instant. It is the probability of component to be available, under specific conditions, at any time of the operating period. Since availability is a success metric for repairable systems, availability is equal to reliability in case of a non-repairable component. For repairable systems, availability is equal to or higher than reliability[9].

Mathematically and similar to reliability, the availability of a system is the probability of the system success at a particular moment of time t

$$\begin{aligned} \text{Availability } &= \frac{\text{System up time}}{\text{System up time } + \text{ System down time}} \\ &= \frac{\text{MTTF}}{\text{MTTF } + \text{ MTTR}} \end{aligned} \tag{2.14}$$

$$\begin{aligned} \text{Unavailability} &= \frac{\text{System down time}}{\text{System up time} + \text{System down time}} \\ &= \frac{\text{MTTR}}{\text{MTTF} + \text{MTTR}} \end{aligned} \tag{2.15}$$

where the MTTR is the time-to-repair. It is the time it takes to repair the component from the time the system went down till it can be up again.

For repairable components, the meant time between failures (MTBF) is an important measurement. MTBF expresses a system that has failed and has been repaired.

$$MTBF = MTTF + MTTR \tag{2.16}$$

MTTF and MTBF have been widely used alternatively. Even though the MTTR is usually small compared to MTTF, it is not valid to neglect it and approximate MTBF to MTTF. MTTR is important to be evaluated to create the research space for seeking improvement in the repair process. The time it takes for a component to be repaired can influence the availability of the component significantly. During availability studies, repairable components failure and repair events can be expressed as in Fig. 2.4.

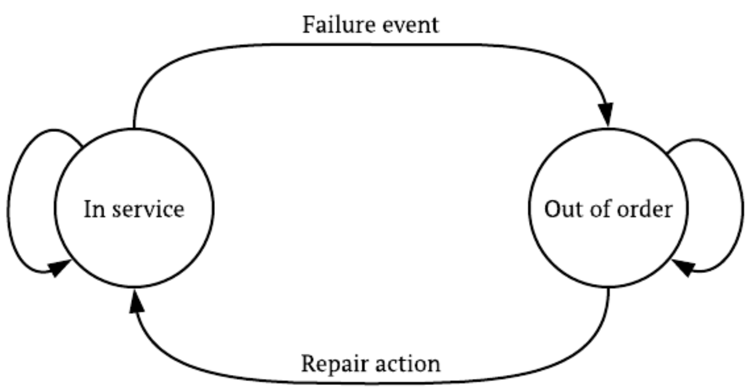

Figure 2.4 Two state diagram for a repairable component

2.7 Types of failures

Failures can be classified into two categories: independent and dependent failures. Failures occurring to an element without affecting other components are called independent failures. This category can be classified further into five types of failures as follows:

1. **Forced failure**. They are failures occurring randomly and out of control. Most of the forced failures in power systems are repairable. Forced failures can be further classified, as shown in the following list.

2. **Planned failure**. Unlike forced failures, planned failures are controlled, and it occurs when maintenance or a replacement is required.

3. **Semi-forced failure**. Those are failures when a physical problem occurs and expected to cause a failure to the component with some time delay. A forced failure is scheduled to fix the issue taking place.

4. **Partial failure**. It is not a severe failure when the component is still operating with a derated status.

5. **Multiple failure**. It is when multiple independent failures are studied. As it is shown later, by using simulation methods, those separate failures can be represented by independent random numbers to show the impacts of those failures in the simulation process.

Forced failures, as mentioned above, can be classified further into:

1. **Repairable failure**. Repairable failures will be modeled in the following chapters using the Up/Downstate transition sampling. It can be defined mathematically, as shown previously in Eq. 2.15.

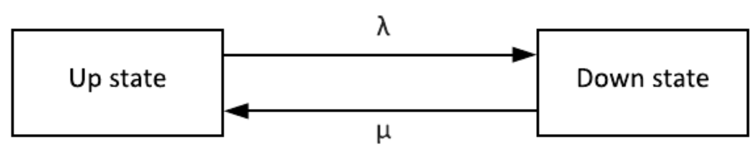

Figure 2.5 Repairable component Up/Down state transition sampling

2. **Non-repairable aging failure**. Aging failures take place at the end-of-life period shown in the bathtub curve in Fig. 2.2. It is a conditional failure depending on the operation history of the component, and since it is in the end-of-life period, the repair is not considered. Aging failures should be considered in design and replacement planning.

3. **Non-repairable chance failure**. During the normal life stage, a non-repairable acute failure can occur, which requires a replacement. Since this is the constant failure rate period, the failure density function can be expressed as an exponential distribution

$$f(t) = \lambda_{ch} e^{-\lambda_{ch} t}. \tag{2.17}$$

Dependent failure is the state when more than one component is affected by a failure event. Dependent failures probability is larger than the probability of independent failures coinciding. Hence, it is important to include them in analysis while working on a reliability model. Dependent failures can be classified as follows:

1. **Common cause failure**. It refers to the simultaneous failure of several components due to a common reason. An example is PV panels failures due to the failure of the PV system.

2. **Component group failure**. It exists when a group of components is affected by one component failure. An example is the failure of DC components due to the failure of the same inverter.

3. **Cascading failure**. This outage occurs when the failure of the first component in a series affects the second component, and the failure of the second affects the third and so on. An example of this failure is the failure of an inverter affecting the failure of the MPPT leading to the failure of the PV system.

4. **Environment related failure**. Natural disasters, such as a big storm, sometimes affects several components of the microgrid system.

Due to the nature of this modeling work, functional dependencies between microgrid components are considered in the reliability assessment proposed in this work.

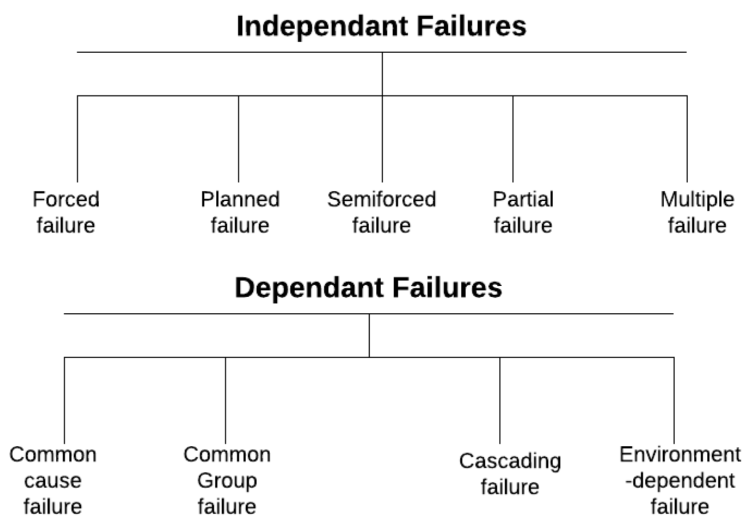

Figure 2.6 Failure models

2.8 Reliability pathways for MG components

Through this work, two major pathways are investigated for improvement. One target is to enhance the reliability of isolated microgrids systems and substantiate their economic viability. The first pathway is based on the reliability function *R(t)*. The reliability function is designed to deal with non-repairable components. In the case of microgrids, the reliability function is essential to estimate the reliability of new components and evaluate their quality in the microgrid setup. This process is essential in the design and development phase. Reliability function is dependant on acquiring historical failure data such as time-to-failure *ttf*.

The empirical reliability function can be calculated using non-parametric methods. The reliability function is then estimated using probability distributions or machine learning. Several techniques to accomplish this pathway will be investigated extensively in Chapter 3.

The second pathway is focused on the stochastic process of component repair. This pathway investigates concepts and models to distinguish repairable components. It is necessary to model repairable systems to study maintenance policies for microgrids. Availability *A(t)* is one of the most outstanding statistical functions to study repairable components. Failure and repair cycles are shown in Fig. 2.3 explains the sequence of events a repairable component is subjected to. The aim of analyzing the Availability pathway is to assess system security and adequacy, build maintenance strategies to mitigate those events, and subsequently improve the reliability of a microgrid.

CHAPTER

3

ESTIMATION AND TESTING OF THE RELIABILITY FUNCTION FOR POWER SYSTEM APPLICATION

The reliability function estimation of a microgrid component is essential to achieve an optimized energy production process. Optimization policies can adapt reliability findings and their related improvement in power security and costs. Reliability studies provide an insight into how to make right decisions to improve the operation and maintenance of a power system. This chapter provides various reliability modeling processes based on analytical modeling and statistical techniques.

3.1 Non-parametric estimation

In Chapter 2, the difference between the usage of reliability and availability functions was illustrated. The reliability function estimation is important to predict the ability of a microgrid component to operate and subsequently support the microgrid system. In this section, we focus on component reliability estimation and prediction as a part of design analysis. It means that for this part maintenance is excluded looking only at the system reliability prediction.

The motivation of using a non-parametric approach is to directly evaluate the reliability from a testing dataset of failure time of a component or a system. By collecting historical data and using an empirical approach, the reliability function $R(t)$ is estimated. Empirical estimation of reliability is the initial step for two pathways of reliability function $R(t)$ prediction. The long-established approach is to fit a probability distribution such as normal, exponential, binomial, and Weibull distributions [10]. Since Weibull distribution is the most commonly used in power systems components, it will be used as the base case in Chapter 4 [2].

3.1.1 Data structures

The starting point in a data-driven prediction approach is a set of failure data. In a testing setup, it can be more than failure times but, most importantly, the failure events and the removal times. The objective is to estimate the primary reliability parameters, improving optimization strategies. In a testing environment and looking at n number of components, a data set is considered to be complete when all unit failure times is obtained. This means that not only all components have been operating within the testing time interval, but also has failed at some point within the interval.

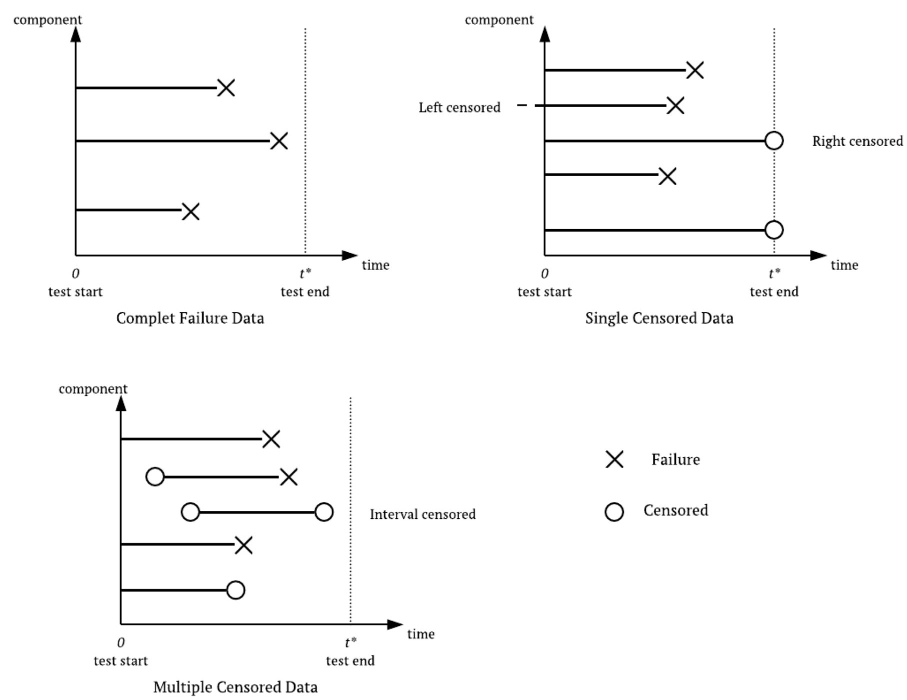

Figure 3.1 Complete and censored failure data

Results are represented as $ttf_1, ttf_2, ttf_3, \ldots, ttf_n$, where ttf_i is the failure time for the ith unit: for a *complete data* case all n units have failure time data point available. By contrast, a *censored data* set is characterized by partly censored or missing data as shown in Fig. 3.1. Censoring is categorized in two different ways:

1. *Individual censored data.* All components go through the same test time *t**. Some fail before

the test is terminated, and others are still operating.

2. *Multiple censored data*. In this case, test duration varies throughout the components. Not only the failure times differ but also the censoring time is different. Components are removed from the test at different times, while components go online at different instants.

Multiply censored data is usually formed in a real-world situation. It is common that it happens when collecting failure times data from on-site components. In contrast, individual censoring usually exists in a testing environment. In a microgrid reliability assessment, it is more likely to have to deal with multiple censoring situations.

Looking at the types of censoring based on the relationship between the failure time and the testing time interval, it is essential to differentiate:

1. *Right censored data*. Only some units failed during the testing time; other units have no failure times data since they did not fail during the text. In this case, those units are usually excluded from the model.

2. *Left censored data*. It is when some units' initial working time and schedule are unknown. It means that even if we know the failure times, it is not descriptive data due to the lack of complete information.

3. *Interval censored data*. Commonly occurring scenario[11], during a testing period, a controlled unit fails between two in-service inspection events.

Non-parametric estimation demands a historical set of data as a minimum requirement. The type of dataset dictates the best prediction models to use for a case study. For microgrids, a fleet of systems, in operation and feeding the energy management unit with real-time data, is ideal for these types of techniques.

3.1.2 Empirical functions and estimators

In survival analysis, special methods have been developed to deal with different types of datasets. For instance, studies dealing with patients' survival utilizes Kaplan-Meier estimator to deal with incomplete or censored data [12]. In this section, the estimators are divided into two categories, as shown in Fig. 3.2. Estimators for complete data will be discussed first, and subsequently, special methods dealing with censored data will be illustrated.

3.1.2.1 Complete data estimators

For a single component failure times dataset, given that $ttf_1, ttf_2, ttf_3, \ldots, ttf_n$, where $ttf_i \leq ttf_{i+1}$, are n ordered failure times in a testing sample, and i is the amount failures occurring up to the time t_i, a direct estimate of reliability function $R(t)$ can be calculated using the *Direct Method* equation:

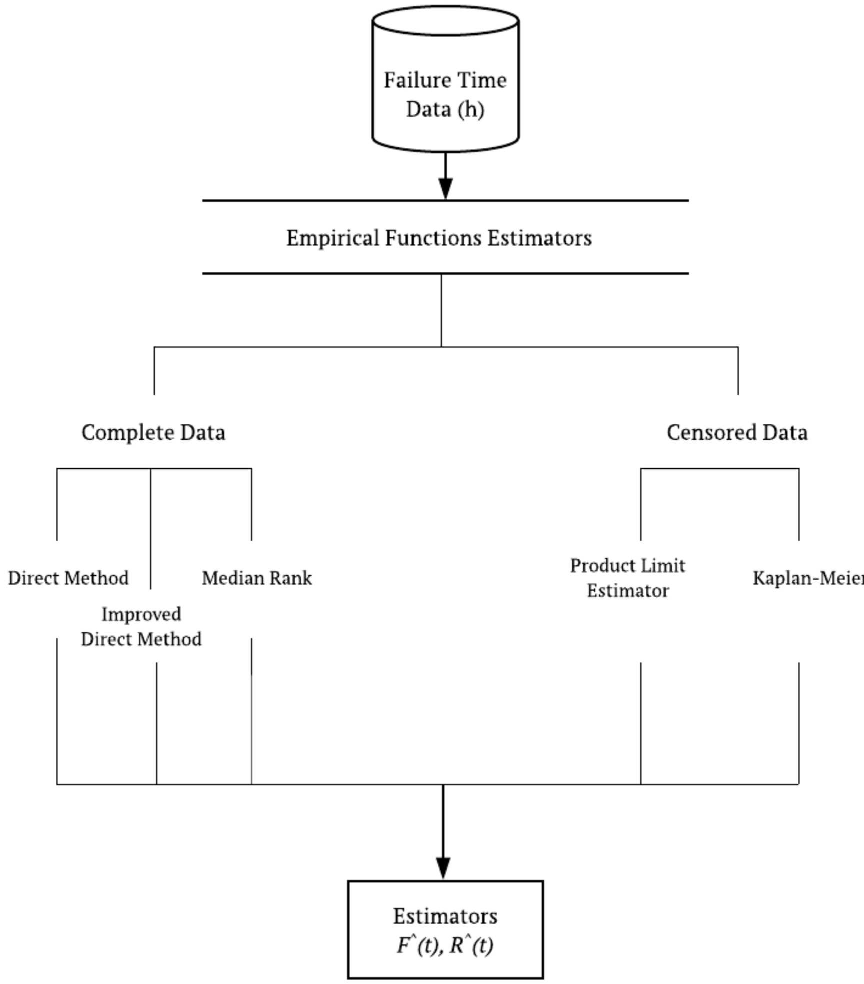

Figure 3.2 Reliability estimation by Empirical functions

$$\hat{R}(t_i) = \frac{n-i}{n} = 1 - \frac{i}{n} \tag{3.1}$$

Direct method estimate can be improved by considering a cumulative failure distribution:

$$\hat{F}(t_i) = \frac{i}{n+1} \tag{3.2}$$

Deriving the reliability function estimator from the failure function above:

$$\hat{R}(t_i) = 1 - \hat{F}(t_i) = 1 - \frac{i}{n+1} = \frac{n+1-i}{n+1} \tag{3.3}$$

This *Improved Direct Method* is widely used as it behaves well in many real-world fields.

On a probability graph, the direct method provides a mean value position on the plot. In cases when the value of i is close to one of the interval bounds, 0 and n, the probability distribution is skewed, and hence a median value would be more descriptive. *Median Rank Method* is a function of both the order of the failure i and the size of the dataset n. MR is derived as

$$\sum_{k=i}^{n} \binom{n}{k} \mathrm{MR}^{k}(1-\mathrm{MR})^{n-k} = 0.50 \tag{3.4}$$

Median rank is tabulated as in [13]. For large failure times datasets, it is acceptable to approximate failure function *F(t)* by

$$\mathrm{MR} \approx \hat{F}(t_i) = \frac{i-0.3}{n+0.4} \tag{3.5}$$

Deriving the reliability function

$$\hat{R}(t_i) = 1-\hat{F}(t_i) = 1-\frac{i-0.3}{n+0.4} = \frac{n+0.7-i}{n+0.4} \tag{3.6}$$

3.1.2.2 Censored data estimators

For a right censored case, assume n to be the number of components in the test setup and r is the number of failures that take place. The test is terminated before we get failure times for each component, i.e., $r \leq n$. Reliability estimator $\hat{R}(t)$ is calculated at test termination as proceeded in the complete date cases. The issue in a right censored data case is that the results will be cut on the right. Based on the improved direct method, *Product Limit Estimator* method is suggested in [14]:

$$\hat{R}(t_i) = \left(\frac{n+1-i}{n+2-i}\right)^{\delta_i} \hat{R}(t_{i-1}) \tag{3.7}$$

In an attempt to improve Product limit estimator, Kaplan and Meier add a variation to the method. Reliability estimator is expressed as

$$\hat{R}(t_i) = \left(1-\frac{1}{n_i}\right)^{\delta_i} \hat{R}(t_{i-1}) \tag{3.8}$$

where δ_i is between [0,1], n_i is the number of components at risk before the ith failure takes place, if failure and censoring take place at ranked failure times t_i and $\hat{R}(0)=1$.

The following example is an application for reliability estimation. A multiple-censored data set of diesel generator fans is collected and documented in Plant Engineer's Handbook[15], the dataset in Table 3.2 is utilized here to apply a product limit estimator and Kaplan-Meier methods to estimate the reliability function of the generator fan using formulas in Table 3.1.

Table 3.3 and Fig. 3.3 show an ordered data of time to failure and their corresponding reliability function *R(t)* estimation using Product Limit Estimator method. Reliability function values are shown with respect to the time to failure points. Comparing different censored data adapted methods shows some interesting trends. As seen in Fig. 3.4 and Table 3.4, Kaplan-Meier method is inclined to underestimate the reliability function with an average of −10% lower than the rest of the methods.

Table 3.1 Reliability estimation by empirical functions for complete and censored data

Empirical function	Data type	$\hat{R}(t_i)$
Direct method	Complete	$\frac{i}{n}$
Improved direct method	Complete	$\frac{n+1-i}{n+1}$
Median rank method	Complete	$\frac{n+0.7-i}{n+0.4}$
Product limit estimator	Censored	$\left(\frac{n+1-i}{n+2-i}\right)^{\delta_i} \hat{R}(t_{i-1})$
Kaplan-Meier	Censored	$\left(1-\frac{1}{n_i}\right)^{\delta_i} \hat{R}(t_{i-1})$

In addition, comparing reliability estimation of complete data and a censored set derived from the same source is serviceable. For the sake of reaching a precise conclusion, a method from each data type is compared. Improved direct method and Kaplan-Meier will be used as they are the two most commonly used methods in real-world applications[7]. Utilizing censored data creates errors throughout the estimation process. However, this is what reliability engineers deal with in real-world microgrid sites, which leads us back to stressing the importance of technological advancement in the field of small power system data collection. Through automating the process, the target of acquiring complete data without consuming resources such as time and money.

In [7], a study made a comparison between complete and censored data reliability estimation results for electric motor parts. The comparison was straightforward due to the availability of a complete and censored data set for the part. Results indicate that Kaplan-Meier for censored data misestimates reliability with a max error of around 20%. This error is an overestimation to the reliability function, and it appears after a large concentration of suspended components. It is also observed that censored data underestimates the reliability function near the end of the lifetime, which is expected from using KM method. Error is generally an overestimation error, with factors such as the number of suspended components and censoring times.

Due to the lack of a complete data set, a table is derived based on the actual censored data set being used for the previous work. Complete data is utilized to observe the influence of censored data, through the developed methods designed for censored datasets, on the reliability estimation process.

The experiment confirmed the findings by comparing Kaplan-Meier results to the improved direct method for complete data. The average error was around 23% representing an overestimation to the reliability function in case of using Kaplan-Meier method, as shown in Fig. 3.5.

Machine learning approaches have been introduced to work on the censored data challenge.

Table 3.2 Generator fan censored dataset

i	Time to failure (hour)	Censored
1	4,500	
2	4,600	*
3	11,500	
4	11,500	
5	15,600	*
6	16,000	
7	16,600	*
8	18,500	*
9	18,500	*
10	18,500	*
11	18,500	*
12	18,500	*
13	20,300	*
14	20,300	*
15	20,300	*
16	20,700	
17	20,700	
18	20,800	
19	22,000	*
20	30,000	*
21	30,000	*
22	30,000	*
23	30,000	*
24	31,000	
25	32,000	*
26	34,500	
27	37,500	*
28	37,500	*
29	41,500	*
30	41,500	*
31	41,500	*
32	41,500	*
33	43,000	*
34	43,500	*
35	43,000	*
36	43,000	*
37	46,000	

Table 3.3 Reliability estimation using Product limit estimator

i	ttf	Censor	$\frac{n+1-i}{n+2-i}$	δ_i	$\hat{R}(t_i)$	
0	0					1.000
1	4,500		0.974	1	R(4,500)=0.971.R(0)=	0.974
2	4,600	*	0.973	0		
3	11,500		0.972	1	R(11,500)=0.970.R(4,500)=	0.947
4	11,500		0.971	1	R(11,500)=0.969.R(11,500)=	0.920
5	15,600	*	0.971	0		
6	16,000		0.970	1		0.892
7	16,600	*	0.969	0		
8	18,500	*	0.968	0		
9	18,500	*	0.967	0		
10	18,500	*	0.966	0		
11	18,500	*	0.964	0		
12	18,500	*	0.963	0		
13	20,300	*	0.962	0		
14	20,300	*	0.960	0		
15	20,300	*	0.958	0		
16	20,700		0.957	1		0.853
17	20,700		0.955	1		0.814
18	20,800		0.952	1		0.775
19	22,000	*	0.950	0		
20	30,000	*	0.947	0		
21	30,000	*	0.944	0		
22	30,000	*	0.941	0		
23	30,000	*	0.938	0		
24	31,000		0.933	1		0.724
25	32,000	*	0.929	0		
26	34,500		0.923	1		0.668
27	37,500	*	0.917	0		
28	37,500	*	0.909	0		
29	41,500	*	0.900	0		
30	41,500	*	0.889	0		
31	41,500	*	0.875	0		
32	41,500	*	0.857	0		
33	43,000	*	0.833	0		
34	43,500	*	0.800	0		
35	43,000	*	0.750	0		
36	43,000	*	0.667	0		
37	46,000		0.500	1		0.334

Table 3.4 Reliability estimation using Kaplan-Meier

i	ttf	Censor	n_i	$1-\frac{1}{n_i}$	δ_i	$\hat{R}(t_i)$	
0	0						1.000
1	4,500		37	0.973	1	R(4,500)=0.973.R(0)=	0.973
2	4,600	*	36	0.972	0		
3	11,500		35	0.971	1	R(11,500)=0.973.R(4,500)=	0.945
4	11,500		34	0.971	1	R(11,500)=0.945.R(11,500)=	0.917
5	15,600	*	33	0.970	0		
6	16,000		32	0.969	1		0.889
7	16,600	*	31	0.968	0		
8	18,500	*	30	0.967	0		
9	18,500	*	29	0.966	0		
10	18,500	*	28	0.964	0		
11	18,500	*	27	0.963	0		
12	18,500	*	26	0.962	0		
13	20,300	*	25	0.960	0		
14	20,300	*	24	0.958	0		
15	20,300	*	23	0.957	0		
16	20,700		22	0.955	1		0.848
17	20,700		21	0.952	1		0.808
18	20,800		20	0.950	1		0.768
19	22,000	*	19	0.947	0		
20	30,000	*	18	0.944	0		
21	30,000	*	17	0.941	0		
22	30,000	*	16	0.938	0		
23	30,000	*	15	0.933	0		
24	31,000		14	0.929	1		0.713
25	32,000	*	13	0.923	0		
26	34,500		12	0.917	1		0.653
27	37,500	*	11	0.909	0		
28	37,500	*	10	0.900	0		
29	41,500	*	9	0.889	0		
30	41,500	*	8	0.875	0		
31	41,500	*	7	0.857	0		
32	41,500	*	6	0.833	0		
33	43,000	*	5	0.800	0		
34	43,500	*	4	0.750	0		
35	43,000	*	3	0.667	0		
36	43,000	*	2	0.500	0		
37	46,000		1	0.000	1		0.000

Table 3.5 Generator fan ordered failure time complete dataset

i	Time to failure (hour)
1	4,500
2	4,800
3	11,500
4	11,500
5	15,000
6	16,000
7	17,000
8	18,000
9	18,400
10	18,600
11	18,700
12	18,900
13	20,000
14	20,200
15	20,400
16	20,700
17	20,700
18	20,800
19	22,100
20	30,100
21	30,300
22	30,600
23	30,700
24	31,000
25	32,100
26	34,500
27	37,600
28	37,700
29	41,400
30	41,500
31	41,600
32	41,700
33	43,200
34	43,400
35	43,700
36	43,800
37	46,000

Table 3.6 Reliability estimation using Improved direct method and Kaplan-Meier

i	ttf	ttf(Cen)	Censor	IDM	KM
0	0	0		1.000	1.000
1	4,500	4,500		0.974	0.973
2	4,800	4,600	*	0.947	
3	11,500	11,500		0.921	0.945
4	11,500	11,500		0.895	0.917
5	15,000	15,600	*	0.868	
6	16,000	16,000		0.842	0.889
7	17,000	16,600	*	0.816	
8	18,000	18,500	*	0.789	
9	18,400	18,500	*	0.763	
10	18,600	18,500	*	0.737	
11	18,700	18,500	*	0.711	
12	18,900	18,500	*	0.684	
13	20,000	20,300	*	0.658	
14	20,200	20,300	*	0.632	
15	20,400	20,300	*	0.605	
16	20,700	20,700		0.579	0.848
17	20,700	20,700		0.553	0.808
18	20,800	20,800		0.526	0.768
19	22,100	22,000	*	0.500	
20	30,100	30,000	*	0.474	
21	30,300	30,000	*	0.447	
22	30,600	30,000	*	0.421	
23	30,700	30,000	*	0.395	
24	31,000	31,000		0.368	0.713
25	32,100	32,000	*	0.342	
26	34,500	34,500		0.316	0.653
27	37,600	37,500	*	0.289	
28	37,700	37,500	*	0.263	
29	41,400	41,500	*	0.237	
30	41,500	41,500	*	0.211	
31	41,600	41,500	*	0.184	
32	41,700	41,500	*	0.158	
33	43,200	43,000	*	0.132	
34	43,400	43,500	*	0.105	
35	43,700	43,000	*	0.079	
36	43,800	43,000	*	0.053	
37	46,000	46,000		0.026	0.000

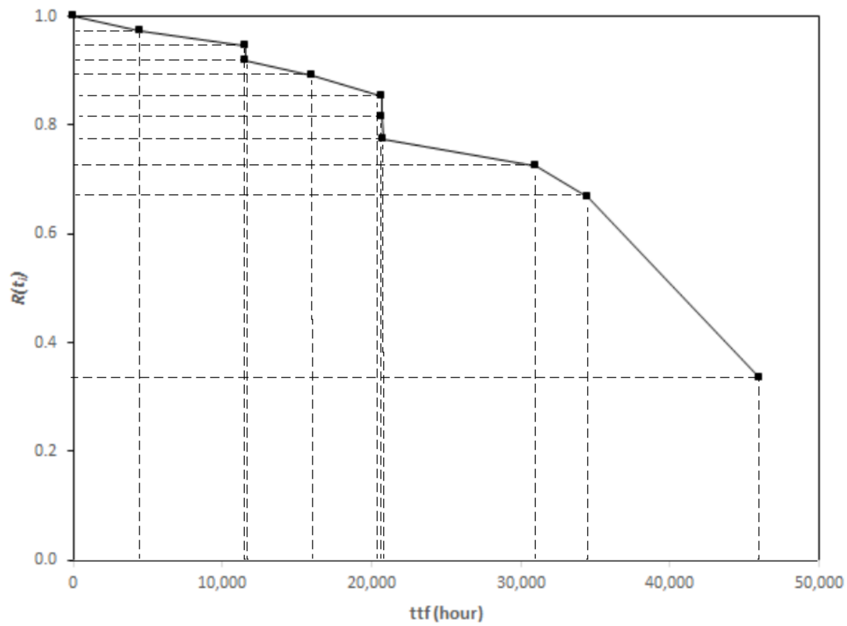

Figure 3.3 Reliability plot for Product limit estimator

In [16], several machine learning models are introduced as a solution to investigate improvement in the performance in the cases of censored data experiments. Neural networks are specifically investigated in [17], with the networks designed to estimate censored data derived from complete data. Genetic algorithms in [18] were also introduced to enhance the reliability estimation process.

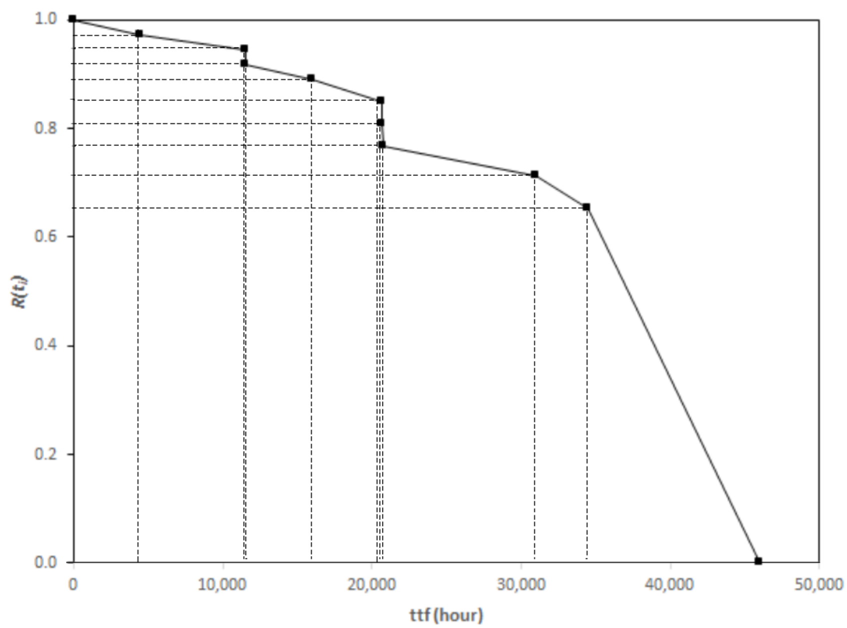

Figure 3.4 Reliability plot for Kaplan-Meier

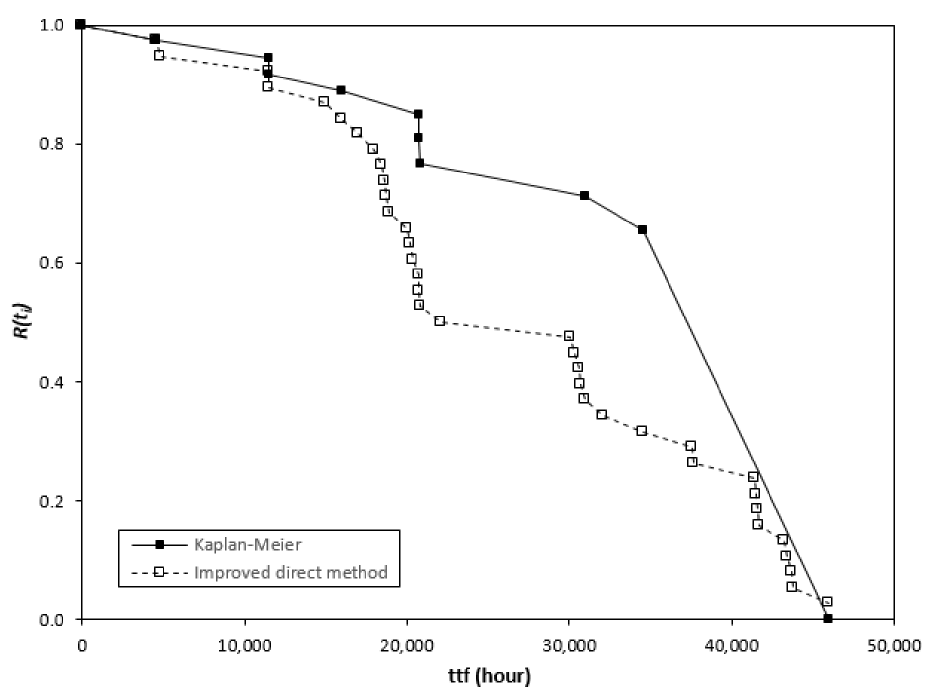

Figure 3.5 Reliability plot for IDM and KM

3.2 Parametric estimation

Reliability parametric estimation is always recognized as a more accurate and reliable method of estimation. However, this method requires more complex work upfront to guarantee good performance. Due to the approach's accuracy, it is preferred. Those functions are based on several parameters and get identified by them to express the stochastic properties of a probability function. This approach always follows the empirical function calculations. Before building the model, it is the initial step to calculate the empirical value and derive the parameters from there.

3.2.1 Probability distributions

This section introduces the most commonly used probability distributions for the application of reliability evaluation and failure function representation. Many distributions are tested for reliability application; however, three distributions are selected here due to their strong history with electrical components. The probability density function determines the probability of the failure and repair events happening.

3.2.1.1 Exponential distribution

The exponential distribution is essential in the reliability world as it has a constant failure rate parameter. It has been used in evaluating the lifetime of an electrical component. The distribution is suitable for used components that can be treated as new if they have not failed. This restriction must motivate the limitation of using this distribution since the memoryless property might not apply to numerous components.

In general for such distribution and a continuous random variable *x*, the probability density function can be expressed as:

$$f(x) = \lambda \mathrm{e}^{-\lambda x}, \quad x > 0 \tag{3.9}$$

Respectively, the cumulative function is:

$$F(x) = \int_{-\infty}^{x} f(x)\mathrm{d}x = 1 - \mathrm{e}^{-\lambda x} \tag{3.10}$$

Deriving the mean function, we get mean time to failure as:

$$\mathrm{MTTF}(x) = \int_{-\infty}^{+\infty} [x f(x)]\mathrm{d}x = \frac{1}{\lambda} \tag{3.11}$$

Evaluating reliability using the generic exponential function equations and considering an exponential probability distribution for failures, the following equation represents reliability function *R(t)*, failure function *F(t)* and failure rate *f(t)*:

$$R(t) = \mathrm{e}^{-\lambda t} \tag{3.12}$$

$$F(t) = 1 - e^{-\lambda t} \tag{3.13}$$

$$f(t) = \frac{dF(t)}{dt} = \lambda e^{-\lambda t} \tag{3.14}$$

Some of the exponential distribution properties will be discussed to stress on the benefits of using this distribution with some reliability applications.

1. *Memoryless property.* The exponential distribution is a continuous distribution allowing

$$P\{T \geq t\} = P\{T \geq t + s | T \geq s\} \quad \text{for } t > 0, s > 0 \tag{3.15}$$

   This indicates what has been discussed before that the component that survived till time s is similar to a new component. This property makes the exponential distribution suitable for Markov chain applications, as presented later in this chapter. Those components will remain "good-as-new" until some failure condition arrives, such as a power surge and cause failure assuming no degradation.

2. *Failure rate confidence interval.* For exponential distributions that are independent and identical with random variables, $T_1, T_2, \ldots, T_n$, having a constant failure rate λ,

$$2\lambda \sum_{i=1}^{n} T_i \sim \chi^2(2n) \tag{3.16}$$

   where $\chi^2(2n)$ is a chi-squared distribution with $2n$ degrees of freedom, which is a useful property as it allows us to have a confidence interval for the failure rate λ

3.2.1.2 Normal distribution

Normal distribution is suitable for measuring components vulnerability and external environment stress factors. It has been used to study many mechanical systems failures due to wear out reasons. The well-know bell curve for the normal distribution is symmetrical around the mean and the spread is defined by the variance. Failure and reliability cumulative distributions are given by:

$$F(t) = \int_{-\infty}^{t} \frac{1}{\sigma\sqrt{2\pi}} e^{-\frac{1}{2}\left(\frac{s-\mu}{\sigma}\right)^2} ds \tag{3.17}$$

$$R(t) = \int_{t}^{\infty} \frac{1}{\sigma\sqrt{2\pi}} e^{-\frac{1}{2}\left(\frac{s-\mu}{\sigma}\right)^2} ds \tag{3.18}$$

where μ is mean and σ is the standard deviation. Tables for normal distribution density function is available to find probabilities for the distribution.

3.2.1.3 Weibull distribution

The memoryless property of the exponential distribution is limiting to those components that can be dealt with as new until they fail. Weibull distribution is more of a general form for the exponential distribution. This time-dependant failure model is one of the most useful parametric distributions in the field of reliability. Weibull function can be express as:

$$f(x) = \frac{b}{a}\left(\frac{x}{a}\right)^{b-1} \exp[-(\frac{x}{a})^b], x > 0 \tag{3.19}$$

where a and b are the scale and shape parameters respectively:
The value of the shape parameter b implies the nature of the failure:

1. $b < 1$. It expresses infant mortality where the components are subject to failing at the beginning of the mission. The purpose of the acceptance test is to bypass this period at the start of the component lifetime.

2. $b = 1$. It suggests a random failure system which means that the failure function is memoryless implying an exponential probability density function as shown previously $\lambda = 1/a$.

3. $1 < b < 4$. It implies a wearout in the early stages of the operation, which reflects on the optimization problem that declares the best time to replace the component and avoid the high cost of the unplanned failure.

4. $b \geq 4$. By the end of the component lifetime, the expected wearout due to old age is expressed here. The normal distribution can approximate the probability density function in this case due to the failure probability symmetry. Failure occurs due to aging reasons such as material degradation or stress corrosion.

The cumulative failure function based on Weibull probability distribution is

$$F(x) = 1 - \exp[-\left(\frac{x}{a}\right)^b] \tag{3.20}$$

Using the gamma function

$$\Gamma(X) = \int_0^\infty y^{x-1} \mathrm{e}^{-y} \,\mathrm{d}y \tag{3.21}$$

Mean-time-to-failure can be expressed by

$$\begin{aligned} \mathrm{MTTF}(x) &= \int_{-\infty}^{+\infty} [x f(x)] \mathrm{d}x = \int_0^{+\infty} [x f(x)] \mathrm{d}x \\ &= a\Gamma\left(1 + \frac{1}{b}\right) \end{aligned} \tag{3.22}$$

Failure rate function is

$$
\begin{aligned}
\lambda(x) &= \frac{f(t)}{R(t)} \\
&= \frac{b}{a}\left(\frac{x}{a}\right)^{b-1}
\end{aligned}
\tag{3.23}
$$

Since the reliability function *R(t)* can be defined as the probability of the component surviving beyond operation time under defined normal conditions.

$$
R(T) = P(\mathrm{ttf} \geq T) = \int_T^\infty f(x)\mathrm{d}x \tag{3.24}
$$

where T is the operation time, reliability function can be expressed as

$$
R(T) = \exp\left[-\left(\frac{T}{a}\right)^b\right], T > 0 \tag{3.25}
$$

3.2.2 Fitting method

As previously stated in Section 3.2 introduction, the parametric estimation process is accurate yet complex to achieve. For each distribution, the right parameters have to be estimated to fit the data on the distribution curve accurately. There are several techniques to perform curve fitting, such as the least square method and maximum-likelihood estimation method. The techniques are designed to help in deriving point estimators.

3.2.2.1 Least-squared estimation

This method is based on minimizing the sum of the squared distances between the best fit line and the actual data. This line can be expressed as $y = a + bx$, where y is the dependent variable that can be seen as the reliability function in this work, x is the independent explanatory variable seen as the time to failure, a is the line intercept with y-axis and b is the slope of the line.

3.2.2.1.1 Fitting exponential distribution

Using this method with the exponential distribution, the first step is to transform the distribution function in the form of the line equation $y = a + bx$:

$$
F(t) = 1 - \mathrm{e}^{-\lambda t} \tag{3.26}
$$

Transformed to be

$$
-\ln[1 - F(t)] = \lambda t \tag{3.27}
$$

where $y = -\ln[1 - F(t)]$, $x = t$, $b = \lambda$ and $a = 0$. Since for the fitting line, the slope represents the failure rate λ estimation and according to the least squares method

$$b = \hat{\lambda} = \frac{\sum_{i=1}^{n} x_i y_i}{\sum_{i=1}^{n} x_i^2} \tag{3.28}$$

where $y_i = \ln(\frac{1}{1-F(t_i)})$ and $x_i = t_i$.

3.2.2.1.2 Fitting Weibull distribution

Similarly, the Weibull cumulative function in Eq. 3.29 is transformed to fit the line Eq. 3.30, we obtain

$$F(t) = 1 - \mathrm{e}^{-(t/\alpha)^{\beta}} \tag{3.29}$$

$$\ln\ln\left(\frac{1}{1-F(t)}\right) = \beta\ln t - \beta\ln\alpha \tag{3.30}$$

Similarly, $y_i = \ln\ln(\frac{1}{1-F(t_i)})$, $x_i = \ln t_i$, $b = \beta$ and $a = -\beta\ln\alpha$ where

$$b = \hat{\beta} = \frac{\sum_{i=1}^{n}(x_i - \overline{x})(y_i - \overline{y})}{\sum_{i=1}^{n}(x_i - \overline{x})^2} \tag{3.31}$$

and

$$a = -\hat{\beta}\ln\hat{\alpha} = \overline{y} - b\overline{x} \tag{3.32}$$

Since in this case the scale parameter a is a function of the shape parameter b, $\hat{\beta}$ is calculated first and then $\hat{\alpha}$ is deduced from it.

3.2.2.1.3 Fitting examples

Based on the generator fan complete failure time data in Table 3.5 and the improved direct method failure function results from Table 3.6, the two distributions, and their least square estimation is performed and evaluated in this section.

Starting with exponential distribution in Table 3.7, y_i is calculated using $y_i = \ln(\frac{1}{1-F(t_i)})$. Parameter a=0, since it is an exponential distribution. From the table results, parameter b is calculated using Eq. 3.28 to get:

$$b = \hat{\lambda} = 0.0000401.$$

To measure the performance of linear regression and line fitting, a fitting index r is calculated using

$$r = \frac{\frac{1}{n}\sum_{i=1}^{n}(x_i - \overline{x})(y_i - \overline{y})}{\sqrt{\sum_{i=1}^{n}\frac{(x_i-\overline{x})^2}{n}}\sqrt{\sum_{i=1}^{n}\frac{(y_i-\overline{y})^2}{n}}} \tag{3.33}$$

For this case study, a linear regression line equation can be written as $y_i = 0.0000401x_i$, with a fitting index calculated using Eq. 3.33 to obtain $r = 0.899$. The goodness of fit is measured by how

Table 3.7 Curve fitting of an exponential distribution

ttf (hour)	$\hat{F}(t_i)$	y_i
4,500	0.026	0.027
4,800	0.053	0.054
11,500	0.079	0.082
11,500	0.105	0.111
15,000	0.132	0.141
16,000	0.158	0.172
17,000	0.184	0.204
18,000	0.211	0.236
18,400	0.237	0.270
18,600	0.263	0.305
18,700	0.289	0.342
18,900	0.316	0.379
20,000	0.342	0.419
20,200	0.368	0.460
20,400	0.395	0.502
20,700	0.421	0.547
20,700	0.447	0.593
20,800	0.474	0.642
22,100	0.500	0.693
30,100	0.526	0.747
30,300	0.553	0.804
30,600	0.579	0.865
30,700	0.605	0.930
31,000	0.632	0.999
32,100	0.658	1.073
34,500	0.684	1.153
37,600	0.711	1.240
37,700	0.737	1.335
41,400	0.763	1.440
41,500	0.789	1.558
41,600	0.816	1.692
41,700	0.842	1.846
43,200	0.868	2.028
43,400	0.895	2.251
43,700	0.921	2.539
43,800	0.947	2.944
46,000	0.974	3.638

close r is close to 1. For the cumulative failure function of the data, the exponential distribution fitting equation can be written as

$$F(t) = 1 - \mathrm{e}^{-\lambda t} = 1 - \mathrm{e}^{-0.0000401 t}.$$

Similarly, the Weibull distribution parameters are calculated to compare the results of both distribution fitting and make a decision to which is better for a generator fan component failure analysis. In Table 3.8, x_i and y_i are calculated using $x_i = \ln t_i$ and $y_i = \ln\ln(\frac{1}{1-F(t_i)})$ respectively. From the table results, parameters b and a is calculated using Eq. 3.31 and 3.32 to get:

$$b = \hat{\beta} = 1.851,$$

$$a = -\hat{\beta} \ln \hat{\alpha} = -19.196$$

and

$$\hat{\alpha} = e^{-\frac{a}{b}} = 31,878.48.$$

The fitting line can also be expressed as $y_i = -19.196 + 1.851 x_i$ and fitting index was calculated using Eq. 3.33 to obtain $r = 0.969$. For the cumulative failure function of the used data, the Weibull distribution fitting equation can be written using Eq. 3.29 as

$$F(t) = 1 - \mathrm{e}^{-(t/31,878.48)^{1.851}}.$$

Looking at the fitting index r, we can deduce that the Weibull distribution is more accurate by obtaining an r value closer to 1. To have a better understanding of the performance of the least-squares results of the two distributions are plotted in Fig. 3.6 and 3.7.

The exponential distribution approximation is not adequate, not only seen by evaluating the fitting index values, but only through the plot, the exponential distribution does not fit the used failure time data good enough. On the other hand, Weibull distribution had a good data fitting, seen in the plot, with a good fitting index of 0.969. With the fitting results from Weibull distribution, it is obvious that for a typical failure process evaluation and analysis, the distribution is well suited. As shown in Fig. 3.8 and 3.9, the Weibull distribution fits the real-world data much better than the exponential distribution.

By plotting the failure function derived from each distribution against the empirical function results, the previous findings is confirmed.

Table 3.8 Curve fitting of an Weibull distribution

ttf (hour)	$\hat{F}(t_i)$	x_i	y_i
4,500	0.026	8.412	-3.624
4,800	0.053	8.476	-2.918
11,500	0.079	9.350	-2.498
11,500	0.105	9.350	-2.196
15,000	0.132	9.616	-1.958
16,000	0.158	9.680	-1.761
17,000	0.184	9.741	-1.592
18,000	0.211	9.798	-1.442
18,400	0.237	9.820	-1.308
18,600	0.263	9.831	-1.186
18,700	0.289	9.836	-1.074
18,900	0.316	9.847	-0.969
20,000	0.342	9.903	-0.871
20,200	0.368	9.913	-0.778
20,400	0.395	9.923	-0.689
20,700	0.421	9.938	-0.604
20,700	0.447	9.938	-0.522
20,800	0.474	9.943	-0.443
22,100	0.500	10.003	-0.367
30,100	0.526	10.312	-0.291
30,300	0.553	10.319	-0.218
30,600	0.579	10.329	-0.145
30,700	0.605	10.332	-0.073
31,000	0.632	10.342	-0.001
32,100	0.658	10.377	0.070
34,500	0.684	10.449	0.142
37,600	0.711	10.535	0.215
37,700	0.737	10.537	0.289
41,400	0.763	10.631	0.365
41,500	0.789	10.633	0.443
41,600	0.816	10.636	0.526
41,700	0.842	10.638	0.613
43,200	0.868	10.674	0.707
43,400	0.895	10.678	0.812
43,700	0.921	10.685	0.932
43,800	0.947	10.687	1.080
46,000	0.974	10.736	1.291

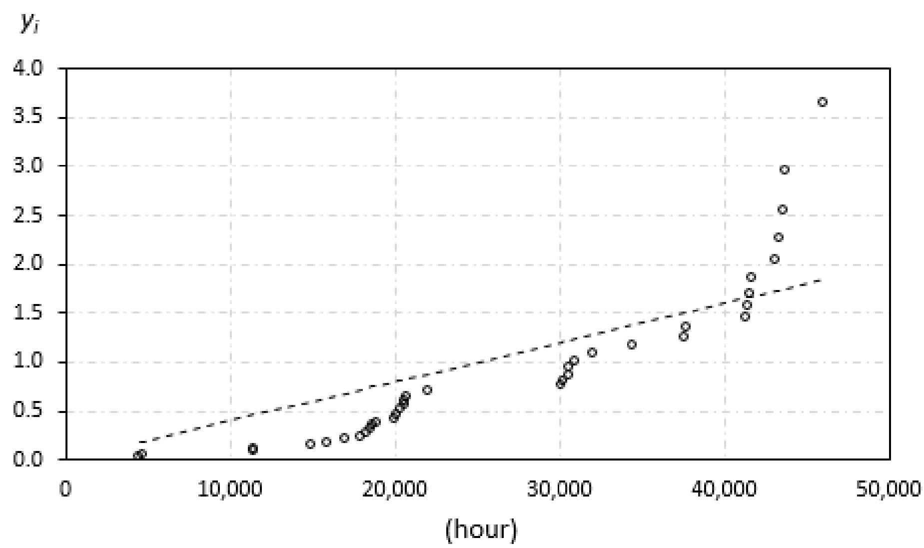

Figure 3.6 Least-squares method for exponential fitting

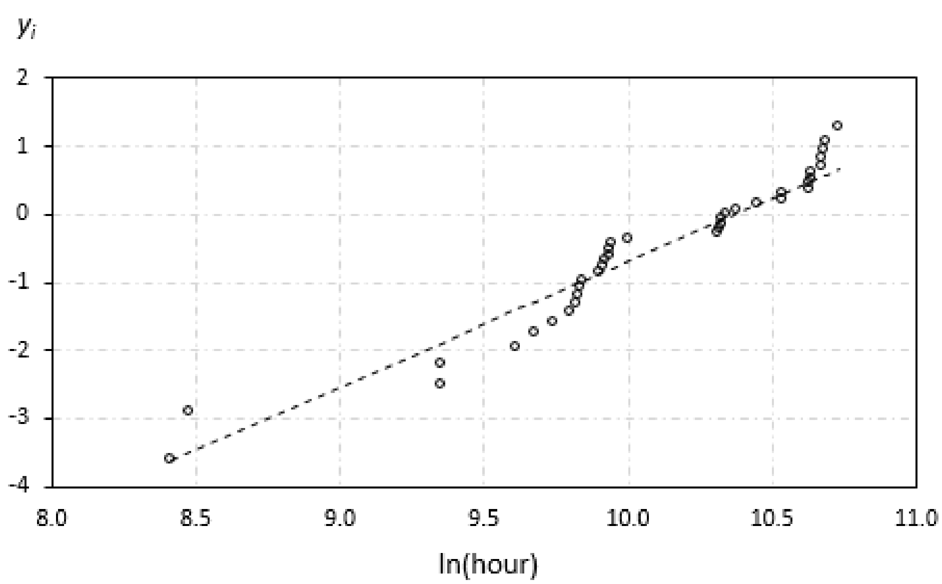

Figure 3.7 Least-squares method for Weibull fitting

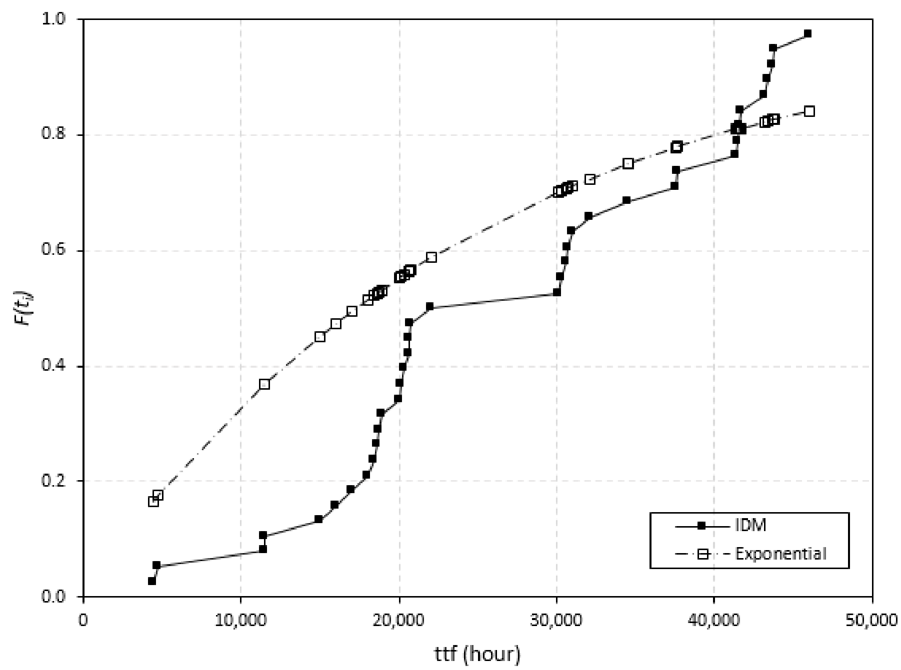

Figure 3.8 Empirical failure function vs. Exponential distribution

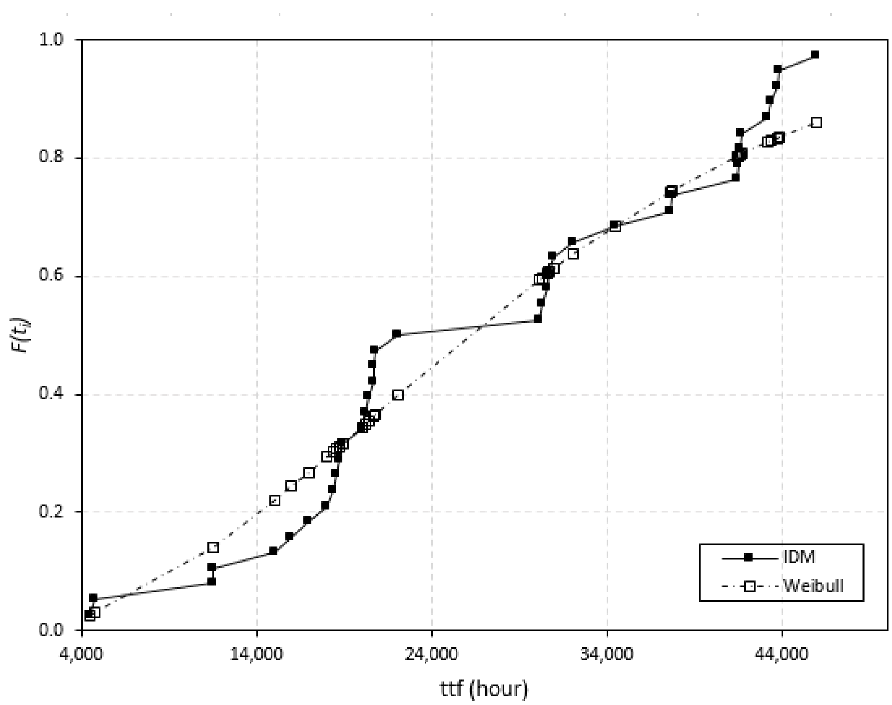

Figure 3.9 Empirical failure function vs. Weibull distribution

3.3 Reliability block diagrams

Before this section, all the work is performed on a single component. Microgrids are hybrid systems with several components working together to deliver power to load. This section focuses on the methodology required to set up components' configuration. The reliability assessment is then performed on the final structure of the microgrid.

Reliability schemes is designed to dictate and study the running configuration for the correct and incorrect operation of the energy production and transmission systems. The design depends on the operating conditions and the interconnections between system components. In Fig. 3.10, a parallel configuration is shown. It is essential to understand the load requirements and the system capacity in parallel configurations. The components can be stacked in parallel as a form of redundancy, where one component is capable of supplying load independently. Otherwise, even if the components are on a parallel functional configuration, in terms of reliability, they should not be represented by reliability block diagram parallel configuration. On the other hand, the series configuration is strictly for systems where all components are critical to ensure a correct operation.

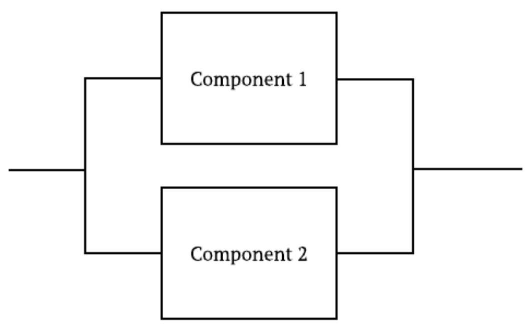

Figure 3.10 Parallel configuration

3.3.1 Series configuration

A reliability block diagram for components connected in series is shown in Fig. 3.11. For a series of components, $C_1, C_2, C_3, \ldots, C_n$, the system will fail should one component fail and the system's reliability R_S can be expressed as

$$\begin{aligned} R_S = & P(X_1)\,P(X_2/X_1)\,P(X_3/X_1X_2) \\ & \times \cdots \times P(X_n/X_1X_2\ldots X_{n-1}) \end{aligned} \tag{3.34}$$

where $P(X_i)$ is the probability of the operating event of component i. For independent events the equation changes to

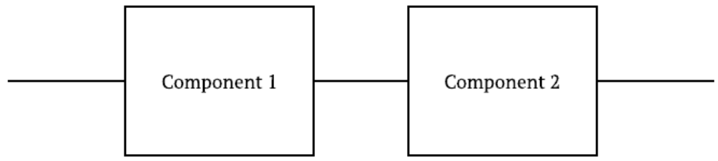

Figure 3.11 Series configuration

$$R_S = P(X_1)P(X_2)P(X_3)\dots P(X_n) \tag{3.35}$$

In terms of system reliability for a period of time T

$$\begin{aligned} R_S(T) &= R_1(T)R_2(T)\dots R_n(T) \\ &= \prod_{i=1}^{n} R_i(T) \\ &= \mathrm{e}^{-\int_0^T \sum_{i=1}^{n} \lambda_i(t)\mathrm{d}t} \end{aligned} \tag{3.36}$$

where $\lambda_i(t)$ is the failure rate of the ith component for a time interval T. For the failure distribution of the system in an unconditional failure rate series setup, it is expressed by the following equation:

$$f_S(t) = \sum_{i=1}^{n} f_i(t)\left(\prod_{j \neq i} R_j(t)\right) \tag{3.37}$$

The failure distribution depends on the ith component failure given the other components in the system is operating $j \neq i$. For the system failure rate $\lambda_S(t)$

$$
\begin{aligned}
\lambda_S(t) &= \frac{f_S(t)}{R_S(t)} \\
&= \frac{\sum_{i=1}^{n} f_i(t)\left(\prod_{j\neq i} R_j(t)\right)}{R_S(t)} \\
&= \frac{\sum_{i=1}^{n} f_i(t)\frac{\left(\prod_j R_j(t)\right)}{R_i(t)}}{R_S(t)} \\
&= \sum_{i=1}^{n} \lambda_i(t) \\
&(\text{since} R_S(t) = \prod_j R_j(t))
\end{aligned}
\tag{3.38}
$$

This means that if the failure rate of components is constant, i.e., probability of failure is the same all the time, the system failure rate is also constant. For the mean time to failure of the system $MTTF_S$, as in Eq. 3.11 for a single component

$$
\mathrm{MTTF}_S = \int_0^\infty R_S(t)\mathrm{d}t = \int_0^\infty \mathrm{e}^{-\int_0^t \lambda_S(x)\mathrm{d}x}\mathrm{d}t \tag{3.39}
$$

Similarly, if the failure rate $\lambda_i(t)$ is constant for all components

$$
\mathrm{MTTF}_S = \frac{1}{\lambda_S} = \frac{1}{\sum_{i=1}^{n} \lambda_i(t)} = \frac{1}{\sum_{i=1}^{n} \frac{1}{\mathrm{MTTF}_i}} \tag{3.40}
$$

3.3.1.1 Series configuration example

A PV system consists of the PV array (to be considered as one whole component for the sake of simplicity in this example), Maximum Power Point Tracker (MPPT), and the inverter. This configuration is based on the objective of power delivery to the load in a microgrid. Following a study of PV systems installed in Taiwan, the MTTF is estimated to be 3.96 years[19]. In [20], a boost MPPT converter is simulated with several power ratings and operating modes. Reliability analysis was performed based on MIL-HDBK-217 standards [21]. Results shown in [20], suggest that switches have the highest failure rates and for an MPPT with rating 1000 W the MTBF is 53,590 hours. Assuming a multi-string inverter case, the reliability study performed in [22] works shows that a MTTF of 48,279 hours considering a low-quality factor.

In reliability block diagram terms, a PV system satisfies a series configuration. Since each component failure events will lead to a whole system failure without considering the rest of the components. Constructing this example, all system components will be assumed to be non-repairable with probability distribution of time to failure to be random following an exponential distribution. From studies mentioned, the following MTTF values will be considered in the example:

$$
\begin{aligned}
\mathrm{MTTF}_{\text{PV modules}} &= 34,690h; \\
\mathrm{MTTF}_{\text{MPPT}} &= 53,690h;
\end{aligned}
$$

$$\mathrm{MTTF}_{\mathrm{Inverter}} = 48,279h.$$

Calculating the failure rate of the system using Eq. 3.38

$$\lambda_S(t) = \sum_{i=1}^{3} \lambda_i(t) = 6.817 \times 10^{-5}\mathrm{h}^{-1}.$$

Applying Eq. 3.36 to calculate system reliability

$$\begin{aligned} R_S(T) &= R_1(T)R_2(T)R_3(T) \\ &= \mathrm{e}^{-\int_0^T \sum_{i=1}^{n} \lambda_i(t)\mathrm{d}t} \\ &= \mathrm{e}^{-\int_0^T \left(\frac{1}{34,690} + \frac{1}{53,690} + \frac{1}{48,279}\right)\mathrm{d}t} \\ &= \mathrm{e}^{-6.817\times 10^{-5}T} \end{aligned}.$$

Evaluating the reliability of this system by considering two period of times; six months and one year missions times

$$\begin{aligned} \mathrm{R}_S(T = 4,380) &= 0.742; \\ \mathrm{R}_S(T = 8,760) &= 0.550. \end{aligned}$$

According to [7], the failure density function of the PV system can be expressed by

$$\begin{aligned} f_S(t) &= \sum_{i=1}^{n} f_i(t)\left(\prod_{j\neq i} R_j(t)\right) \\ &= \left(\lambda_{\mathrm{Valve}_1} + \lambda_{\mathrm{Valve}_2} + \lambda_{\mathrm{Pump}}\right) \\ &\times \left(\mathrm{e}^{-\lambda_{\mathrm{Valve}_1} t}\,\mathrm{e}^{-\lambda_{\mathrm{Pump}} t}\,\mathrm{e}^{-\lambda_{\mathrm{Valve}_2} t}\right) \\ &= \lambda_S \mathrm{e}^{-\lambda_S t} \end{aligned} \tag{3.41}$$

$$\begin{aligned} f_S(t = 4,380) &= \lambda_S \mathrm{e}^{-\lambda_S \times 4380} \cong 5.057 \times 10^{-5}\mathrm{h}^{-1}, \\ f_S(t = 8,760) &= \lambda_S \mathrm{e}^{-\lambda_S \times 8760} \cong 3.752 \times 10^{-5}\mathrm{h}^{-1}. \end{aligned}$$

Figures 3.12, 3.13, 3.14 and 3.15, represent the patterns of the PV system's reliability function $R(t)$, failure function $F(t)$, failure probability density $f(t)$ and failure rate $\lambda(t)$ with respect to the mission time studied taking into consideration an exponential distribution for all the components and the system itself.

3.3.2 Parallel configuration

As mentioned in the introduction of this section, parallel configuration represents redundancy in the system. This means that for the system to fail, every component in such configuration should fail.

System reliability is presented in this case as

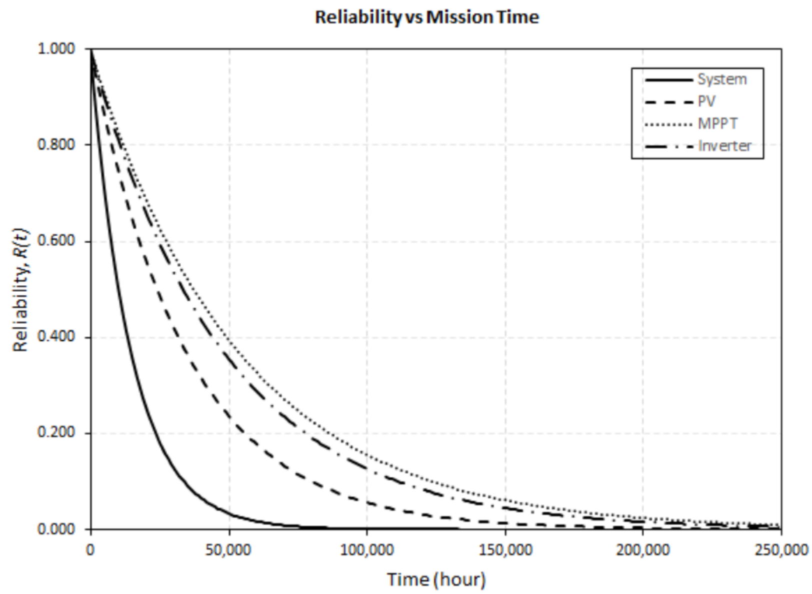

Figure 3.12 PV system series configuration exponential distribution, R(t)

$$\begin{aligned} R_S(T) &= 1 - F_S(T) \\ &= 1 - [1 - R_1(T)] \ldots [1 - R_n(T)] \\ &= 1 - \prod_{i=1}^{n} [1 - R_i(T)], \end{aligned} \tag{3.42}$$

where $F_S(T)$ is the system failure function at time mission T, n is the number of components and $R_i(T)$ is the reliability function of the ith component.

$$R_S(T) = 1 - \prod_{i=1}^{n} \left(1 - \mathrm{e}^{-\int_0^T \lambda_i(t) \mathrm{d}t}\right) \tag{3.43}$$

Similar to the series configuration system reliability, in Eq. 3.43, λ_i is the failure rate of the ith component. Considering a full redundancy and unconditional failure, system failure probability density can be expressed as

$$f_S(t) = \sum_{i=1}^{n} \left(f_i(t) \prod_{j \neq i} \left[1 - R_j(t)\right] \right) \tag{3.44}$$

It is a function of the failure probability density of component i when the rest of the components are already in a state of failure. For the system failure rate

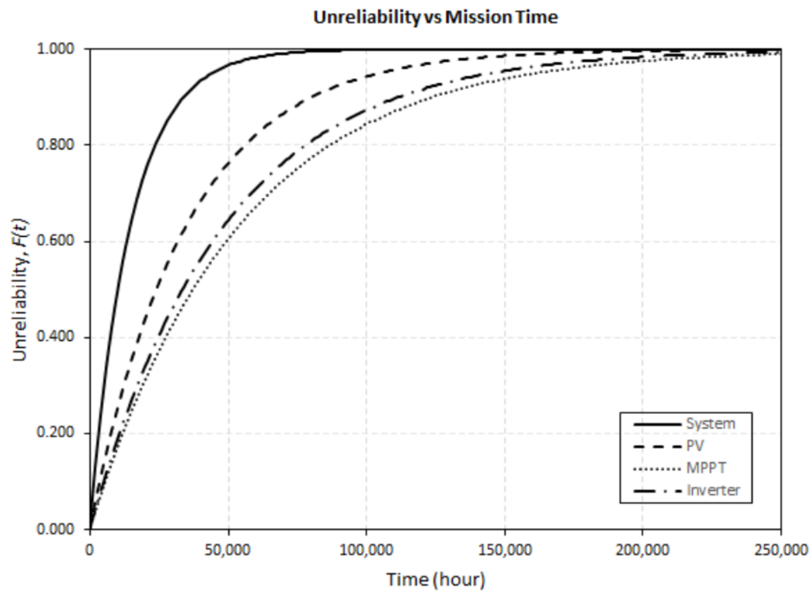

Figure 3.13 PV system series configuration exponential distribution, F(t)

$$\begin{aligned}\lambda_S(t) &= \frac{f_S(t)}{R_S(t)} \\ &= \frac{\sum_{i=1}^{n}\left(f_i(t)\prod_{j\neq i}\left[1-R_j(t)\right]\right)}{1-\prod_{i=1}^{n}\left(1-\mathrm{e}^{-\int_0^t \lambda_i(x)\mathrm{d}x}\right)}\end{aligned} \tag{3.45}$$

3.3.2.1 Parallel configuration example

In a redundant microgrid system, all the energy production components are designed to take the load solely. In this example, this assumption is considered in addition to considering only physical failure. This means that the primary energy source is assumed to be always available, which is not the case in terms of renewable energy sources. Adequacy assessment is another field of reliability engineering and hence needs to be investigated in the case of microgrids. In this example, it is assumed to have a PV system, an energy storage system, and a diesel generator.

The PV system will be considered from the previous example with $\mathrm{MTTF}_{PV} = 14,670h$. In an attempt to improve the reliability of ship machinery, the works of [23] is aimed to evaluate the problems occurring in autonomous engine rooms for commercial ships. The machinery in the engine room is including a diesel generator. For the study, data is collected from several years of an on-site operating diesel generators. It is found that the meantime to failure of the diesel generator is $\mathrm{MTTF}_{DG} = 4,043h$.

For the energy storage system, a Lithium-ion (Li-ion) battery is considered. In the works of

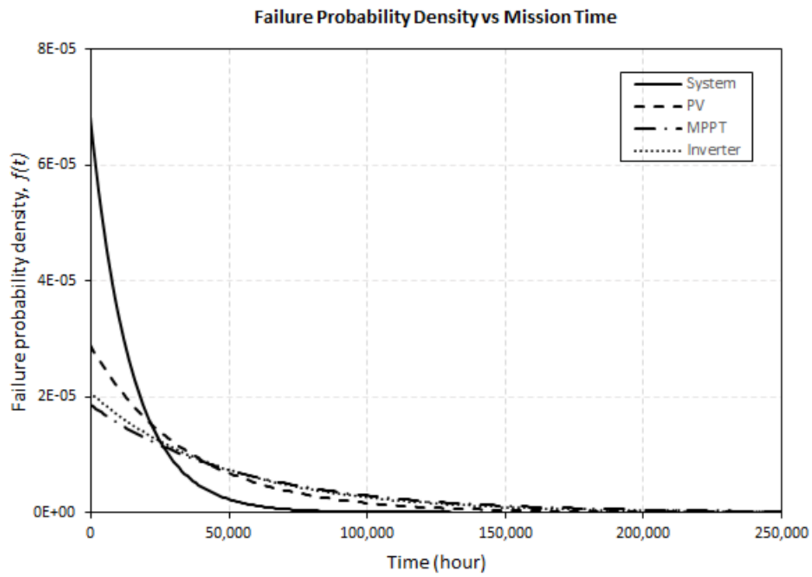

Figure 3.14 PV system series configuration exponential distribution, f(t)

[24–28], the MTTF of a Li-ion battery is evaluated as a function of the number of cycles. Reliability assessment of Li-ion batteries can be divided into three categories; initial performance tests, lifetime endurance, and safety tests [25]. In this example, battery safety is considered, the battery is evaluated by having two states; it is either operating under normal conditions or out of order. For the Li-ion battery in the microgrid case study, the specification, the fitting distribution, the cycle-to-hour *MTTF* conversation model, the satisfactory block diagram modeling and degradation modeling will be studied extensively. However, in this example, the battery as a parallel component and a direct conversion of life cycles to hours is considered. Assuming a daily cycle, *MTTF* in cycles calculated in [25] is converted to hours. $\mathrm{MTTF}_{Li} = 1024 cycles = 24,576h$.

From studies mentioned, the following MTTF values will be considered in the example:

$$\mathrm{MTTF_{PV}} = 14,670h;$$
$$\mathrm{MTTF_{Li}} = 24,576h;$$
$$\mathrm{MTTF_{DG}} = 4,043h.$$

Applying Eq. 3.42 to calculate system reliability

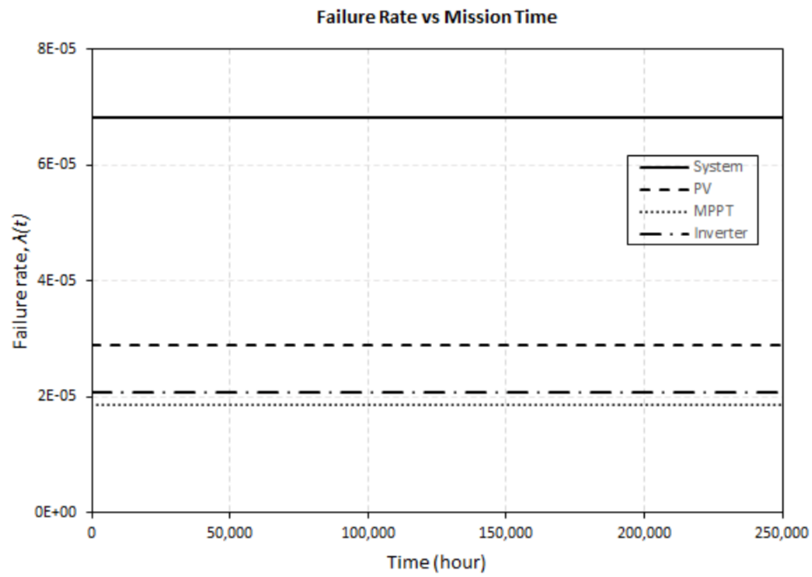

Figure 3.15 PV system series configuration exponential distribution, $\lambda(t)$

$$
\begin{aligned}
R_S(T) &= 1-[1-R_{PV}(T)][1-R_{Li}(T)][1-R_{DG}(T)] \\
&= R_{PV}(T)+R_{Li}(T)+R_{DG}(T)-R_{PV}(T)R_{Li}(T) \\
&-R_{PV}(T)R_{DG}(T)-R_{Li}(T)R_{DG}(T) \\
&+R_{PV}(T)R_{DG}(T)R_{Li}(T) \\
&= \mathrm{e}(-\frac{T}{14,670})+\mathrm{e}(-\frac{T}{24,576})+\mathrm{e}(-\frac{T}{4,043}) \\
&-\mathrm{e}(-1.09\times 10^{-4}T)-\mathrm{e}(-2.88\times 10^{-4}T) \\
&-\mathrm{e}(-3.16\times 10^{-4}T)+\mathrm{e}(-3.56\times 10^{-4}T)
\end{aligned}
$$

Evaluating the reliability of this system by considering two period of times; six months and one year missions times

$$
\begin{aligned}
\mathrm{R}_S(T=4,380) &= 0.972; \\
\mathrm{R}_S(T=8,760) &= 0.881.
\end{aligned}
$$

According to [7], the failure density function of the PV system can be expressed by

$$
\begin{aligned}
f_S(t) = &\sum_{i=1}^{n}\left(f_i(t)\prod_{j\neq i}\left[1-R_j(t)\right]\right)\\
=&f_{PV}(t)+f_{Li}(t)+f_{DG}(t)+f_{PV}(t)R_{Li}(t)R_{DG}(t)\\
&-f_{Li}(t)R_{PV}(t)R_{DG}(t)+f_{DG}(t)R_{PV}(t)R_{Li}(t)\\
&-f_{PV}(t)[R_{Li}(t)+R_{DG}(t)]\\
&-f_{Li}(t)[R_{DG}(t)+R_{PV}(t)]\\
&-f_{PV}(t)[R_{Li}(t)+R_{PV}(t)]
\end{aligned} \tag{3.46}
$$

$$
\begin{aligned}
f_S(t = 4,380) =&\cong 1.480\times 10^{-5}\mathrm{h}^{-1},\\
f_S(t = 8,760) =&\cong 2.512\times 10^{-5}\mathrm{h}^{-1}.
\end{aligned}
$$

Similarly, failure rate of the system can be expressed as

$$
\begin{aligned}
\lambda_S(t) = &\sum_{i=1}^{n}\left(\lambda_i(t)\prod_{j\neq i}\left[1-R_j(t)\right]\right)\\
=&\lambda_{PV}(t)+\lambda_{Li}(t)+\lambda_{DG}(t)+\lambda_{PV}(t)R_{Li}(t)R_{DG}(t)\\
&-\lambda_{Li}(t)R_{PV}(t)R_{DG}(t)+\lambda_{DG}(t)R_{PV}(t)R_{Li}(t)\\
&-\lambda_{PV}(t)[R_{Li}(t)+R_{DG}(t)]\\
&-\lambda_{Li}(t)[R_{DG}(t)+R_{PV}(t)]\\
&-\lambda_{PV}(t)[R_{Li}(t)+R_{PV}(t)]
\end{aligned} \tag{3.47}
$$

$$
\begin{aligned}
\lambda_S(t = 4,380) =&\cong 2.473\times 10^{-5}\mathrm{h}^{-1},\\
\lambda_S(t = 8,760) =&\cong 6.764\times 10^{-5}\mathrm{h}^{-1}.
\end{aligned}
$$

Figures 3.16, 3.17, 3.18 and 3.19, represent the patterns of the microgrid system's reliability function $R(t)$, failure function $F(t)$, failure probability density $f(t)$ and failure rate $\lambda(t)$ with respect to the mission time studied taking into consideration an exponential distribution for all the components and the system itself.

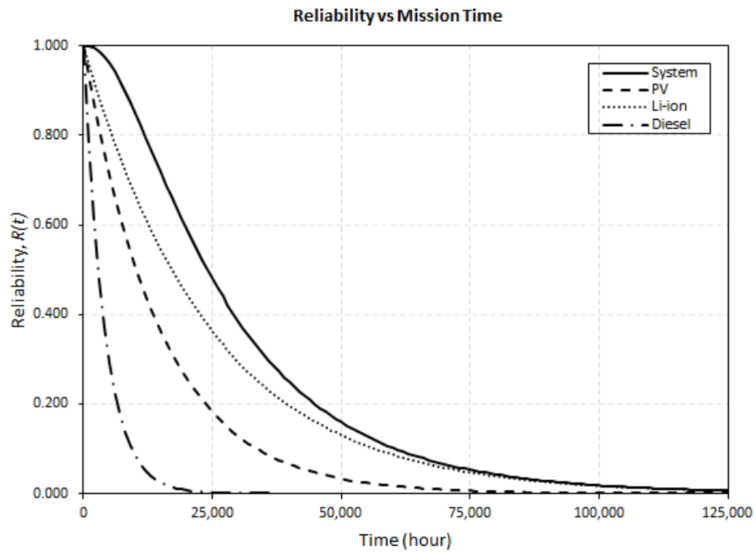

Figure 3.16 Microgrid parallel configuration exponential distribution, R(t)

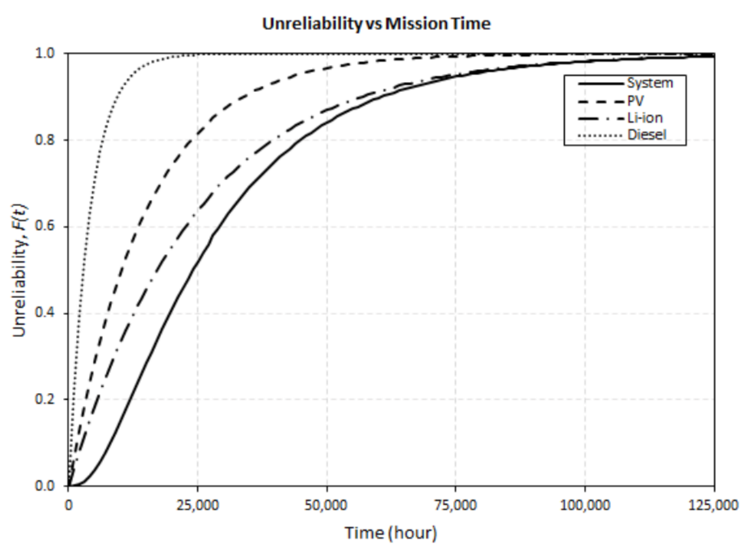

Figure 3.17 Microgrid parallel configuration exponential distribution, F(t)

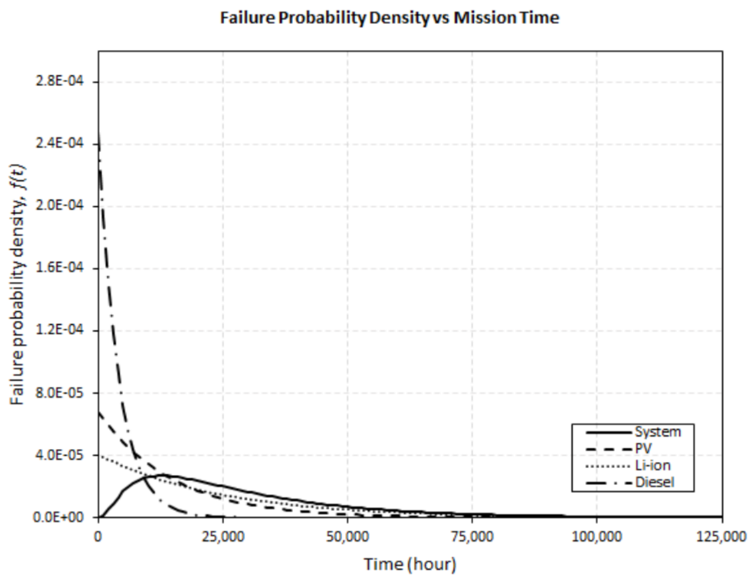

Figure 3.18 Microgrid parallel configuration exponential distribution, f(t)

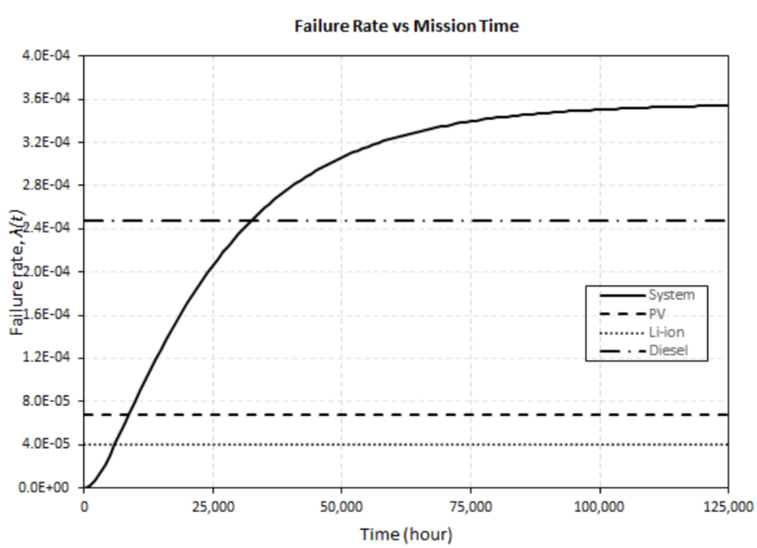

Figure 3.19 Microgrid parallel configuration exponential distribution, $\lambda(t)$

CHAPTER

4

MONTE CARLO METHODS AND RANDOM STATE SAMPLING FOR MICROGRID RELIABILITY ESTIMATION

4.1 Introduction to Monte Carlo methods

Monte Carlo method is a process based on random numbers and probability theory to solve optimization and number generation problems. S. Ulam and Nicolas Metropolis invented the term *Monte Carlo* in reference to the games of chance, which is a popular activity in Monte Carlo, Monaco [29, 30]. It is a class of mathematical models based on random sampling. Monte Carlo Simulation is used to solve an integral to get an expected value

$$I = \int_T F(x) d\mu(x) = E_\mu[F(X)], \tag{4.1}$$

where $X = (X_1, \dots, X_n)$ is a vector of random variables following a distribution with μ as the mean. The method is based on the *Law of Large Numbers* and the *Central Limit Theorem*[31].

- *Law of Large Numbers.* Let $F(X_1), F(X_2), \dots, F(X_n)$ be a sequence of independent random variables following the same distribution with mean $\mu < \infty$

$$\frac{F(X_1) + F(X_2) + \cdots + F(X_n)}{n} \to \mu, \text{ as } n \to \infty. \tag{4.2}$$

- *Central Limit Theorem.* Let $F(X_1), F(X_2), \ldots, F(X_n)$ be a sequence of independent, random variables following the same distribution, each with mean μ and variance σ^2. The distribution will tend to a standard normal as $n \to \infty$

$$P\left\{\frac{F(X_1)+F(X_2)+\cdots+F(X_n)-n\mu}{\sigma\sqrt{n}} \le a\right\} \quad \to \quad \frac{1}{\sqrt{2\pi}}\int_{-\infty}^{a} e^{-x^2/2} dx F \tag{4.3}$$

If $\mu = E[F(X)]$. The unbiased estimator for a sample size n with Monte Carlo is

$$\mu = \frac{1}{n}\sum_{i=1}^{n} F(x_i) \tag{4.4}$$

Taking the Monte Carlo Simulation approach in reliability assessment and deducing the availability complementary function, Unavailability, U, from Eq. 4.5

$$U = \frac{1}{N}\sum_{i=1}^{N} x_i \tag{4.5}$$

where x_i is a zero-one operator variable obtained as an output from the MCS

$$x_i = 1 \text{ if the sampled component state is failure,}$$
$$x_i = 0 \text{ if the sampled component state is success.}$$

and N is the component state samples. The sample variance is defined as

$$V(U) = \frac{V(x)}{N} = \frac{1}{N(N-1)}\sum_{i=1}^{N}(x_i - U)^2 \tag{4.6}$$

The unavailability estimated is also a random variable depending on the number of the state samples and the sampling process. Uncertainty of the estimate can be calculated by checking the variance of the sample mean

$$V(x) = \frac{1}{N-1}\sum_{i=1}^{N}(x_i - U)^2 \tag{4.7}$$

The standard deviation of the sample mean can be given as

$$\sigma = \sqrt{V(U)} = \frac{\sqrt{V(x)}}{\sqrt{N}} \tag{4.8}$$

From Eq. 4.8, it is shown the two measures that can reduce the standard deviation of MCS estimate; decreasing the sample variance and increasing the size of the sample. Hence, it is essential to consider a large number of samples.

4.2 Availability function with Monte Carlo simulation

The application of Sequential Monte Carlo Simulation (SMCS) analysis is valid in the case of studying a repairable component. The "good as new" and the "bad as old" hypotheses are assumed, which indicates that the time to failure and repair data is used without distinguishing the first failure/repair from the rest of the events. The analysis is based on a renewal process, where probabilistic recurrent events are assumed. The parametric distributions from the previous section are utilized in the analysis. PV system series configuration in the previous works will be simulated in the following subsection to maintain simplicity in the illustration of the algorithm through analysis steps and a flowchart.

4.2.1 Availability analysis steps

In this section, Monte Carlo Simulation is executed for repairable components of the PV system; PV modules, an MPPT, and an inverter. In this generic example, the same exponential distribution is used for all components. By the application of the chronological MCS for a specific mission time, we can obtain the up/down state plot for each component and the system. Also, the point availability of the components and the system is estimated. The main steps of using sequential Monte Carlo Simulation for system reliability assessment can be expressed as:

1. The historical time to failure (MTTF) and the time to repair (MTTR) of all the system components is inserted. These numbers can also be expressed through failure rate λ, and failure duration μ. As stated previously, the sample size has to be large enough to obtain valuable results. Hence, the sample size (N) is also inserted as an input. The last input for the simulation is the mission time (T), for reliability and availability studies, the mission time is a vital part of the function expression. Along with the mission time, the availability values estimated are illustrative.

2. The state residence time or, in other words, the MTTF and MTTR generated through a probability distribution. The random numbers for sampled failure data are a function of the historical numbers of each component and the shape of the most suitable distribution describing the randomness. In this generic example, distributions for the three components are exponential,

$$\begin{aligned} \mathrm{h}_{up,i} &= -\mathrm{MTTF}_i . \ln U, \\ \mathrm{h}_{dn,i} &= -\mathrm{MTTR}_i . \ln U', \end{aligned} \tag{4.9}$$

   where h_{up} and h_{dn} are the generated residence times for each component i, U and U' are random numbers in the interval [0, 1].

3. The h_{up} and h_{dn} are utilized to determine how long the component will be in the "UP" and "DOWN" states. This information is used to create an *Up/Down* plot for the components and

subsequently the system. The process is done through system state update at each residence time (t) limited by simulation time limit (s),

$$\text{State}(t) = \begin{cases} 1 & t < h_{up} \\ 0 & h_{up} \leq t \leq h_{up} + h_{dn} \\ 1 & t > h_{dn} \end{cases} \tag{4.10}$$

4. The residence times generation process is repeated for a sampling size (N) times.

5. The simulation time is then calculated using the events that occurred throughout the process,

$$T_{sim} = \sum_{i=1}^{N} h_{up}(i) + \sum_{i=1}^{N} h_{dn}(i), \tag{4.11}$$

where T_{sim} is the simulation time in hours or years.

6. Finally, the availability function A(t) is calculated where t is the mission time,

$$\text{Availability} = \frac{\sum_{i=1}^{N} h_{up}(i)}{T_{sim}}. \tag{4.12}$$

7. Subsequently, the unavailability of the system is estimated,

$$\text{Unavailability} = 1 - \text{Availability}. \tag{4.13}$$

The analysis is executed as shown in Fig. 4.1 using Algorithm 1.

4.2.2 PV system configuration results

The flowchart, shown in Fig. 4.1, is implemented for the PV example. Figure 4.2 is constructed from the MCS results for series PV system. The figure is documenting the state of the components and the system through a specific interval of time. This mission time is set to be $t = 150,000$.

One of the main purposes of running the simulation is to calculate the availability of the components and the system. One of the performance metrics is the mean availability, as shown in Eq. 4.12. Moreover, point availability A (t) is the availability at a specific time t, which represents the probability of the system being available at time t. To calculate this value, a counter was designed in the simulation code. The counter's function is to increment the amount of time the system was in operation up until this specific time t. As in Eq. 4.14, This summation is then divided by the mission time stamp until time t. In Fig. 4.3, the point availability is then compared to the point reliability, the point reliability is calculated using the same exponential distribution as executed in Section 3.2. The comparison is useful to clear the common confusion between the reliability and the availability functions.

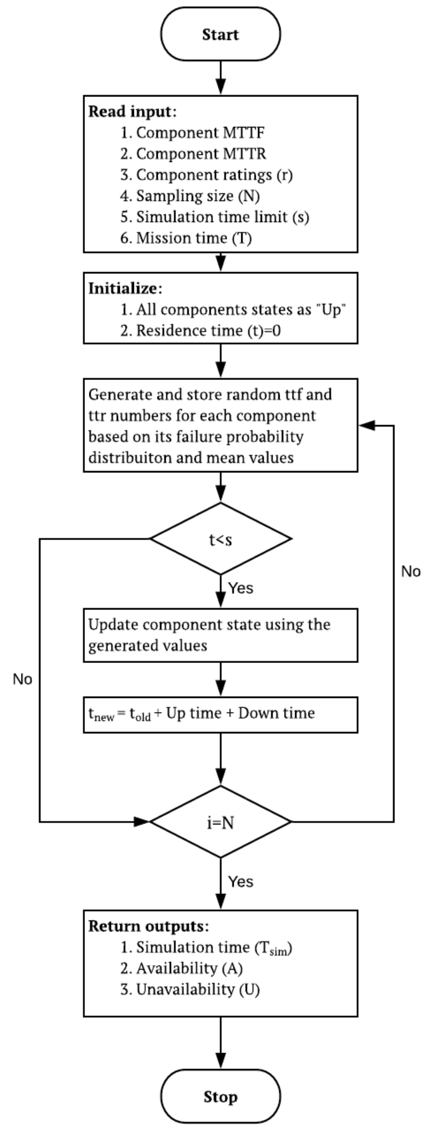

Figure 4.1 Components availability analysis Flowchart

$$A(t') = \frac{\sum_{i=1}^{t'} \text{state}_{up}(i)}{t'}. \tag{4.14}$$

Simulation results for components' availability, expected number of failures (ENF), expected mean time to failure (EMTTF), up time, down time and the system point availability at the end of the mission time is shown here:

$$\text{Availability}_{PV} = 0.9928;$$
$$\text{Availability}_{MPPT} = 0.9953;$$
$$\text{Availability}_{Inverter} = 0.9947;$$

Algorithm 1 Availability analysis using SMCS

Input:
MTTF, MTTR, T, t, N, s
Initialize:
state=ones(T,1)
$t_0 = 0$
for i = 1 to N **do**
  $h_{up} =$ exprnd(MTTF)
  $h_{dn} =$ exprnd(MTTR)
  $T_{up}(i) =$ round(h_{up})
  $T_{dn}(i) =$ round(h_{dn})
  if $t < T$ **then**
    state$(t + T_{up}(i) : t + T_{up}(i) + T_{dn}(i) = 0$
    $t = t + T_{up}(i) + T_{dn}(i)$
  end if
end for
Output:
T_{sim}, Availability, Unavailability

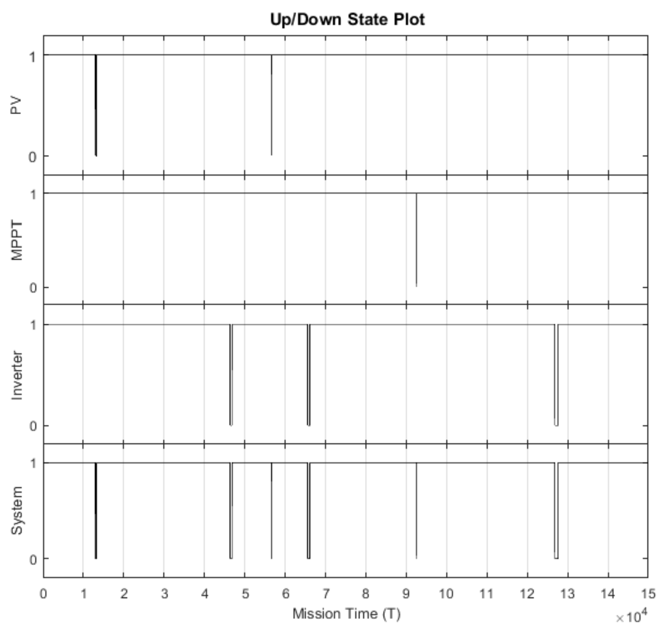

Figure 4.2 Series PV Example, Repairable Systems, Up/Down state plot

$$\text{ENF}(t = 150,000) = 6;$$
$$\text{EMTTF} = 25,000h;$$
$$\text{UpTime} = 147,838h;$$
$$\text{DownTime} = 2,162h;$$
$$\text{A}_s(t = 150,000) = 0.986.$$

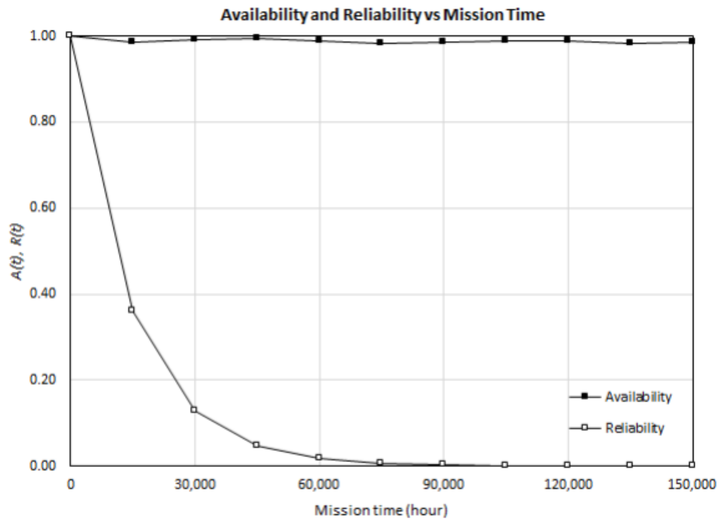

Figure 4.3 Point reliability R(t) and availability A(t) for the PV example mission time interval

In the following section, the work is applied for a microgrid system case study. To evaluate the impact of system reliability on operation, adequacy indices will be introduced.

4.3 Microgrid system case study

4.3.1 Case setup

Microgrid as defined by the department of energy (DOE) "a group of interconnected loads and distributed energy resources within clearly defined electrical boundaries that acts as a single controllable entity with respect to the grid. A microgrid can connect and disconnect to the grid to enable to operate in both grid-connected or island-mode"[32]. To quantify the risk of investing in microgrids, designs, maintenance policies, and renewable energy adequacy need to be investigated. Microgrids have the potential of delivering renewable-based electric services at high-reliability levels. More recently, various consumers are keen on progressing to total renewable energy systems as a means of carbon footprint reduction. In conjunction with the increasing interest in renewables, the costs associated with solar PV and energy storage technologies are dropping remarkably. Moreover, fossil fuel is scarce for rural and remote communities in some developing regions. Before deployment, hybrid generation systems need to be assessed to assure the expected reliability requirements.

The utility grid connection influences the setup of a microgrid, in addition to the studied system constraints and, most importantly the main objectives of the microgrid system. Microgrids objectives can be very versatile, depending on the studied project. One of the most common objectives of any project is to minimize the cost of the system. For an existing project, it is usually minimizing the running cost of the system. For new projects, the cost element is looked at as an optimization problem for the initial investment costs and the running cost. In the field of reliability, the objectives can be system reliability and availability based such as having a four 9's or six 9's system (99.99% or 99.9999%). However, it can also be cost-based through monetizing the impact of outages through cost of not serving the load or the cost of losing system components.

Microgrids can be operating by several modes or a mix of logic. While the grid connection is essential to be considered in the process of operation logic design, the microgrid connection to the grid can be one of three systems. The first system is the energy-saving mode; this system works such that the available microgrid power is meant to be a backup source of power. It works such that in cases of grid unavailability, the microgrid supplies the load with the reserved power through the system components. Self-consumption is the second system to consider. The dependency on the grid, in this case, is minimized. The microgrid is mainly trying to cover the load with its available power until the grid is required. The third system is off-grid systems. Those are the microgrid system where the grid connection is unavailable. In this case, the microgrid is responsible for covering the load all the time. In these off-grid systems, the reliability requirements are usually more relaxed than grid-connected systems. As mentioned earlier, microgrids can be working through a mix of those systems, in the effort to reach the desired objectives and optimize the process of load-serving.

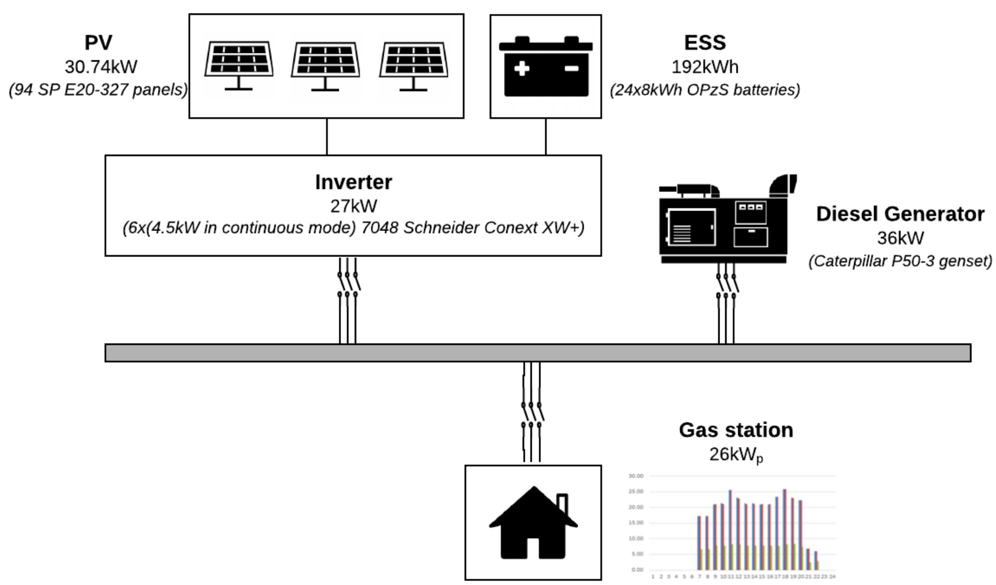

Figure 4.4 Microgrid Case Study Setup

In Figure 4.4, the case study used in this assessment is expressed. The microgrid tested is an off-grid system. We will consider this system as our base case for the following designed use cases.

Those cases is built to express the influence of different aspects of microgrids as a way to show the influence of reliability assessments on investment decisions for those types of systems.

The PV systems considered in this example consists of ninety-four PV modules. The system rated power is $31kW_p$. The energy storage system is a stack of twenty-four $8kWh$ lead-acid batteries. The PV and the energy storage system are connected to a $27kW$ inverter system; this system consists of six $4.5kW$(in continuous mode) design. Finally, the Diesel generator used is a $36kW$ genset unit. This microgrid is designed to serve a profile of loads with a $26kW_p$ daily peak. The derived failure and repair data in Section 3.3 is used for this system.

4.3.2 System operation

The microgrid is set up to work as an off-grid system, as mentioned in the previous section. This system works such that it prioritizes the harnessing of renewable resources before depending on the available conventional power resources. In this microgrid case, the renewable resource is the photovoltaic power generated from the PV system. The energy storage system logic mostly governs the microgrid operation. The logic in Fig. 4.5 is utilized for this example. The load is being served by what is available from PV power first. Then, the battery charges or discharges depending on the remaining or shortage in PV power to satisfy the load. The battery is also maintaining its operation at a certain State of Charge (SoC) limit to avoid over-discharging and extend the useful battery life. After the battery decision-making process, the generator will be used to pick up the rest of the unserved load until its maximum capacity.

During this process, the SMCS results of generated failure events for components is considered. The capacity and the state of the component is considered to evaluate the available power at each location of the microgrid. For instance, if the inverter has a failure event during the operation, all DC systems connected to the inverter are set as open until the inverter is back in service.

4.3.3 Simulation analysis

To calculate the availability measures of the microgrid components, the flowchart in Fig. 4.1 is applied to the previously mentioned system. The sampling size is set to be $N = 10,000$ trials, the simulation time limit is $s = 5,708$ years and the mission time $T = 5$ years. A test is run to determine the tendency of the average *ttf* events generated to approach the actual *MTTF* to find and demonstrate the minimum sampling time required for this application of SMCS. The test results for the components simulations are shown in Fig. 4.6, 4.7, 4.8 and 4.9.

4.3.3.1 Components availability

The results for the microgrid components are shown in Table 4.1. All components' availability for the simulation time is above 99% except for the Diesel generator due to the fact that it has a much lower MTTF than all the rest of the components. The Diesel generator has an availability of about 94%. Subsequently, the diesel generator has the lowest simulation years, which force the experiment to be

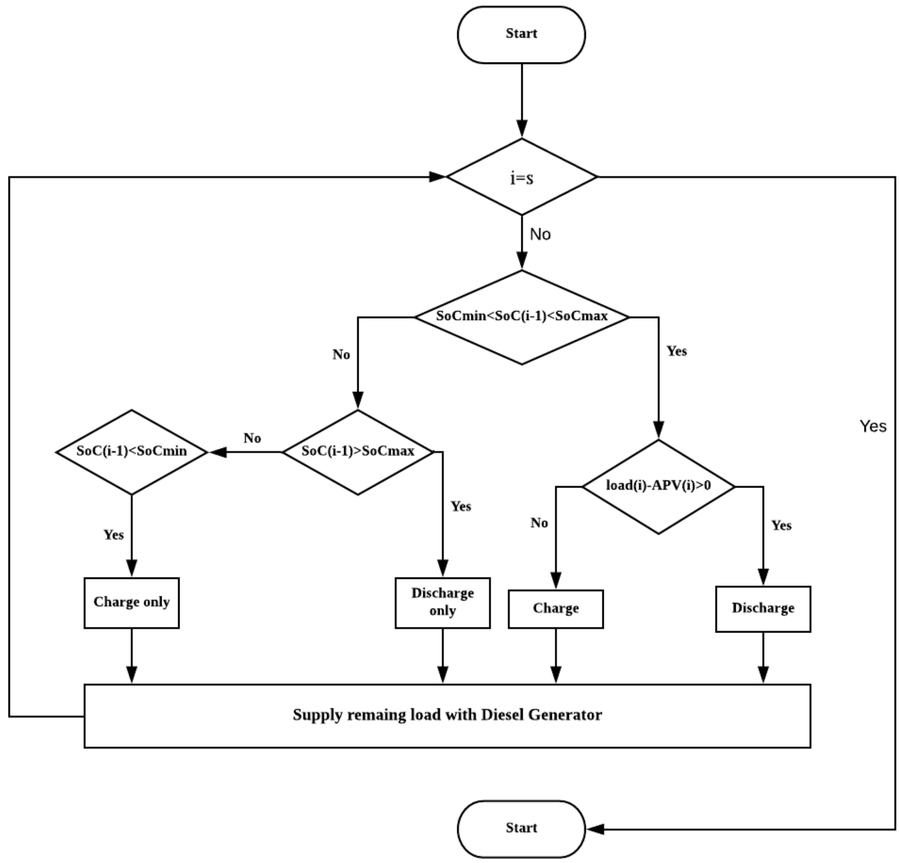

Figure 4.5 MG Battery Operation Logic

limited in that number of years to maintain a simultaneous component time-to-failure simulation process.

4.3.3.2 Components Up/Downstate plot

The next step in the model is building up a Up/Downstate plot for each component. The idea is to go through the operation for the simulation time since this allows the MG operation and logic to be implemented along with the failure events generated to evaluate the reliability of the system.

Mission time is a snapshot of the simulation results. It helps to build a plot that represents what is going on throughout the simulation time, as it is impossible to present the whole period of simulation, which does not mean that the rest of the evaluation is based on this fragment of the simulation. The complete simulation is still utilized to generate the rest of the experiment results. The mission time plot also gives an insight to how it would look like for the microgrid operating for a certain number of years, in this case, five years. Figure 4.10 shows the components states for the five years of mission time.

The results show that the inverter could be operating for five years without any failures occurring.

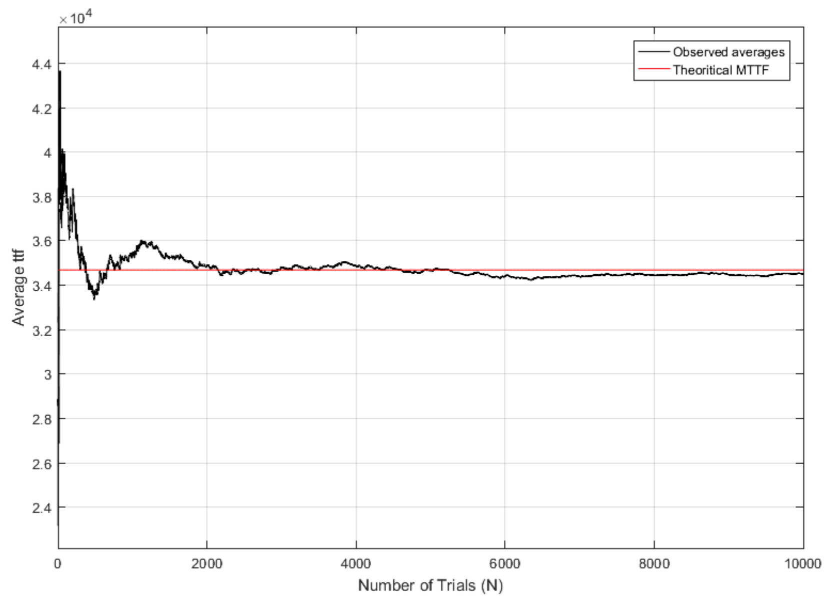

Figure 4.6 PV Average generated failure events vs. MTTF at different number of trials

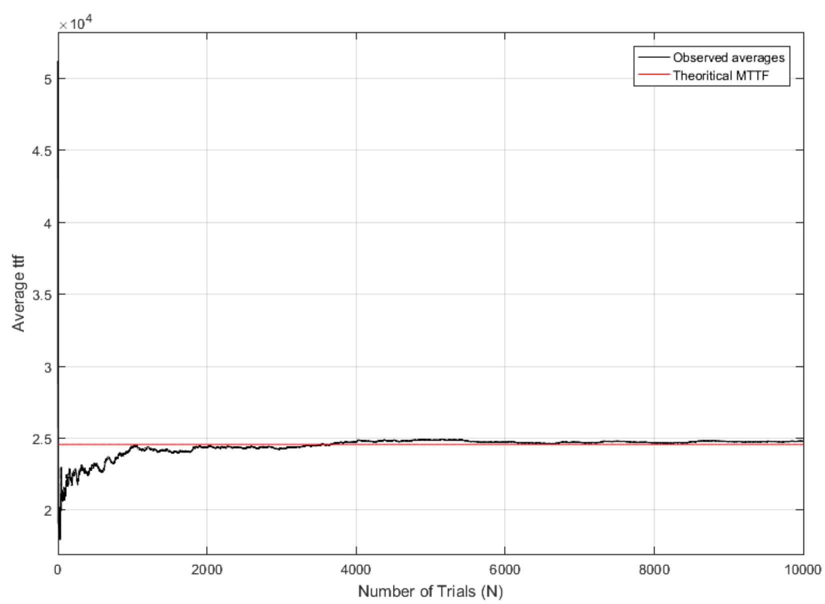

Figure 4.7 ESS Average generated failure events vs. MTTF at different number of trials

On the other hand, the diesel generator has failed at six events during the same time. PV system and the battery had only one failure event each for the same duration. The results show that for five years, there could be eight maintenance orders required to be made.

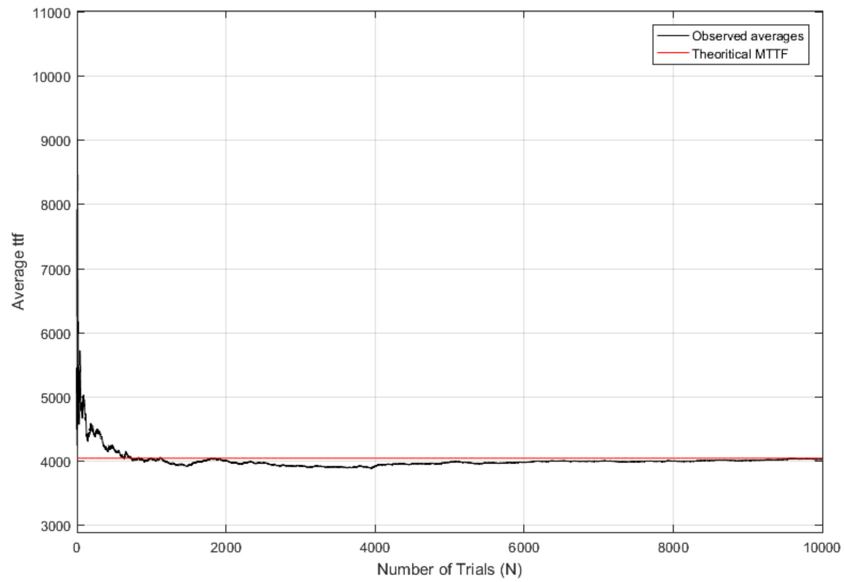

Figure 4.8 Diesel Generator Average generated failure events vs. MTTF at different number of trials

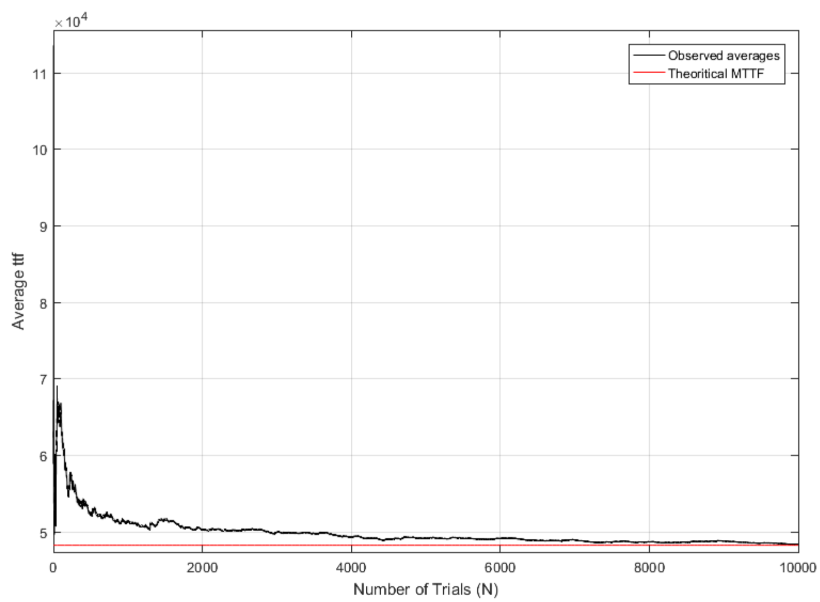

Figure 4.9 Inverter Average generated failure events vs. MTTF at different number of trials

4.3.3.3 MG system state plot

During the simulation time, the states for the components are stored for the same time series. These states, with the capacities of the components, are used to structure the states for the MG system.

Table 4.1 Components Availability Results

	PV	ESS	DG	Inverter
Availability	0.99276	0.99005	0.94177	0.99486
Unavailability	0.00724	0.00995	0.05823	0.00514
Simulation years	39,682	28,591	4,879	55,562

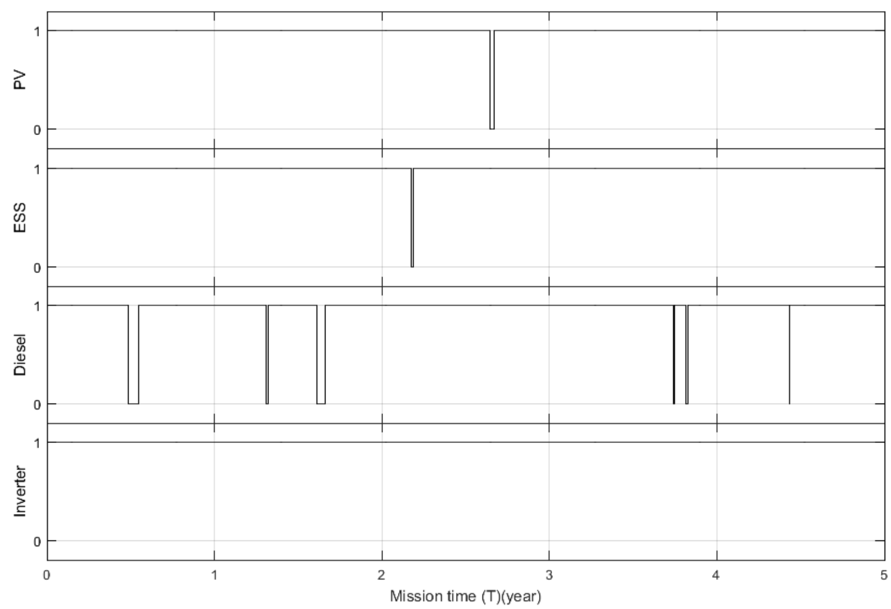

Figure 4.10 MG Components Up/Down State Plot at Mission time $T = 5 years$

The flowchart in Fig. 4.11 illustrates the adequacy assessment section of the algorithm. A snapshot is also taken for this process and is shown in Fig. 4.12 for a mission time of five years.

The results, shown in Fig. 4.12, show several interesting behaviors for the MG system. The plot shows that the system does not get affected by the failure of either the PV or the battery system. It is only influenced by the state of the Diesel generator. The second observation from the plot is that even when the system is down, it does not follow the generator behavior precisely. The downtime for the system does not look smooth as much as the components downtime.

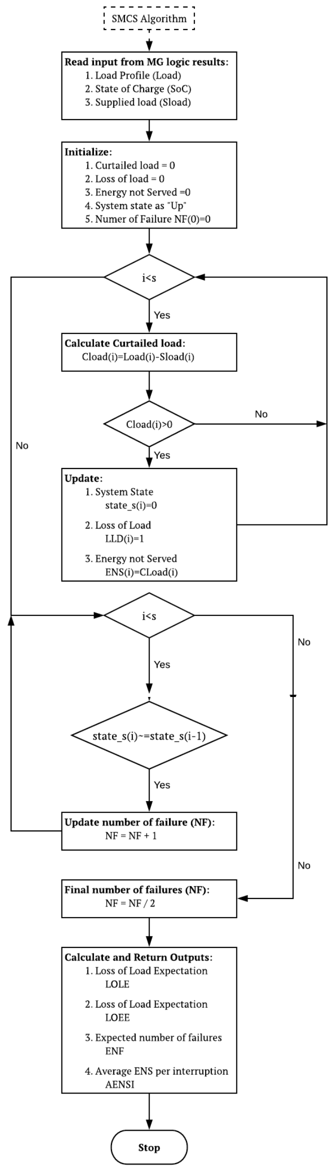

Figure 4.11 System Adequacy Assessment Flowchart

The five-year mission time is divided into yearly plots in Fig. 4.13 to investigate what is happening. It shows in the graph that during the six generator failures, the system seems to be restored several times within the time of the generator failure, which leads to the ragged MG system state plot. To have a clear view of the system behavior through these failure times, a three-week and a one-day event were plotted. In 4.14 and 4.15, the details of the operation and the system response in smaller time snaps are observed.

The results show that due to the process dynamics of evaluating the system state, the representation of the expected system failures is describing more failures than the actual expected values. The system state evaluation works such that every time the system does not serve the load ultimately, it

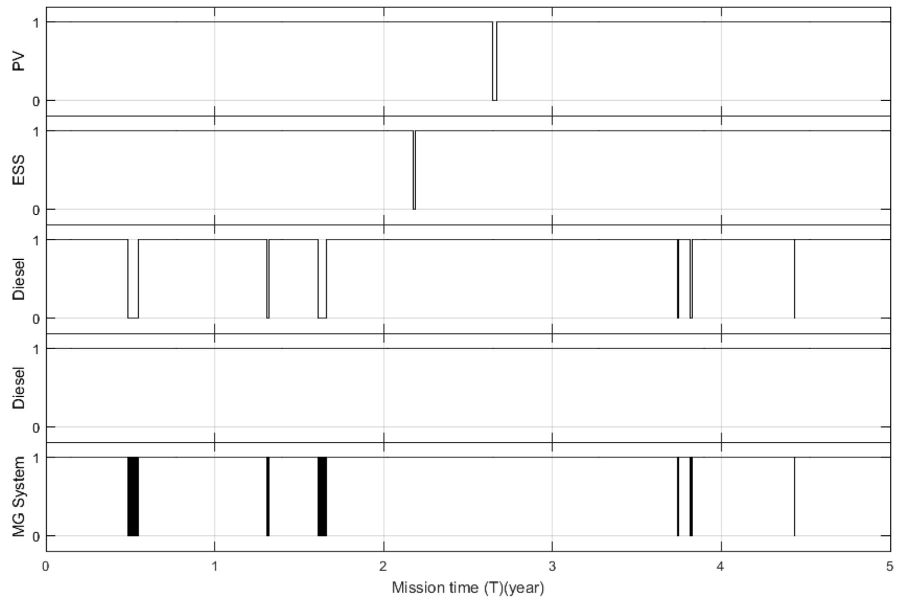

Figure 4.12 MG System Up/Down State Plot at Mission time $T = 5 years$

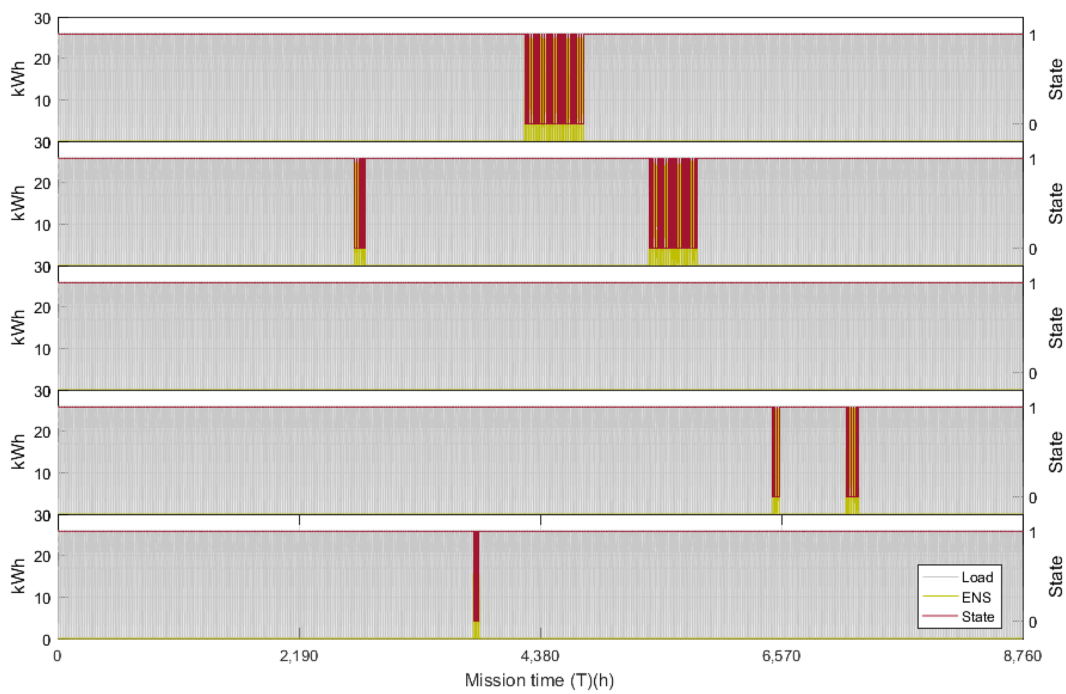

Figure 4.13 Load, Curtailed load and MG Up/Down Plot at Mission times $T = 1 years$

goes from an Up to a Downstate. This evaluation process not includes the times when an actual component's failure occurred and lead to the system failure, but also every time the system was able to serve the load for a while and went to not serving the load status during a long duration failure.

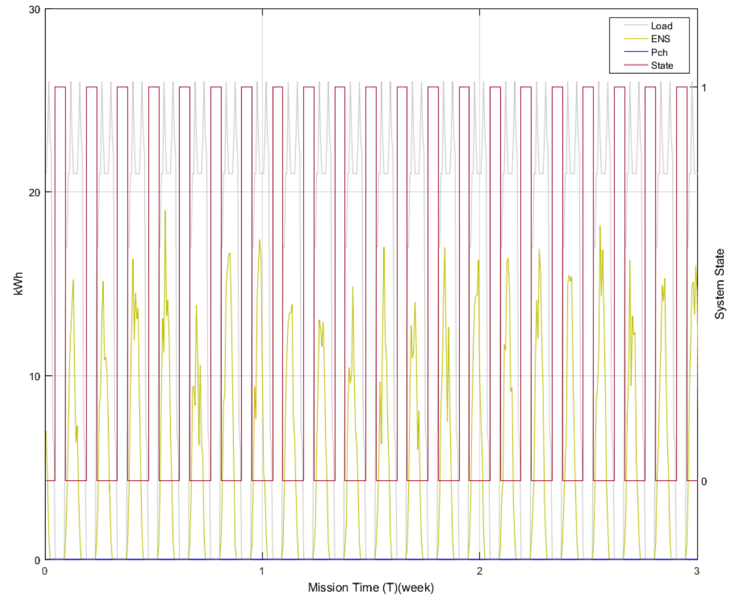

Figure 4.14 Diesel generator three-week failure event

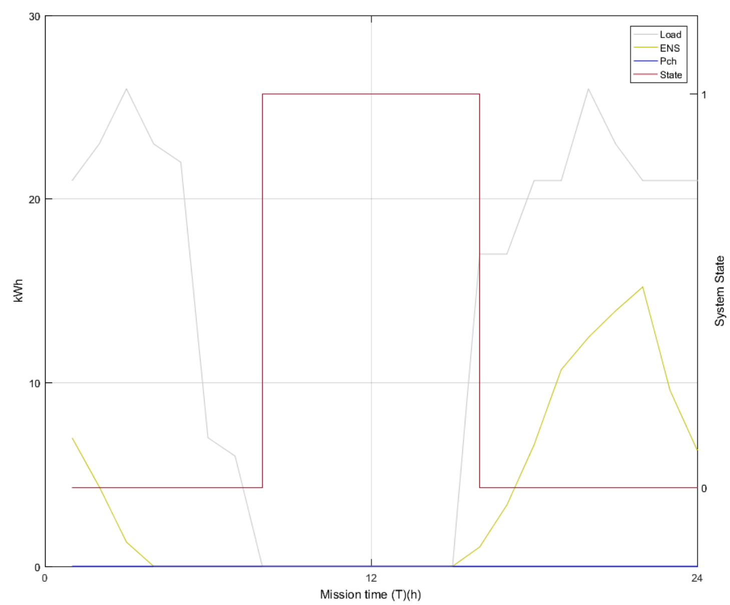

Figure 4.15 Diesel generator one-day failure event

This leads to expressing one failure into a series of failures, which represent the expected number of failure number by larger values than the ones to be expected.

Table 4.2 MG System Availability Results

	PV	ESS	DG	Inverter	MG System
Availability	0.99276	0.99005	0.94177	0.99486	0.96698
Unavailability	0.00724	0.00995	0.05823	0.00514	0.03302
Simulation years	39,682	28,591	4,879	55,562	5,708

4.3.3.4 MG System availability

The system expected yearly availability results are shown in Table 4.2. The analyzed microgrid system is expected to be available for about 96.7% of the year.

4.3.3.5 MG adequacy assessment

The second stage of a MG reliability assessment is to evaluate the system capability to satisfy the load throughout its lifetime or for a certain mission duration. Adequacy assessment is the evaluation being used to make expectations for the system with respect to the load-serving. The assessment can be divided into two phases. The first step depends on the MG operation design assigned for the case and the system states, previously structured, through the simulation time.

The first step outcomes are:

1. **Loss of Load Duration (LLD)**. It is the number of times the MG system has failed to serve the load entirely or partially. The commonly used unit for this metric is the number of hours for the simulation period.
2. **Energy not Served (ENS)**. It is the number of the required energy units that were not supplied to the load at each time step. The ENS is measured with the same unit to be used for the energy balance calculations in the model. In this case, this metric is estimated in kWh. ENS is another definition of the concept of the curtailed load previously presented in the study.

Finally, the second step in the adequacy assessment to measure a group of expected values to represent the system reliability for a certain period of time. This duration is usually preferred to be in years. The expected values are calculated to give us a sense of how reliable the system is in the specific project to be evaluated. The following adequacy assessment indices are used for this process,

1. **Loss of Load Expectation (LOLE)**. This index represents the expected number of hours through which the load will not be served partially or fully. This value and the rest of the adequacy indices will be calculated on a yearly basis. Therefore, in this case, it is the number of hours in

Table 4.3 MG system adequacy assessment indices

Loss of load expectation (LOLE) (hours/y)	**Loss of energy expectation (LOEE) (kWh/y)**	**Expected Number of failures (ENF)**	**Average ENS per Interruption (kWh/int.)**
289	3,604	21	169

a year expected to have an unserved load. This value can be calculated from the *LLD* values previously calculated as expressed here,

$$LOLE = \frac{\sum_{i=1}^{N} LLD_i}{N} (h/y). \tag{4.15}$$

2. **Loss of Energy Expectation (LOEE)**. It is the amount of the expected energy not to be served to the load over a year period of time. The total *ENS* value is used to estimate this index,

$$LOEE = \frac{\sum_{i=1}^{N} ENS_i}{N} \quad (kWh/y). \tag{4.16}$$

3. **Expected Number of Failures (ENF)**. The model generates a large number of failure events over the simulation duration. The expected number of outage events is calculated by this index as follows,

$$ENF = \frac{\sum_{i=1}^{T_{sim}} NF_i}{T_{sim}} (/y). \tag{4.17}$$

4. **Average Energy not Served per interruption (AENSI)**. Finally to have a sense of what to expect at each failure event, the expected amount of energy not to be served at each failure event is then calculated,

$$AENSI = \frac{ENS}{TotalCustomerInterruptions} \quad . \tag{4.18}$$

Following the adequacy assessment explained, the results for the MG system evaluated in this example are presented in Table 4.3.

4.3.4 Results

Results show that the MG system is expected not to thoroughly pick up the load for 3% of the year. It will not serve 4% of the total load energy requirement. The system is estimated to suffer 21 failures with an average of 169kWh not supplied at each of those events. It is clear from the results that the microgrid design is not optimized. As discussed, the generator is the only component that leads to the system down states. Moreover, the ESS is barely working. Since the battery is following a logic that dictates to only charge when there is a PV surplus power after serving the load. This situation rarely occurs; hence, a sizing capability, in addition to operation and logic selection, is suggested to be associated with the designed model to help with the planning of new microgrid projects.

The suggested modifications are presented in the following steps:

1. **Failure events counter**. The number of failures for the presented case study is not descriptive. Although the availability of the microgrid was high, 97% of the time, the number of failures presented seems large for that high availability system. After investigating the issue and taking snapshots of some failure events in the simulation, it is shown that the failure events counter is not offering meaningful results. The failure events being counted are not only the actual yearly component failure events. In addition to that, the transitional times when the state of the system goes to no-load curtailment and then back again to curtailment status during one failure event. This occurs due to situations such as when the PV picks up the load in the morning and then not able to cover it at night while an actual component is at failure state. To solve this issue, the suggestion of separation of load curtailment and failure events counting is presented in Chapter 5.

2. **Frequency of load curtailment**. To separate the number of failure events and load curtailment incidents, a new index is introduced in Chapter 5. The frequency of load curtailment will help as a part of describing the system adequacy towards the served load. It also presents the rate of occurrence of times when the system is forced only to serve a part of the load. This index is implemented in the model along with the results are presented for the case study in the following chapter.

3. **Adequacy indices probability distribution**. Previously, the expected values of the studied adequacy indices are presented in this chapter. It is proposed to present not only expected and mean values to describe the results but also present the probability distribution of the indices. A probability distribution can be very helpful to give a more complete picture of the results shown.

The first section of this chapter is developed to discuss minor modifications in the designed base model. In the rest of the chapter, several pathways for model improvement are proposed. The improvement suggestions are created to increase the capabilities of the model. The chapter also takes on microgrid development topics such as sizing and design. The cost of outages and failures will be quantified in here as well.

4.4 Reliability assessment estimates modifications

4.4.1 Failure events counter

In the algorithm developed, the failure events counter is modified here. The idea is to separate failures and load losses in the reliability and the adequacy assessment, respectively. The failure counter is now more related to the actual failures of the components. During the simulation, the counter is incremented by one each time one of the components suffered a random failure. The counter is being reset at each year of the simulation, and the results are stored to be used later to evaluate the expected number of failures (ENF) in the adequacy indices section in the results. The expected value of the yearly number of failures is calculated as shown in Eq. 4.17.

4.4.2 frequency of load curtailment

The load curtailment events are now evaluated independently. Load curtailment frequency is proposed in the case study to present the number of times a load curtailment is imposed on the system. A new index is also introduced here to evaluate the expected value of this frequency. Expected Frequency of Load Curtailment (EFLC) can be expressed by

$$EFLC = \frac{\sum_{i=1}^{N} FLC_i}{N} \quad (/y). \tag{4.19}$$

4.4.3 Yearly adequacy indices evaluation

The adequacy indices expected values are previously calculated by the end of the simulation for the yearly values. In this part, these calculations are done through two steps instead. The simulated values of loss of load duration, energy not served, load curtailment, and the number of failures are aggregated for every simulated year. The yearly values are then being handled to estimate the expected values for a year. The following equations illustrate the process,

$$A_N = [\sum_{i=1}^{8760} State_s(i)/8760]_N \quad (-), \tag{4.20}$$

$$LOL_N = [\sum_{i=1}^{8760} LLD(i)]_N \quad (h), \tag{4.21}$$

$$LOE_N = [\sum_{i=1}^{8760} ENS(i)]_N \quad (kWh), \tag{4.22}$$

$$NF_N = [\sum_{i=1}^{8760} NF(i)]_N \quad (occ.), \tag{4.23}$$

$$LC_N = [\sum_{i=1}^{8760} LC(i)]_N \quad (occ.), \tag{4.24}$$

where N is the simulated year order. These N number of values are then utilized to estimate the expected values for each index. This can be expressed as

$$EA = \frac{\sum_{i=1}^{N} A_i}{N} \quad (/y), \tag{4.25}$$

$$LOLE = \frac{\sum_{i=1}^{N} LOL_i}{N} \quad (h/y), \tag{4.26}$$

$$LOEE = \frac{\sum_{i=1}^{N} LOE_i}{N} \quad (kWh/y), \tag{4.27}$$

$$ENF = \frac{\sum_{i=1}^{N} NF_i}{N} \quad (occ./y), \tag{4.28}$$

$$EFLC = \frac{\sum_{i=1}^{N} FLC_i}{N} \quad (occ./y). \tag{4.29}$$

4.5 Analysis results for modified base model

4.5.1 Reliability assessment results

The same use case shown in Chapter 4 is applied to the modified model. The results for the reliability and adequacy assessment are shown in this section. Conclusions deduced from the modifications are discussed later.

The reliability assessment for the MG system case study is evaluated and shown in Table 4.4. System availability is expected to be 96.697. It is conceivably very similar to the previously calculated values since the process did not change a lot in the part of estimating system availability. The evaluation suggests an expected yearly 2.523 failures. Comparing it to the previous numbers, the

Table 4.4 MG system reliability assessment using the modified model

Simulation years (y)	Expected availability (%)	Expected Number of failures (ENF) (occ./y)
5707	96.697	2.523

Table 4.5 MG system adequacy assessment indices using the modified model

Loss of load expectation (LOLE) (hours/y)	Loss of energy expectation (LOEE) (kWh/y)	Expected frquency of load curtailment (EFLC) (occ./y)	Probability of load Curtailment (PLC)
289	3,605	1.752	0.0002

expected number is now tenfold less than the previous value. This number shows more consistency and relevance to the rest of the evaluation. Since the presented calculation is based on the actual failure events of the components, the estimates represents a more realistic system reliability.

4.5.2 Adequacy assessment results

Expected values for the adequacy indices are shown in Table 4.5. The results indicate that the loss of load and energy expectations are similar to the base model results. With these few similarities, it is still beneficial that the expected values are calculated through the explained two steps. Without this procedure, the process of showing the following results of indices probability distribution would not be possible otherwise. The newly introduced indices dealing with load curtailment are also shown in the table.

It is observed that the expected frequency of load curtailment is lower than the expected number of failures previously mentioned, which shows that the load curtailment event does not necessarily occur with every component failure event. This is an expected result of having distributed generation units in a microgrid setup. This also indicates the benefit of separating those two counters, as previously discussed.

4.6 Conclusions

4.6.1 Reliability indices custom formulation

The reliability indices used to present power systems' reliability are abundant. The modeling work in Chapter 4 illustrates the importance of specifying ways to measure the reliability of every system setup. The modifications done in this chapter made the results more meaningful and descriptive to the actual pattern meant to be discussed in this work. Separating the number of failures and the load curtailment indices is one example of this.

4.6.2 Repair time modeling impact

By implementing the probability distribution to the set of the results shown, it gives more essential insights. The probability distributions results for the modified base model are presented in Fig. 5.2, 5.3, 5.4, 5.5 and 5.6. Observing these results, it is clear that even though the expected values of reliability and adequacy indices show good performance, the distributions are wide showing bad performance values for much less amount of simulation years.

An investigation to explore the indications of having these shapes rather than concentrated tall curves is highly motivated. After going through the model, it is clear that these wide shapes are a result of the randomness of the repair process. As stated previously, both failure and repair events are generated randomly using a set of distributions which can be avoided by through planning.

It means that even if the failure times randomness is necessary to be included in the model, the repair process randomness can be avoided to improve the results. This shows the importance of improving the maintenance process through both the planning or the executions phases. These observations are the drive for proposing an investigation of the introduction of maintenance strategies to the model (work proposed for Chapter 7).

4.7 Proposed model improvement and upgrade areas

4.7.1 Sequential Monte Carlo improvement

During the structuring of the SMCS model, the steps of improvement in the modeling and the coding showed a great impact on the computational cost. This is one factor that is necessary to be considered in simulation works. Hence, the sequential sampling process in the model is yet to be improved to reach the minimum computational cost possible. These improvements also allow the increase of the simulation years to be requested in the analysis process. Finally, SMC helps to express the adequacy indices in the form of the expected values and its probability distribution. The adequacy assessment results are now more meaningful, and the value of showing the probability distributions will be shown in the next chapter.

4.7.2 Cost of reliability/unreliability feature

The cost analysis is essential to investigate the viability of such projects. The cost of high reliability is reflected in the initial investment cost as one element that is required to be looked at if high reliability is a priority for projects. This cost is one important element to be included in the optimization problem. The other cost related to microgrid reliability is the cost of not serving. This cost accounts for all the costs that can be a consequence of the events where the microgrid is not satisfying the connected loads. This cost is quantified as a running cost, and it can be modeled as a function of several variables such as the energy-not-served in kWh. This cost is required to be evaluated and monetized as a way to present the reliability results differently (in terms of money losses).

4.7.3 MG operation and ESS logic selection

In the base case experimental results, it is shown that manipulating and customizing the battery logic can lead to reliability improvements. For this reason, it is essential to investigate several logics and compound logic systems before suggesting an investment or upgrade to existing systems. This process is also important to implement in the design and development phase.

4.7.4 Testing with different MG setups and systems

It is essential to validate the model by testing it with different microgrid setups. The replication of the evaluation in a different environment surely provides more insights in terms of model evaluation and improvement suggestions.

4.7.5 Reliability-based sizing

Using the cost analysis mentioned above, MG grid sizing can be evaluated based on reliability requirements and cost minimization objectives. A sizing feature gives the model a high value since the model is designed to estimate reliability values for long term project evaluation. Sizing of those projects based on the results of the model can indicate another use to the reliability analysis.

CHAPTER

5

MICROGRID RELIABILITY ASSESSMENT IMPROVEMENT BASED ON SEQUENTIAL MONTE CARLO SIMULATION

It is shown in Chapter 4 that transforming the reliability assessment tool, to a sequential Monte Carlo based method, has resulted in a high computational cost. This chapter is developed to discuss the rising challenges with using sequential simulations. The mitigation plan to reduce the computational time is then proposed. Then, the SMC reliability assessment tool is explained in steps. The rest of the chapter analyzes case studies and the validation criteria for the proposed methodology. Moreover, several suggested tool capabilities are proposed to use the assessment with the developed optimizer in Chapter 6. The last section presents various case studies.

5.1 Introduction to sequential simulations

Sequential Monte Carlo methods are a general MCS class of techniques. Sequential Monte Carlo methods are random-sampling based techniques to approximate Bayesian inference. SMCS is a powerful tool to simulate rare events. For composite power system reliability, a historical time series analysis such as SMCS is suitable to simulate operation and contingencies immanent in a MG system [6, 33, 34]. It provides a weighted sample from a series of distributions by sequencing importance sampling and resampling mechanisms [35]. This approach can be harnessed to model failures of a power system. In a sequential Monte Carlo Simulation (SMCS), each component state is connected to the previous state of that component. This sequential process is useful when the power system is partially determined by the historical evolution of the system [33]. The flexibility of SMCS is derived from the ability to represent non-exponential residence times, which make them useful for chronological processes. The initial state is always sampled from a non-sequential MCS [36]. The use of the sequential technique is effective in evaluating a set of reliability indices, including failure frequency and outage duration, which helps to assess the value of losses[6]. Therefore, the sequential class is suitable to consider correlated events and functional dependencies.

This work presents a reliability evaluation methodology, where components' states are generated using probability distributions and random numbers. Unlike the work in [37], component random failure events are generated and updated at each simulation trial. Previously, component up and downtimes are generated for N times based on the failure and repair mean values. Each component availability is estimated using these numbers. Finally, outages are generated for one year of operation to estimate indices. In this chapter, system reliability is analyzed at each transition of a component. At each trial, the minimum residual time for a component is set to be the transition time when the composite system is analyzed. A new failure number is randomly generated for the down component, and the rest of the components get their residual time updated by subtracting the analyzed simulation trial duration.

Simulation time is advanced to the next transition incident, and the simulation proceeds until the variation associated with the calculated index is minimized. Compared to previous work in this area, the proposed methodology is more reasonable since the system reliability is studied at each occurring state transition. Moreover, failure events are generated in series only if required, as opposed to being generated all at once at the beginning of the simulation. This technique cuts down the required computational time, despite the fact that sequential approaches are usually slow to converge. The other factor contributing to process efficiency is reducing simulation trials based on achieving a reasonable coefficient of variation. The chapter also aims to present a MG cost analysis in order to evaluate the economics of a proposed system with respect to the achieved renewable penetration. A net present cost (NPC) is calculated for the evaluated MG design. The assessment considers the fixed and running costs for the associated components, as well as the cost of unreliability.

5.2 Reliability assessment challenges

The previously discussed high computational time challenge occurs based on the complexity of the evaluated system. While assessing the reliability of a power system to estimate the availability and/or the energy adequacy, the system complexity can be driven by:

1. **A complex reliability structure**. While using a hybrid system of different technologies, the reliability structure of the integrated system can be very sophisticated, given a large-scale system.

2. **Different failure distribution for sub-component level**. The failure distribution for a MG component can be estimated using the failure history of the component. However, A more accurate estimation is more feasible by having more detailed historical data about the failure reason and the failed sub-component. Thus, applying the failure distributions of sub-components, a more complex simulation is required.

3. **Lack of components data**. It is prevalent that the more mature components, such as generators, would have more extensive sets of data, giving them an advantage over new technologies such as battery systems.

4. **Different repair distributions**. The randomness in the repair process is previously discussed while applying reactive maintenance. Thus, the repair distributions can be different between components, leading to an increase in the complexity.

5.3 Motivation

While evaluating a power system reliability, it is more sound to simulate the system component simultaneously to resemble the real-life operation. The states of the composite system are sampled sequentially based on the component failure events. The transition between system states is simulated using probability distributions of components' state duration and random number generation. Take component i as an operating microgrid component. The probability of failure of this component dictates the system reliability associated with this component failures. Assuming that the component up duration is given by T_i, then the probability of the system transition at time t can be given by,

$$R = P(T_i \leq t) \tag{5.1}$$

and can be illustrated as in Fig. 5.1,

Therefore, the sequential method is based on the previous MC approach of random sampling. However, the method correlates the system transitions to the random sampling of components' events. Sequential Monte Carlo is used to generate a more distinctive assessment for microgrid reliability. This group of methods are characterized by estimating expectations with probability distributions.

By combining an efficient sequential Monte Carlo simulation with an empirical Bayes method, the explained challenges can be tackled. SMC is a powerful tool to solve complex systems with components and sub-components failure behavior following various probability distributions. Such a problem is impossible to solve with classical statistics. SMC can be applied to any form of power network as long as the functional structure can be obtained. The method is successful for large-scale systems in principle, taking into consideration the expected increase of the computational time.

SMC can easily integrate components with *a priori* information [38]. Components with high reliability that is subject to reliability testing with a small field population can be assessed by

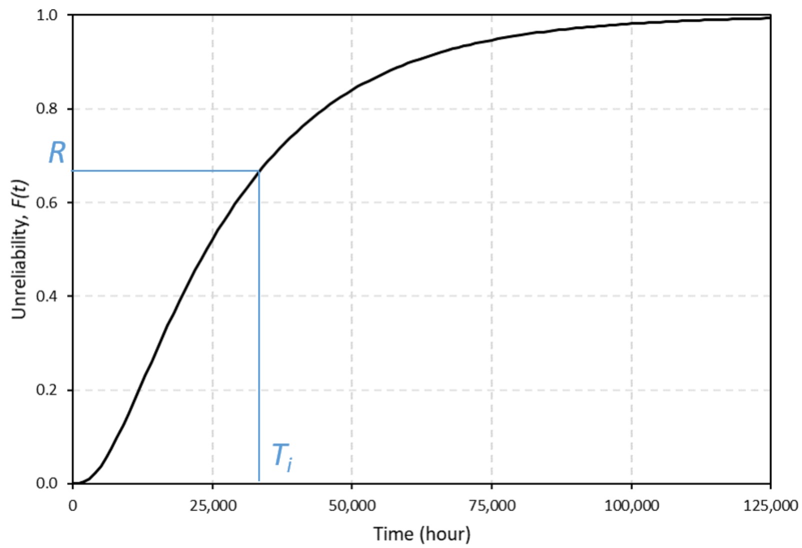

Figure 5.1 System transition based on a component failure probability

enlarging the failure information using a Bayesian approach with SMC as in [39]. Finally, SMC can be used to estimate the mean time between failure *MTBF* and the availability of a system based on random and/or condition-based failures. Thus, this method can be used to simulate arbitrary reactive and planned maintenance systems. It will be shown in the proposed methodology using the reliability assessment model is easy and does not require knowledge about how it works. By implementing the information of the included system, a full reliability assessment can be executed, returning the results in the form of various indices. SMC provides a detailed view of the calculated indices. The probability distribution histograms, for the indices, expected values presented below can give us more insights about the estimates. The distributions are plotted for the frequency in several simulation years as shown in Fig. 5.2, Fig. 5.3, Fig. 5.4, Fig. 5.5 and Fig. 5.6.

In conclusion, Sequential Monte Carlo methods are commonly used to simulate stochastic failure behavior and estimate composite reliability. The reliability analysis of a microgrid system is performed considering each component operation and maintenance nature. The historical field maintenance and factory testing records for the considered components are a key element in the reliability estimation process. Therefore, acquiring microgrid components maintenance history is essential to predict and simulate the system behavior in a MG setup. System state transition sampling techniques are often used to evaluate power system reliability. Sequential Monte Carlo methods are random-sampling based techniques to approximate Bayesian inference. SMCS is a powerful tool to simulate rare events. For composite power system reliability, a chronological time series analysis such as SMCS is suitable to simulate operation and contingencies immanent in a MG system.

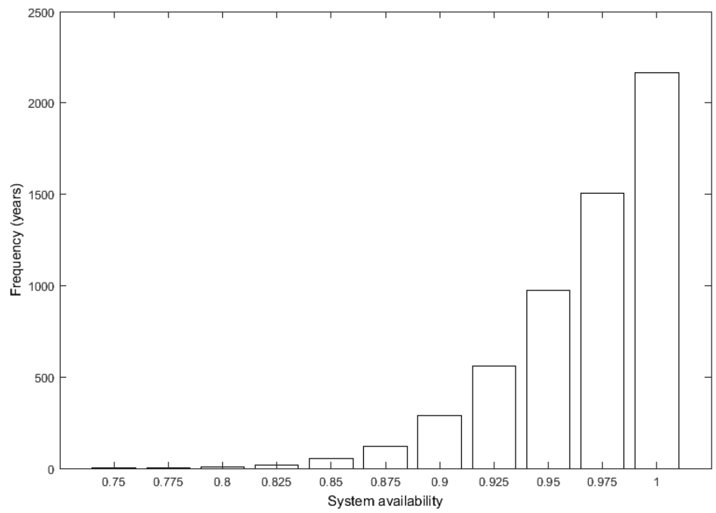

Figure 5.2 System availability probability distribution

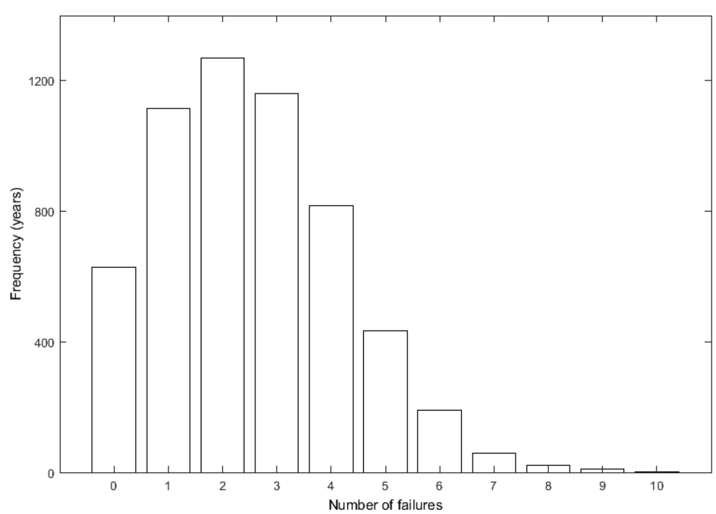

Figure 5.3 Number of failures probability distribution

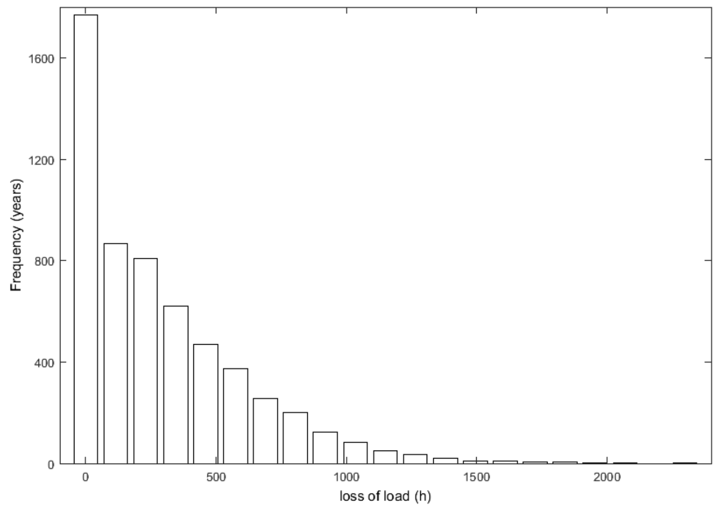

Figure 5.4 Loss of load probability distribution

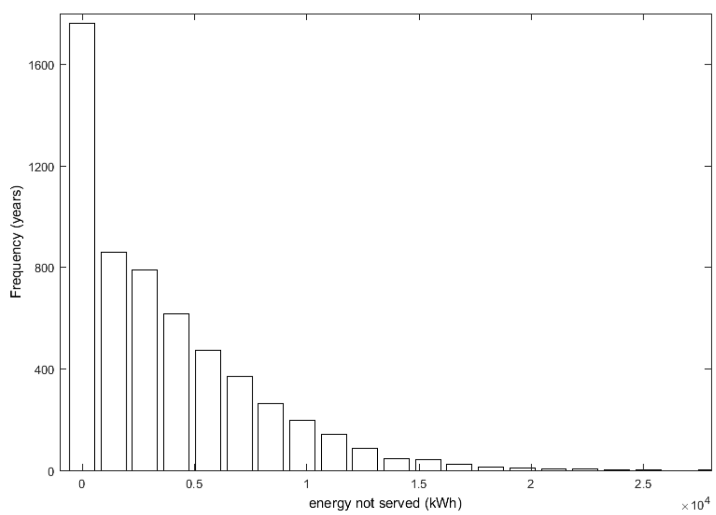

Figure 5.5 Loss of energy probability distribution

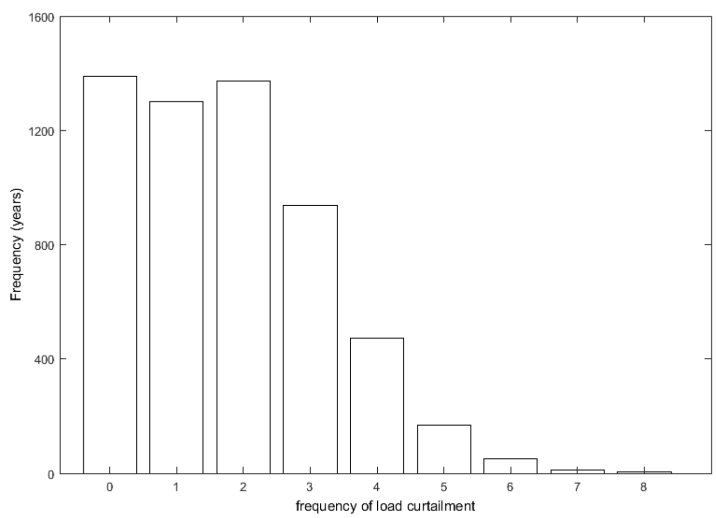

Figure 5.6 Frequency of load curtailment probability distribution

5.4 Proposed SMC reliability assessment methodology

The time-series simulation is performed to resemble the microgrid operation and assess the system performance with respect to meeting the required demand. Being analyzed sequentially, a simulation trial presents a contingency event from the integrated system perspective. By considering the system design, the operation logic, and components constraints, the system is evaluated at each transition. The operation of the hybrid system is simulated for several trials, while randomly generating failure events for the components, to estimate system reliability. SMC considers the chronological format of time-series problem, where the load demands and renewable resources historical data is introduced. A battery storage cycling logic is implemented to meet the demand and maximize renewable utilization. Based on the degree of meeting the load, the system states are sampled. Apart from the challenge of acquiring chronological data, the SMC high computational effort is mitigated through minimizing the necessary steps to acquire accurate results. The presented results show that the estimated indices are more descriptive and accurate compared to non-sequential approaches.

5.4.1 Initializing the reliability assessment

The assessment tool is designed as a function where case-dependent required parameters and inputs are required. To initialize the simulation, the following inputs are implemented:

1. **MG Components' ratings**. The sizes of the analyzed microgrid components are required to estimate the available power to meet the demand at each time step. Most generation systems require the size in the form of the kW rating except for storage devices. A dual rating for the energy storage size is necessary and consists of the max charging/discharging power and the capacity in hours or kilowatt-hours.

2. **Fuel-fired units loading curve and limits**. The loading of the fuel-based generation units dictates the efficiency of operation and fuel consumption accordingly. To ensure an efficient operation, manufacturers of generators provide fuel-loading curves and recommendations for the minimum loading to ensure an efficient and environmental operation. A minimum and maximum loading is implemented for each generator in the configuration along with the type of fuel used.

3. **Energy storage cycling limits**. Similar to the generator loading limits, the battery system is cycled within a specific State-of-Charge range (SoC) to maximize battery health and prevent over degradation. These limits are implemented as a percentage of the system capacity and used to apply a rule-based logic to maintain the system within the given range.

4. **Failure data or probability distribution**. An important precursor in the used methodology is the analysis of the components' failure behavior. The assessment is able to use data samples to generate failures or a typical distribution representing the component failures. In the case

of using a probability distribution, the necessary number of parameters will depend on which distribution is considered.

5. **Demand profile**. The system operates to meet the demand at each time step of the simulation and evaluate accordingly. Thus, Load information such as the seasonal and daily peaks as well as the daily and annual average is required. A full year load profile would be the best-case scenario, but peak and average values are sufficient by applying regular variations.

Further inputs to accommodate the requirement of the optimizer is discussed in the upgraded tool section.

5.4.2 Simulation steps

The presented simulation steps can be divided into subgroups of steps. Given that the approach is based on time-series analysis, the first group illustrates the methodology to update the required timestamps in the simulation.

5.4.2.1 Simulation times update

The order of the simulation trials, N, is the number of times the simulation is executed to reach the desired level of accuracy in the results. N is used as the index of the times used in the simulation. Therefore, all the following described times are calculated before the start of each simulation trial and stored as the trial values.

1. **Composite random event generator**. The simulation starts by generating time-to-failures for the components and store it in the component time to next transition array using the following equations,

$$TTF_i = -\ln(1-U)/\lambda_i \tag{5.2}$$

$$T_i^{tr} = TTF_i \tag{5.3}$$

   where λ is the exponential distribution parameter in this case. However, the number and the nature of these parameters vary based on the component distribution. Failure times are then stored as the time to next transition for each component.

2. **System time to transition**. The system transition to be analyzed in the current simulation trial is indicated based on the minimum value in the component time to next transition array as in Eq. 5.4,

$$\left[T_s^{tr}, f\right] = \min\left(T_i^{tr}\right) \tag{5.4}$$

where T_s^{tr} is the system to the next transition and f is the order of the failed component. A reactive repair action, *TTR*, is generated for the component causing the transition using the assigned probability distribution for repair duration.

3. **Simulation time**. The simulation advances by adding the system time to transition as follows,

$$t_{N+1} = t_N + T_s^{tr} + TTR \tag{5.5}$$

4. **Component residual times**. The component residual time is the time remaining for the generated failure to take place. The residual time for the components is then updated using Eq. 5.6 as shown in Algorithm 2,

$$T_i^{rs} = \begin{cases} 0, & \text{if} i = f \\ T_i^{tr} - T_s^{tr}, & \text{otherwise} \end{cases} \tag{5.6}$$

where T_i^{rs} is reset to zero for component f and updated for the rest of the components by subtracting the system time to next transition from component time to next transition.

5. **Component time to next transition**. The time to next transition is updated considering the residual time as in Eq. 5.7,

$$T_i^{tr} = \begin{cases} -\ln(1-U)/\lambda_f, & \text{if} i = f \\ T_i^{rs}, & \text{otherwise} \end{cases} \tag{5.7}$$

where T_i^{rs} is created for component f using a new randomly-generated time-to-failure with a distribution U and its failure rate λ_f. On the other hand, T_i^{rs} is set as the residual time value for the rest of the components.

6. **Component state sampling**. The component's time to next transition, with the repair duration for the failed components, is used to sample the states of the components for the trial period.

The described time values are calculated between each two simulation trials. This update process can be integrated into the simulation steps, as shown in Fig. 5.7

5.4.2.2 Microgrid operation and system evaluation

The system operation is simulated after all the times are updated for the subsequent trial. The microgrid dispatch strategy is based on a load-following approach while maximizing renewable energy utilization and efficiently operating generators. The strategy is applied, and the performance of the system is evaluated by various reliability counters. At each simulation trial, the strategy is applied as follows,

1. **Power time-series**. The operation starts by calling the load profile for the simulation trial period. Components rating and constraints data are implemented to consider the power

Algorithm 2 Sequential Monte Carlo

Input:

Components' rating and loading limits, Component failure history and distributions, Solar irradiation data, Load profile

for i = 1 to N **do**

Randomly generate failure events for all components

Find the minimum residual time, T_f^{rs}

Update system time to transition T_s^{tr}, Residual times T_i^{tr}, component time to transition T_i^{tr} and simulation time t_{N+1}

for $J = 1$ to t_N **do**

Simulate the system operation

Record contingency events in *ENS* and *LLD*

end for

Calculate reliability estimates *LOEE* and *LOLE*

Calculate coefficient of variation *CV* and test convergence

end for

Calculate *Availability* and *Adequacy*

Calculate renewable and environmental metrics

Calculate the generators fuel consumption

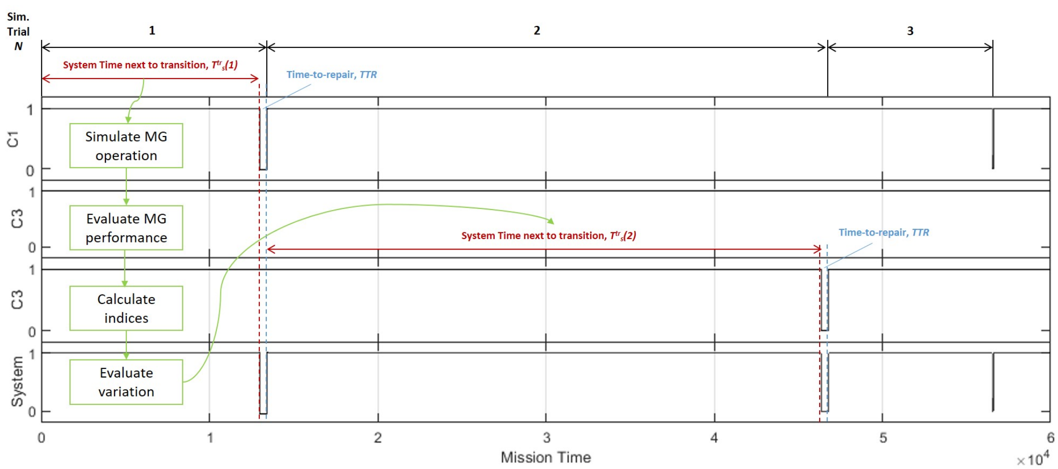

Figure 5.7 Simulation times update

limits during the operation. Moreover, the solar irradiation profile for the PV system is called for the studied period. Finally, the states of the components, previously sampled in the time updates stage, are taken into account to estimate the available power for each component in the system.

2. **Battery storage cycling**. The battery cycling takes place by applying the load following algorithm. The operating power for each component is simulated with different strategy for three stage of charge regions. The boundaries for the three regions are the battery operation limits, where the decision to charge or discharge the battery is taken accordingly. The cycling logic

can be described as in Fig. 5.8,

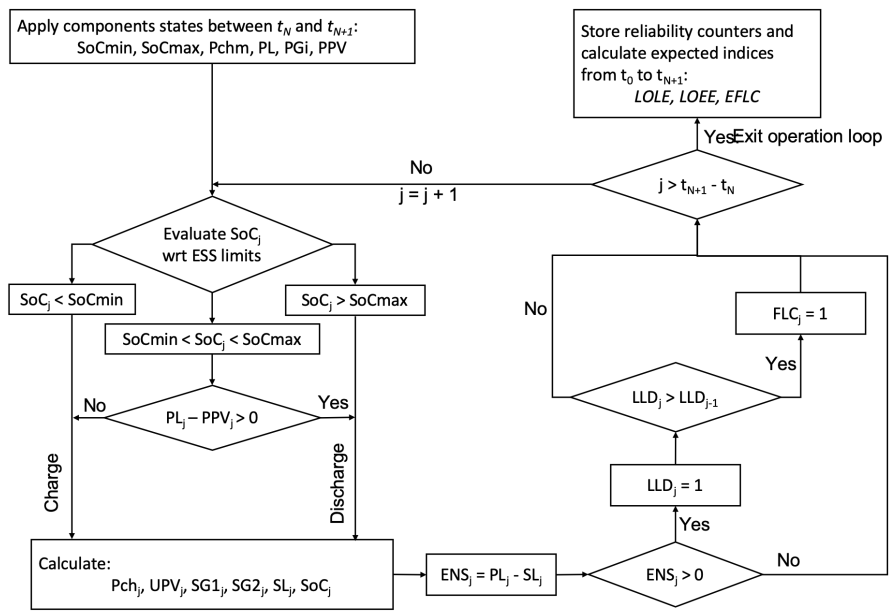

Figure 5.8 System operation and performance evaluation

where the available power, considering the components' states, is called, and the required counters are initialized as an array of zeros. SoC_j is the State of Charge of time step j is located within the three cycling zones by comparing it to the cycling limits. The battery is only allowed to charge if it is below the minimum state of charge, *SoCmin*, and is only allowed to discharge if it exceeds the maximum charging limit, *SoCmax*. In the case of occurring in the normal operation zone, the battery is only charged and discharged based on the available PV power in comparison to the required demand.

When the demand is more than the available PV power, the discharging power, Pch_j, is determined based on the minimum of the remaining load after using PV power, the maximum charging power of the battery $Pchmax$, the available capacity before hitting the state of charge lower limit. On the other hand, when the PV power exceeds the load demand, Pch_j is the minimum of the excess PV power, the battery rated charging power, and the empty battery capacity without exceeding the maximum limit. SoC_j is now updated based on the previous state and the calculated charging/discharging power.

After using the battery capacity while complying with the logic rules, the generators are used to complement the remaining demand efficiently. By exhausting all the available power, the supplied load, SL_j, is calculated to determine later if the demand is met completely. The utilized PV power UPV_j, the battery state of charge, and power, the generators loading SGi_j, and the supplied demand are stored.

3. **System performance evaluation**. The studied power system is evaluated during battery cycling, as shown in Fig. 5.8. The Energy Not Served *ENS* is calculated in *kWh* by comparing the supplied load to the required demand. Then, the Loss of Load Duration *LLD* counter is incremented, and the failure counter *FLC* is only incremented at the first hour of the outage.

Once the trial duration is covered, the system performance is evaluated, and the simulation advances.

5.4.2.3 Estimating reliability indices

After evaluating the system performance using the battery cycling loop, Loss of Energy Expectation *LOEE*, Loss of Load Expectation *LOLE* and the expected number of load curtailments *EFLC* are calculated by estimating an annual estimate for the previously calculated *ENS*, *LLD* and *FLC*. The expected values are estimated for the trial years using,

$$LOEE = \frac{1}{Y}\sum_{i=1}^{Y} ENS(i) \tag{5.8}$$

$$LOLE = \frac{1}{Y}\sum_{i=1}^{Y} LLD(i) \tag{5.9}$$

$$EFLC = \frac{1}{Y}\sum_{i=1}^{Y} FLC(i) \tag{5.10}$$

5.4.2.4 Coefficient of Variation

The simulation is designed to terminate when a certain level of variation is achieved to reduce the computational effort. Coefficient of Variation, *CV*, is a statistical tool to measure dispersion in estimated values around the mean. *CV* is used to measure the risk of the estimated value using random sampling methods. This value is calculated at the end of each trial using,

$$CV = \frac{\sigma(E(F))}{\mu(E(F))} \tag{5.11}$$

where σ, the standard deviation and μ is the mean values of the estimators for the reliability indices. In case the estimators have a zero value when the system is 100% reliable, the CV is not calculated since the mean is zero. Thus, this one special case is dealt with differently where the estimators are calculated for 20 times, and if not deviated from zero, the simulation terminates.

5.4.2.5 Availability and energy adequacy

The reliability indices are finally presented in annual percentage values as in Eq. 5.12 and Eq. 5.12,

$$EA = \left(1 - \frac{LOEE}{Load}\right) \times 100\% \tag{5.12}$$

$$TA = \left(1 - \frac{LOLE}{8760}\right) \times 100\% \tag{5.13}$$

5.4.2.6 Evaluation generators operation

The generators' operation is modeled based on maximizing the efficiency of the combustion and fuel utilization. Fuel consumption model in Fig. 5.9 and Fig. 5.10, is modeled in the assessment to be used to calculate the fuel consumption and implement minimum loading. The fuel curve shows that the fuel combustion is extremely inefficient below 25% loading. Thus, the loading limit is set to 25% open to adjustments. Annual consumption in Gal/year is finally estimated. Other metrics such as the operating hours and the loading are also calculated for the generation unit.

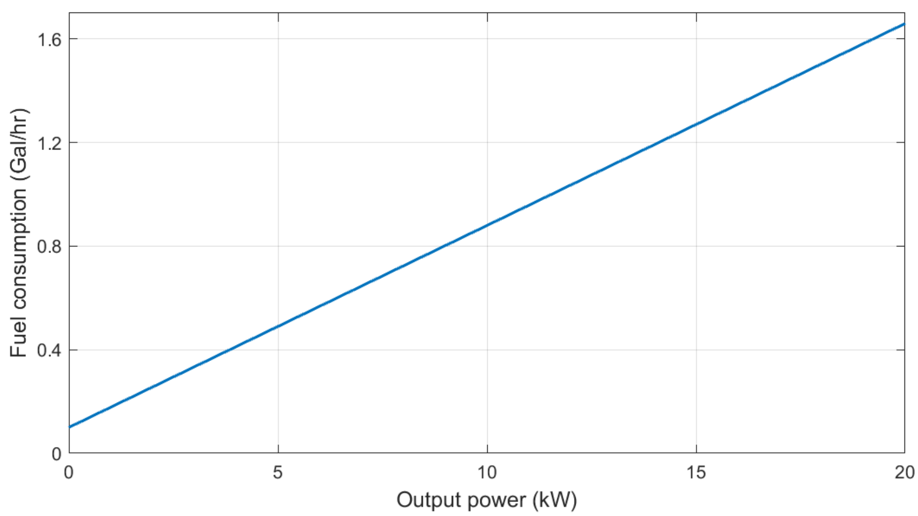

Figure 5.9 Fuel consumption curve

5.4.2.7 Renewable penetration

The renewable percentage is calculated annually, based on the used PV power or the power loading of the fuel-fired units in comparison with the annual load consumption as follows,

$$RP = \left(1 - \frac{SGi}{Load}\right) \times 100\% \tag{5.14}$$

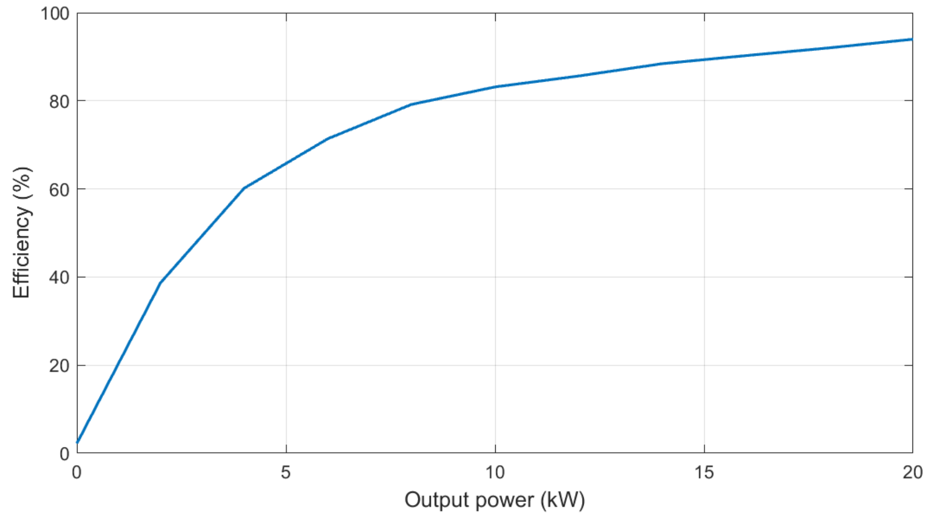

Figure 5.10 Generator efficiency

5.5 Convergence and statistical analysis

5.5.1 Convergence

The accuracy level of Monte Carlo methods is usually determined using the coefficient of variation shown in Eq. 5.11. For the desired accuracy *CV*, the required simulation trials depend on the system unavailability, but it is independent of the size of the system [40]. Hence, MC is more suitable for large complex systems compared to analytical enumeration techniques. ENS is observed to have the largest variation, the lowest convergence rate, so it is used as the convergence criterion to ensure the desired accuracy. In the following example, hybrid system reliability is tested against several accuracy levels. The computational time is recorded and analyzed.

The system components are shown in Table 5.1. Results in Table 5.2 show that convergence accuracy between 10-20% is showing efficient results of around 0.5 seconds until termination.

Table 5.1 Convergence example

PV (kW)	ESS (kW)	GS1 (kW)	GS2 (kW)
70	25	20	20

Table 5.2 Convergence time

CV (%)	5	10	15	20
Time (sec)	11.19	1.63	0.542	0.549
Adequacy (%)	99.737	99.738	99.741	99.741

5.5.2 Reliability indices probability distributions

The probability distributions of the system reliability indices are presented in Fig. 5.11, Fig. 5.12 and Fig. 5.13. Based on the results, LOEE metric is used to identify the variability of the simulation trials where the CoV is maintained below a threshold.

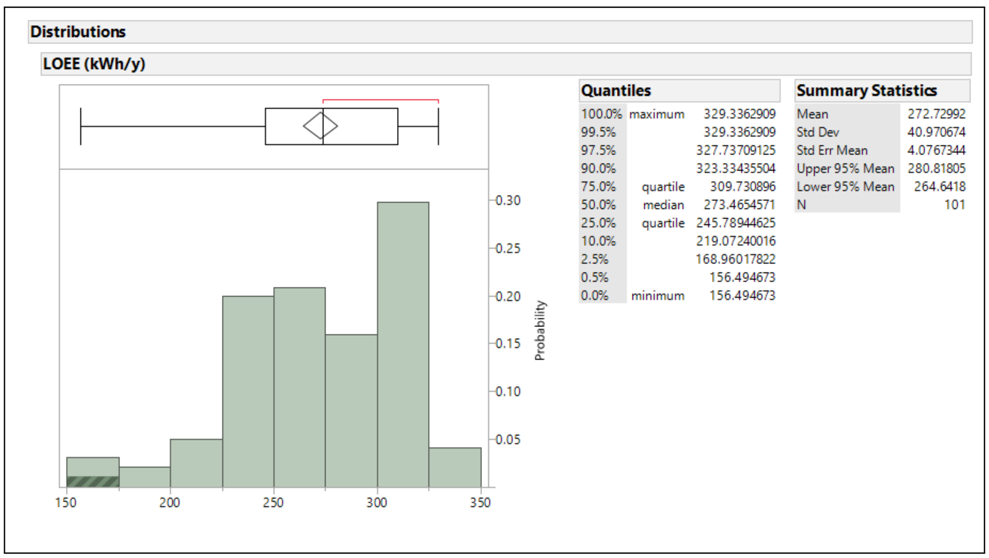

Figure 5.11 Loss of energy expectation prob. distribution

5.5.3 Testing simulation

One of the most common tests in statistics is the student t-test. The test is based on a null hypothesis of no significant difference between one sample and the true mean or between two simulation result samples. Two samples of reliability indices are estimated in Fig. 5.14, Fig. 5.15 and Fig. 5.16, where 25 and 30 experiments are executed and a t-test is applied to the two independent sets. All P-values of the tests are shown to be greater than the 0.05 p-value, resulting in not rejecting the null hypothesis of no significant difference.

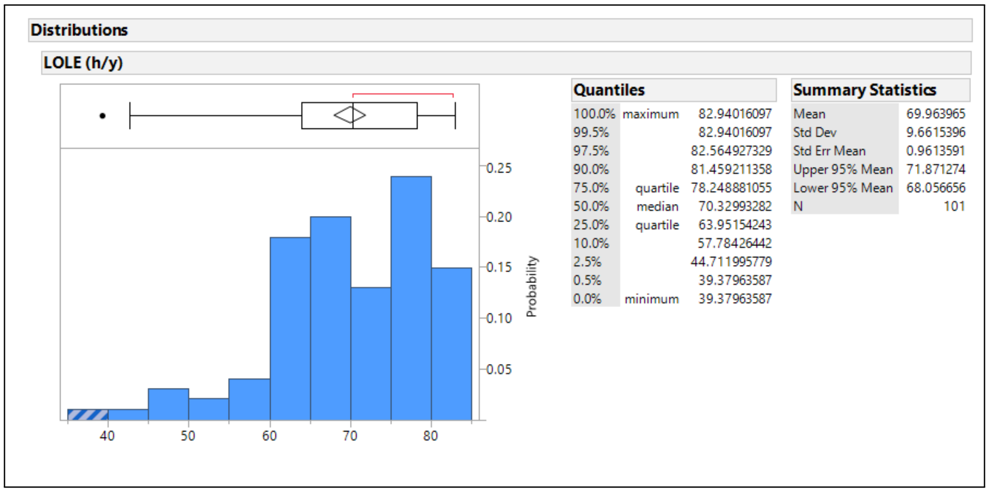

Figure 5.12 Loss of load expectation prob. distribution

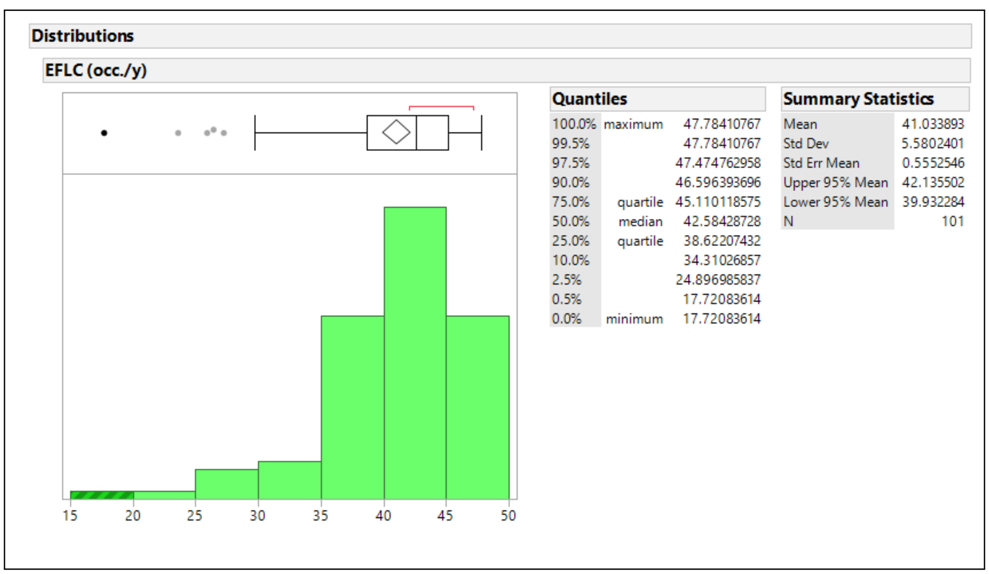

Figure 5.13 Expected frequency of load curtailment prob. distribution

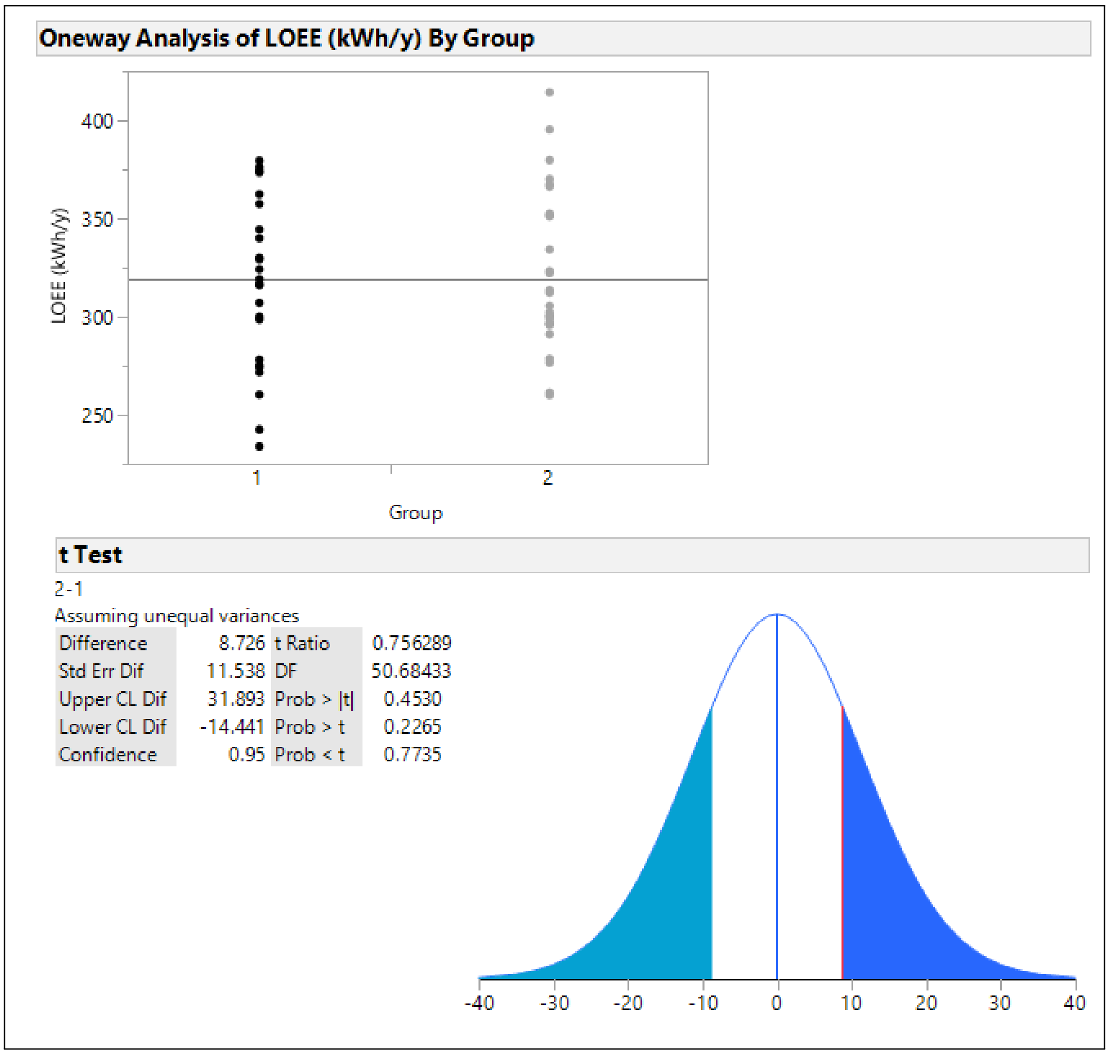

Figure 5.14 t-test for LOEE

Oneway Analysis of LOLE (h/y) By Group

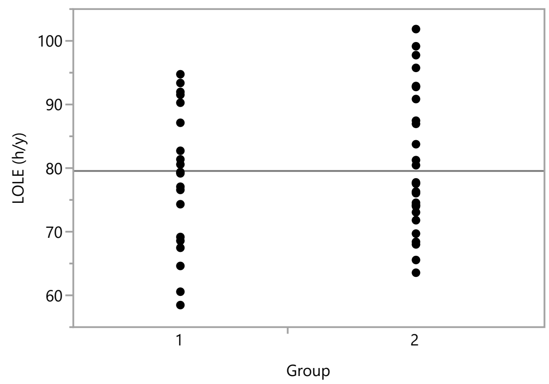

t Test

2-1

Assuming unequal variances

Difference	1.7760	t Ratio	0.617575
Std Err Dif	2.8757	DF	51.15211
Upper CL Dif	7.5488	Prob > |t|	0.5396
Lower CL Dif	-3.9969	Prob > t	0.2698
Confidence	0.95	Prob < t	0.7302

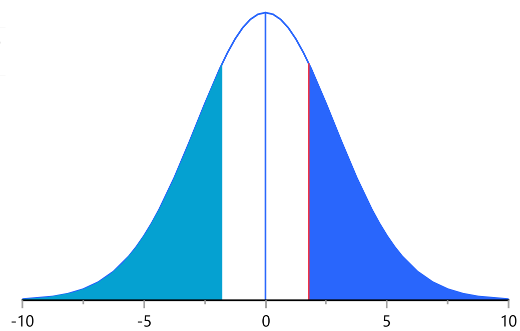

Figure 5.15 Expected frequency of load curtailment prob. distribution

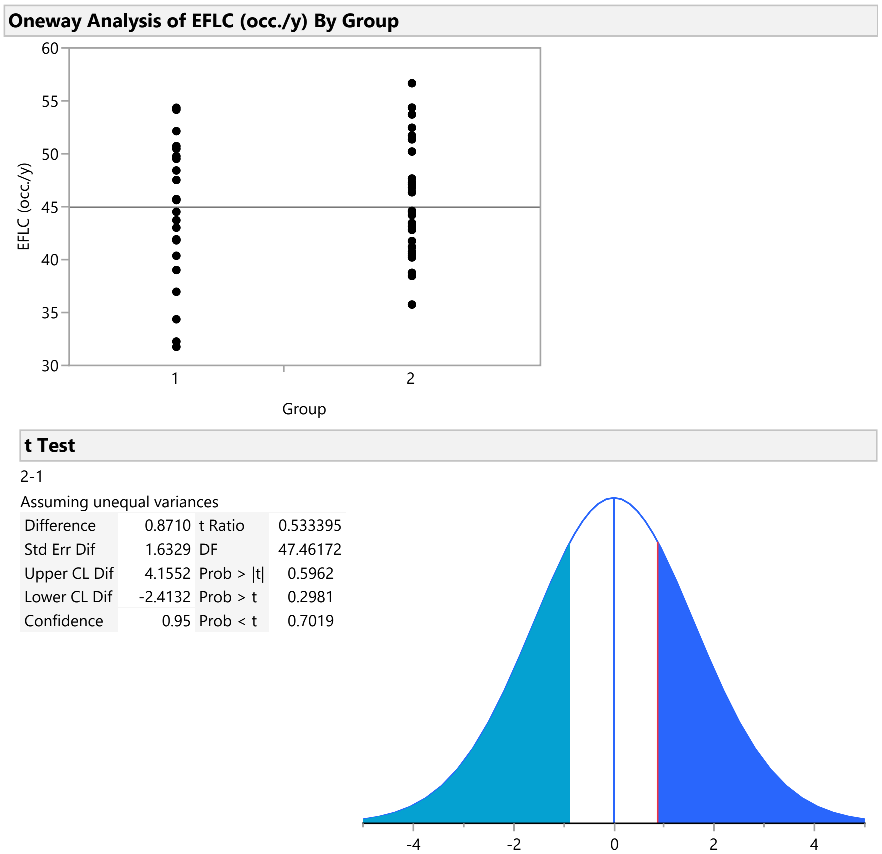

Figure 5.16 Expected frequency of load curtailment prob. distribution

5.6 Case study

The analysis is performed to evaluate and improve the case study customer reliability. To understand reliability, the evaluating metrics have to be determined while considering the relevance to the case study. *LOEE* and *LOLE* are designed to represent the reliability on the energy production side. However, the case study is based on one commercial customer. Therefore, *LOEE* and *LOLE* also represents customer reliability. *LOLE* expresses the outage hour's distribution that the customer will suffer throughout a full year.

5.6.1 Base case

The analyzed case study is for a small commercial load consumer. The peak load is 26 kW, with an average load consumption of 316 kWh/day. The initial system configuration consists of a 35 kW solar PV system, a 14 kWh ESS capacity and a 36 kW Diesel generator. Operation logic is centered on maximizing reliability and consuming the least amount of fuel. Hence, solar power produced is used to serve the load as a priority, then charging the battery. If solar power is not sufficient for this task, the battery discharges to meet the remaining load. Finally, if ESS capacity is at a depth of discharge (DoD) limit, the diesel generator is started.

For this study, the MTTF for the PV system, ESS, and diesel generator is estimated to be four, three, and a half years, respectively. The repair time for all components is also randomly generated with an MTTR of 10 days. Both MTTF and MTTR is following an exponential distribution. For the few first simulations, the CoV is very high due to the low number of years. The simulation proceeds and concludes when both indices achieve a CoV lower than 15%. Applying the base case to the proposed methodology, LOEE and LOLE are estimated to be 3548 kWh/y and 295 h/y. In proportion to the yearly consumption, the simulated microgrid supplied the load with a kWh shortage of 3% and an hour shortage of 3.2%. The outage events mostly occur due to the GS low MTTF. The generator is expected to fail twice a year in this study. During these events, renewable resources are not sufficient to cover the load.

A normal operation day for the MG is shown in Fig. 5.17. In the morning, the Battery SoC is at the DoD limit until the PV yield is more than the projected load. This simulation day represents a clear sky day, where the PV yield is sufficient to supply the load only at noontime. For the rest of the time, the GS unit is constantly complementing the PV system to cover the load requirements. GS is only at no load when ESS SoC is higher than DoD and, added to PV, is sufficient to supply the load.

In Fig. 5.18, a MG outage event is presented. An outage in the simulation represents a partial or complete insufficiency of the system to cover the load. The failure event that triggered this outage is a GS unit failure. This example shows an instance where the renewable generation is partially serving the load during a GS unavailability. In Case 1, the PV system is not designed to cover the load requirements individually. Hence, the energy generated is inadequate when the GS is undergoing maintenance. By analyzing different outage incidents in the simulation, the estimated reliability indices are mostly impacted by GS failure events, as shown in Fig. 3. The first step of the

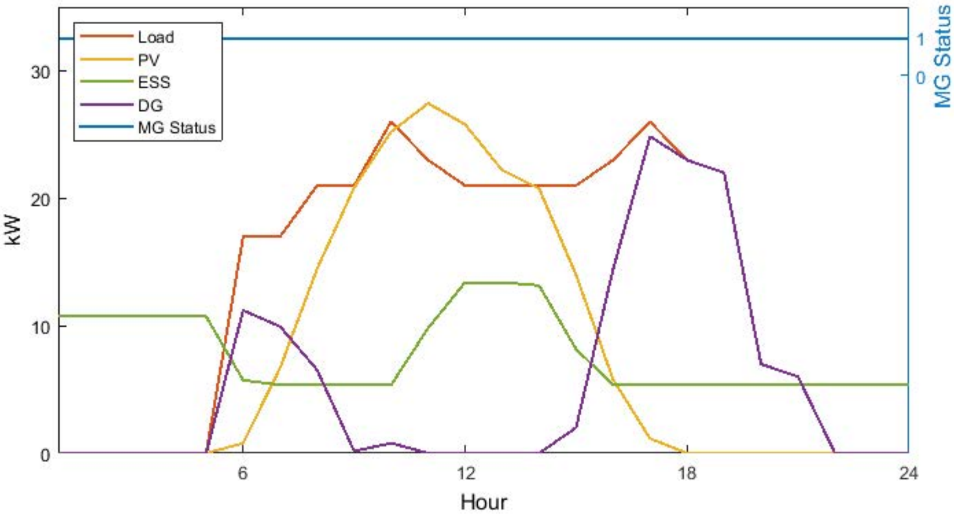

Figure 5.17 Base case healthy scenario

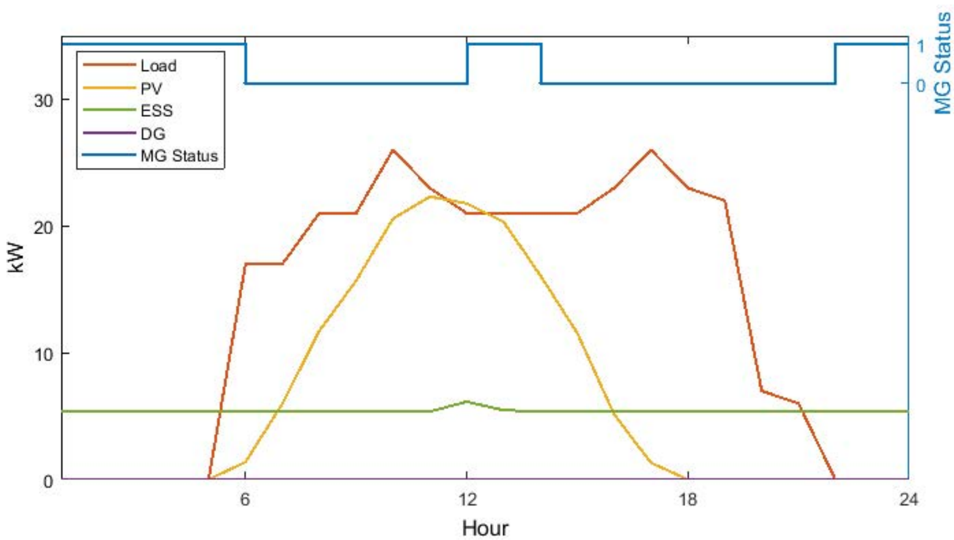

Figure 5.18 Case 1 outage scenario

economic analysis is to evaluate the costs associated with the base case scenario. Then, the results are compared to the suggested alternative systems. The economic metric is calculated following the assumptions presented in Table 5.3. While acknowledging the challenge of estimating the cost associated with outages, the cost of not serving shown is selected based on estimated average values in [41, 42], for small commercial cases.

5.6.2 100% renewable alternative

Case 2 explores the possibility of transforming a MG system to a full renewable solution. In this work, a 100% renewable alternative is analyzed to acquire a good understanding of the benefits and drawbacks of moving towards this solution. The base case is transformed into full renewable

Table 5.3 Base case inputs

Duration	Diesel cost	PV price	ESS price	GS price
15 years	\$1.5/L	\$2900/kW	\$560/kW	\$500/kW
MTTF$_{PV}$	**MTTF$_{ESS}$**	**MTTF$_{GS}$**	**MTTR**	**ENS Cost**
35,040h	26,200h	4,043h	100h	\$0.7/kWh

energy microgrid by eliminating the GS and modifying the PV and the storage system. To achieve Case 1 LOEE reliability level, the PV system is increased to 225 kW, and ESS is increased by a factor of 10. This system is designed to maintain a reliability level by delivering the same kilowatt-hours in the base case scenario. Results show that the proposed system leads to more outage hours and higher global costs. Fig. 5.19 shows that the 134 kWh storage system is depleted each night, one or two hours before expected consumption drops. On the following morning, the PV system fails to deliver the required power in the first hour the consumption picks up. For Case 1, the GS unit was responsible for delivering power mostly early in the day and late at night.

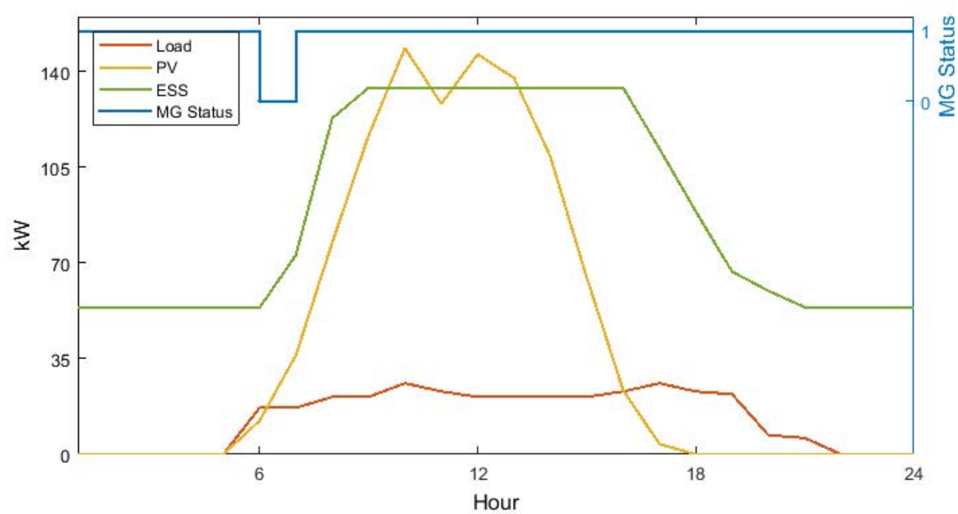

Figure 5.19 Case 2 outage scenario

In the next few steps of the study, the aim is to reduce the rise in global cost and maintain Case 1 number of outage hours. While ensuring to maintain a high penetration level, GS is reintroduced to improve the expected cost and outage hours resulted from Case 2. Fuel based units are implemented to minimize outage hours due to their ability to serve the load at times when renewable sources are scarce. To maintain a high penetration level, a smaller GS model is introduced. Adding a fuel-based unit is expected to minimize the necessary upgrade for PV and storage and subsequently, the global cost while leading to fewer outage hours than Case 2 results.

5.6.3 90% renewable alternative

In Case 3, the renewables target is reduced to 90%. By implementing an 18 kW GS unit, the PV and ESS requirements are reduced to 150 kW and 107.8 kWh, respectively. Fig. 5 illustrates a typical day of the year when the GS is available. In this scenario, PV and storage are sufficiently large to supply the load except in the beginning and the end of the day. In the early hours of the day, GS is coupled with PV to complement the required load. On the other hand, after sunset, the GS is combined with ESS to supply the load during the late-night hours. Unreliability occurring within Case 3 simulation is due to the same reasons illustrated in Case 2. However, unlike Case 2, these outage scenarios happen with a much lower frequency since GS is available most of the year.

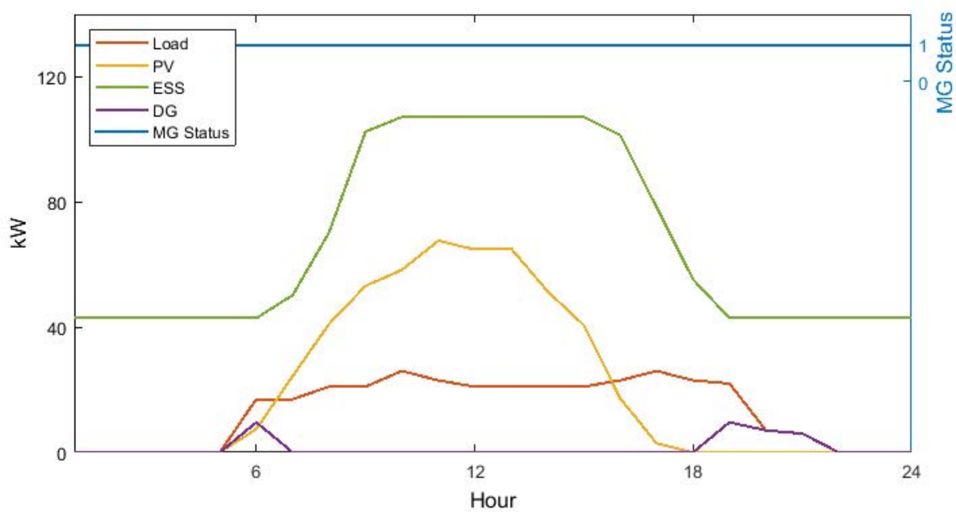

Figure 5.20 Case 3 healthy scenario

Case 3 configuration improves the reliability of the system significantly, as shown in Fig. 5.20. Not only the expected energy not served is dropped by 79% compared to Case 1 results, but also the loss of load hours is reduced by 59%. Since the target is to achieve a reasonable cost increase, Case 4 is designed to reach an 80% renewable penetration while maintaining the reliability targets.

5.6.4 80% renewable alternative

Following the base case manufacturer ratings, a one-step smaller diesel unit is selected. A 22.7 kW unit is paired with a PV and storage system. Subsequently, the PV and storage systems are reconfigured with an objective of 80% renewable penetration. The final system selected consists of a 125 kW PV system, coupled with 53.6 kWh storage capacity and backed up by the diesel genset unit. This system achieves a 79.31% penetration target. Compared to the base case results, the global cost has expectedly increased (by 61%), but the reliability levels have been improved for both metrics. The expected LOEE and LOLE are 1,350 kWh/y and 149 h/y, respectively. The energy not served is reduced by 62%, and the outage hours is dropped by 49.5%. From the results in Table 5.4, we can deduce that extreme renewable policies might result in infeasible and less reliable results. However, it is shown in Case 3 and 4 that the cost elevation can be limited while achieving a high reliability measure by selecting the proper configuration.

Table 5.4 Base case results

Case	PV (kW)	ESS (kW)	GS (kW)	Ren. Pen. %	Cost ($K)	LOEE (kWh/y)	LOLE (h/y)
1	35	5	36	56	343	3,548	295
2	225	50	0	100	754	3,367	493
3	150	40	18	90	615	743	120
4	125	20	22.7	80	552	1,350	149

Fig. 5.21 shows the net present cost associated with all the presented cases. Reliability metrics are presented in percentage of the yearly load consumption. A cost increase to at 160% of the initial value is a minimum requirement to achieve a renewable percentage higher than 80%. It is also essential to observe that the cost difference between the 90% and 100% cases is more than double the cost required to upgrade from 80% to 90% renewable-based system.

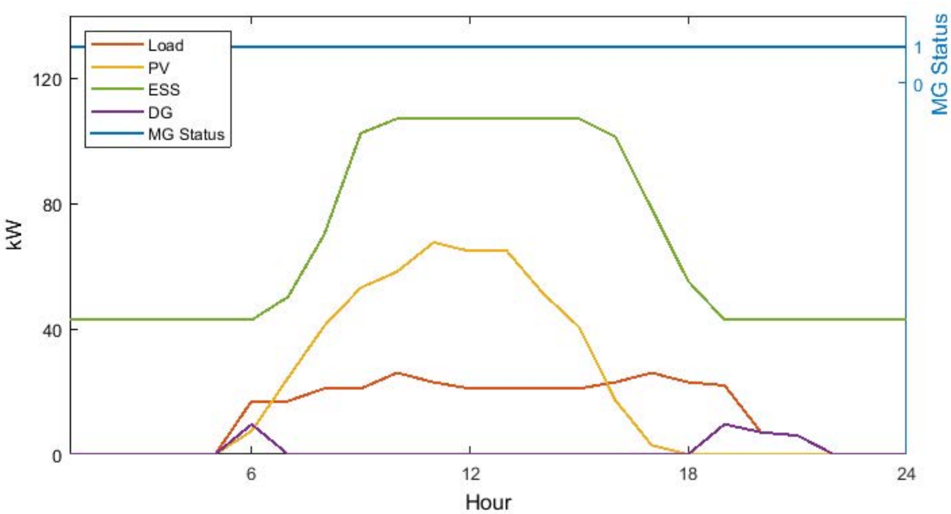

Figure 5.21 NPC vs renewable percentage

5.6.5 Conclusions

In this work, a comprehensive economic and reliability assessment is applied. It is shown that microgrid-sizing problem is a function of several factors such as desired renewable percentage, reliability target, and fuel cost. Sequential Monte Carlo modeling is developed to implement the reliability constraints built on the base case results. Microgrid component failure is accounted for by a statistical analysis performed within the SMCS algorithm. A microgrid supplies the base case with a total capacity of 100 kW. The global cost of this system is estimated to be $342,910. Case 2 is designed to achieve a 100% renewable level with a target to increase the renewable resources' percentage. Accordingly, the estimated cost is increased to 220% of the base case with a deterioration in the outage duration reliability metric, where LOLE is increased by 67% of the initial loss of load hours. By relaxing the renewable percentage requirement to 80% and 90% significant improvement in the reliability metrics is recorded, while minimizing the cost elevation to 161% and 180%. In conclusion, a 100% renewable target can be exponentially costly without achieving the desired reliability levels. On the other hand, MG systems in Case 3 and 4 do not only meet but also exceed the reliability targets. Therefore, the benefits associated with the last two cases' cost elevation is demonstrated in the genset hours of operation reduction and the reliability improvement.

CHAPTER

6

MICROGRID ECONOMIC SIZING USING PARTICLE SWARM OPTIMIZATION

6.1 Microgrid Planning

The island mode of a microgrid makes it an effective solution for improving the reliability of power systems. Microgrids are designed to operate off-grid in case it is more economical or a failure in the main distribution system takes place. On the other hand, the uncertainty of the DERs in a microgrid is challenging from the microgrid reliability point of view. For non-grid-connected microgrid systems, the risk is higher since a failure event could always mean a blackout. The first step to improve microgrid reliability is to look into evaluating and predicting microgrid reliability. Analysis can be done through historical data or by having an online system to analyze site measurements and assess the system conditions and reliability. Business developers and researchers investigate microgrids to improve a wide range of aspects related to the transmission and distribution grid. Microgrids are expected to cover a wide range of applications in addition to power delivery to homes, businesses, and industries. Moreover, the utilized distributed energy resources systems (DER) allow the possibility of increasing renewable energy penetration to meet low carbon policies. Microgrid developers aim to provide cost-effective and flexible solutions to meet customers with precise targets. The rising need for environmental solutions, by various organizations, creates a marketplace for distributed energy generation. Moreover, one of the essential MG functions is to maximize reliability and security to customers with critical loads.

Nevertheless, the economics of new unconventional technologies need to be analyzed, before implementation, to verify their value. Power systems are designed to operate for a long-term duration and meet the projected demands. Therefore, a life-cycle analysis is suited to evaluate MG systems. The analysis is based on determining the most cost-effective solutions with a group of competing alternatives, considering the project expected cash flows. In an LCCA, a design is compared to alternative solutions based on the project cash flows. LCCA can be performed in either constant dollars or present dollars, where a present value for life-cycle costs is produced [43]. The initial investment is represented in capital costs associated with the system components, while the future costs are the running costs associated with operation throughout the project duration.

Distributed systems planning and allocation is a classic optimization problem. Optimization techniques are selected based on the nature of the problem. In [44–47], linear programming approaches, such as MILP, are used to solve a power system placement and sizing problem. Furthermore, heuristic techniques have been recently popular as they are robust and offer near-optimal solutions for a complex system with non-linear constraints [48]. A high computational requirement is expected from these algorithms. However, requirements can be minimized by finding the proper model parameters. Particle Swarm optimization is a metaheuristic evolutionary computation technique developed by Kennedy and Eberhart to deal with highly non-linear constraints [49]. PSO is inspired by the collective intelligence of animals during a search process. PSO is based on the concept of recruiting a population of particles that mutates at each iteration to approach the optimal configuration. PSO can be used for distributed generation complex problems due to its flexibility to be integrated in hybrid frameworks. The work in [50] shows a population that is based on a stochastic process to find the optimal allocation for a distributed generation while considering reliability. PSO is used to run a techno-economic analysis for power system planning applications in [51–53].

This proposed framework is designed to support MG design in the preliminary phase. The developed assessment in Chapter 5 is used to estimate system reliability. The approach is integrated into an optimal sizing model to consider reliability as one problem variable. Moreover, the proposed work addresses the non-linear formulation of the sizing problem. Initial, replacement, operations, and maintenance costs associated with the MG project are included in an LCCA framework considering the rate of return. In this work, the state-of-the-art lies in the flexibility and the seamless reciprocity between the reliability assessment and the PSO algorithm. Moreover, the proposed work addresses the non-linear characteristics of estimating reliability and renewable percentage for a given MG system. While using a PSO heuristic approach with an acceptable computational effort requirement, the candidate system fitness is evaluated using LCC analysis. MG initial, replacement, operations, and maintenance costs are included in the analysis and estimated in terms of net present values.

6.2 The planning problem formulation

An optimal MG design must ensure a normal operation while meeting the load at a certain degree of reliability. While maximizing the use of the available renewable energy resources combined with an energy storage solution, GS are implemented to provide support to reach the expected level of reliability. The proposed approach is successful in finding an optimal system that strategically utilizes the system components. The planning process is executed by finding the best size of the renewable system, coupled with a group of optimally dispatched GS to reduce fuel costs and greenhouse gas (GHG) emissions. However, the optimal system is selected based on the cost performance concerning alternative solutions. Thus, the proposed framework, as shown in Fig. 6.1, is developed in this paper to support the long-term planning of MG and distributed systems.

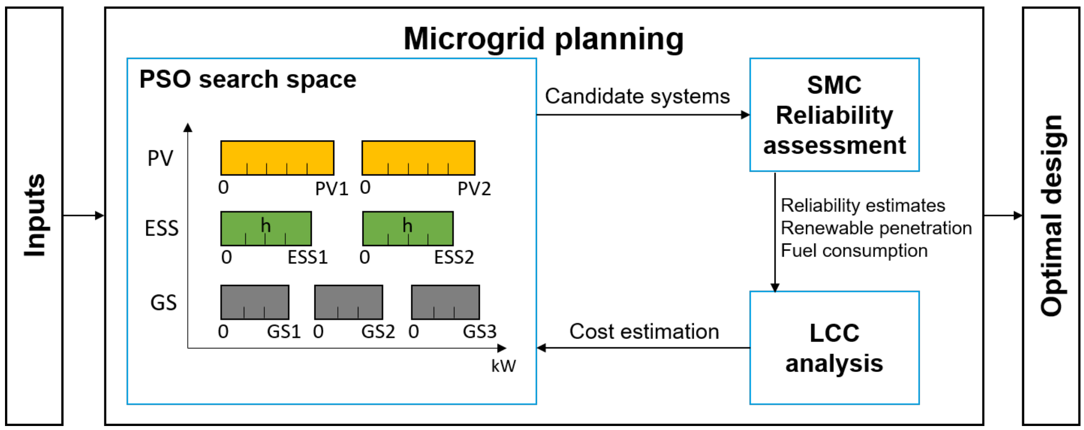

Figure 6.1 Microgrid planning framework

6.2.1 Cost minimization objective function

This cost of the proposed microgrid systems are evaluated considering the costs of the system through the service period. The optimal design benchmark is based on minimizing the life-cycle cost of the proposed system. An overall net present cost is estimated considering all the initial investments and the operating costs throughout the service period of the MG. The problem objective function is expressed in Eq. 6.1, *Minimize* cost of candidate system:

$$IC + \sum_{y=1}^{max} OC_y. \tag{6.1}$$

where IC is the initial capital investments, calculated by multiplying the system component sizes by the technology unit prices. IC represents the investments to acquire the system capacities at year 0. OC_y is the system operating cost at year y. Investment cost is expressed as in Eq. 6.2,

$$IC = \sum_{i=1}^{m} N_i \times C_i \tag{6.2}$$

where m is the number of components used, N is the component size in kW or kWh, depending on the technology, and C is the unit price for each component in \$ /kW or \$ /kWh. Operating cost is calculated for each year of the project duration as in Eq. 6.3

$$
\begin{aligned}
OC_y = \sum_{GS=1}^{G} (OM \times P \times h)_{GS} + FC \times \text{Fuel}_{GS} \\
+ (OM \times P)_{PV} + \sum_{i=1}^{m} (P \times UC \times RO)_i
\end{aligned}
\tag{6.3}
$$

where OM_{GS} is the operation and maintenance costs for generator sets in \$/kW-h, P is the size of the unit and h is the annual hours of operation. FC is the fuel cost in \$/gal multiplied the fuel annual consumption to calculate total fuel cost. $OM_{PV} is the$/kW-yr PV annual operation and maintenance cost as in [54], a function of the PV system size in kW. RO is the replacement operator for MG component i, with a value of 0 or 1 governed by the hours and years of operation counters. m is the number of components, P is the size of component i in kW and UC is the unit price for each component in \$/kW or \$/kWh. For the GSs, a replacement cost is implemented when the hours of operation representing life expectancy is reached. For renewable systems, a component is replaced after life expectancy years, while considering a warranty and augmentation costs for MW size systems. All future costs are represented as an annual negative cash flow in present-day dollars using a discount rate.

6.2.2 Reliability assessment and optimizer constraints

Component power limits and cycling state-of-charges are considered as in Eq. 6.4 and Eq. 6.5,

$$0 < P_i(t) < P \max_i \tag{6.4}$$

$$\text{SoCmin } < SoC(t) < SoC\text{max} \tag{6.5}$$

where $P(t)$ is the required power for component i at time t, Pmin and Pmax are the maximum and minimum design power loading. $SoC(t)$ is the battery state of charge at time t, *SoCmin* and *SoCmax* are the manufacturer-recommended cycling boundaries. The objective function is constrained by the power limits of the components, as in Eq. 6.4. Moreover, the energy storage system is limited by the manufacturer recommended maximum State-of-Charge *SoC* and the depth of discharge *DoD*, shown in Eq. 6.5.

Reliability and renewable metrics are estimated using SMC assessment. An enormous cost is implemented when the system fails to meet the reliability or renewable targets. The large penalty guarantees that the optimizer will reject and improve the candidate configurations that violated any of the targets. Targets are implemented in the cost estimation problem as a fitness indicator shown in Eq. 6.6,

$$\left(Target - Achieved\right) \times \text{Penalty} \tag{6.6}$$

where the achieved energy adequacy, time availability, and renewable percent are compared to the required targets. The penalty is the cost value that ensures the rejection of configurations that violated the target. The availability of components and the reliability target for a given case is taken into account. All the constraints except for the reliability target are implemented in the SMC operation and reliability assessment to be included in the system simulation. The reliability target non-linear constraint depends on the simulation of microgrid operation and components' availability. Therefore, this constraint is added to the cost function as a penalty term, as in Eq. 6.6. If the reliability indices are lower than the preset threshold, the cost function is highly penalized, which ensures that the optimizer will reject or modify the configuration associated with such behavior.

The search space boundaries are individually implemented in the optimizer for each component, considering case preferences and physical space limitations. Low and high bounds are required for the components to initialize the optimization algorithm. The low bound is usually set to zero unless a specific technology capacity preexists or is required in the design. The last constraint is the search space associated with the optimizer. A search space for each microgrid component has to be determined based on the project budget cap or physical space limitations. The optimizer requires a lower bound (LB) and higher bound (HB) for each unit considered in the design. The lower bound can be set as a non-zero value when a minimum size for technology is required in the configuration, which ensures a minimum size in the search space for this technology.

6.3 Applying the sequential reliability assessment

The long-term simulation is performed to represent the microgrid normal and abnormal operation states. The objective of the developed SMC model is to analyze the performance of the studied system and its availability to serve the load compared to the project reliability targets. For each analyzed configuration by the optimizer, a reliability assessment is performed. The number of simulations is based on comparing the reliability indices to mean value of failure and repair, as in Fig. 6.2. The failure and repair events are randomly generated using the assigned probability distribution, and the mean values deducted from historical datasets.

The MG components are dispatched based on the designated logic, and the MG failure is tested throughout the simulation, as in Fig. 6.3 and 6.4. This case shows that a MG can fail to satisfy the load even when all components are normally operating. Similar outages are expected when the design is not made for a 100% reliability target. In contrast, a failure may occur due to physical failure of components such as in Fig. 6.5. Unless one of the gensets fails, the dispatch works in normal operation where PV and a primary GS unit works to serve the load while having the backup unit to operate for few hours at the end of the day as in Fig. 6.6. At each simulation trial, the microgrid system availability is evaluated by considering components' availability and the degree to serve the loads based on the designed operation logic. The overall reliability of the system is evaluated using energy and time availability formulas as in Eq. 5.12, Eq. 5.13. The assessment can be illustrated as in Fig. 6.7

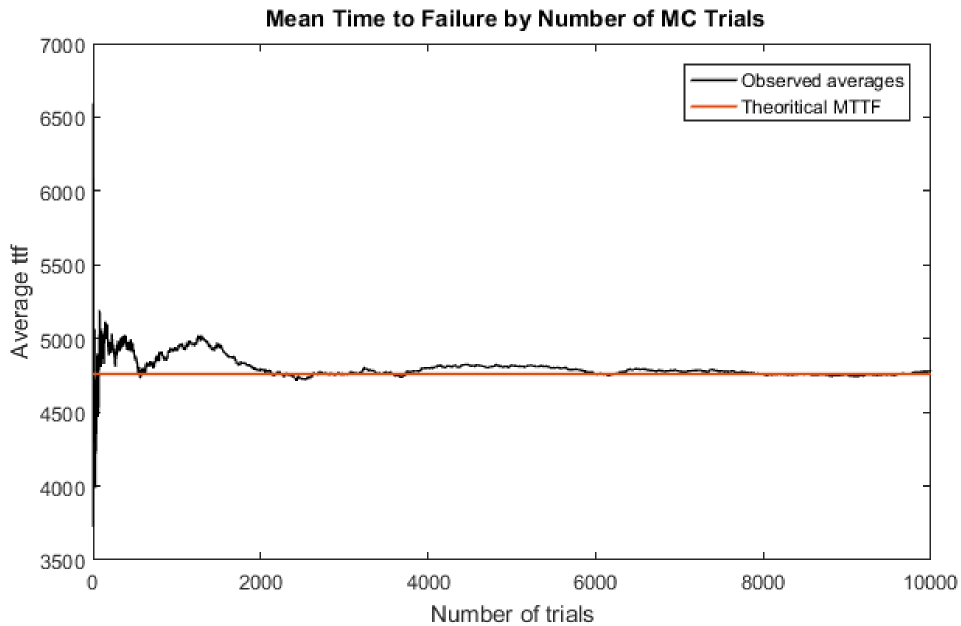

Figure 6.2 Mean time to failure by number of MC trials

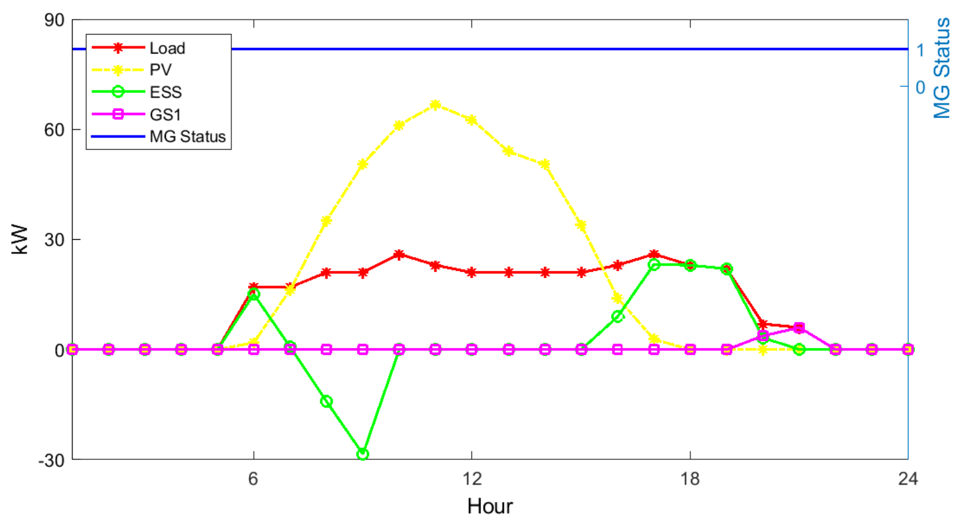

Figure 6.3 PV+ESS+GS case normal operation example

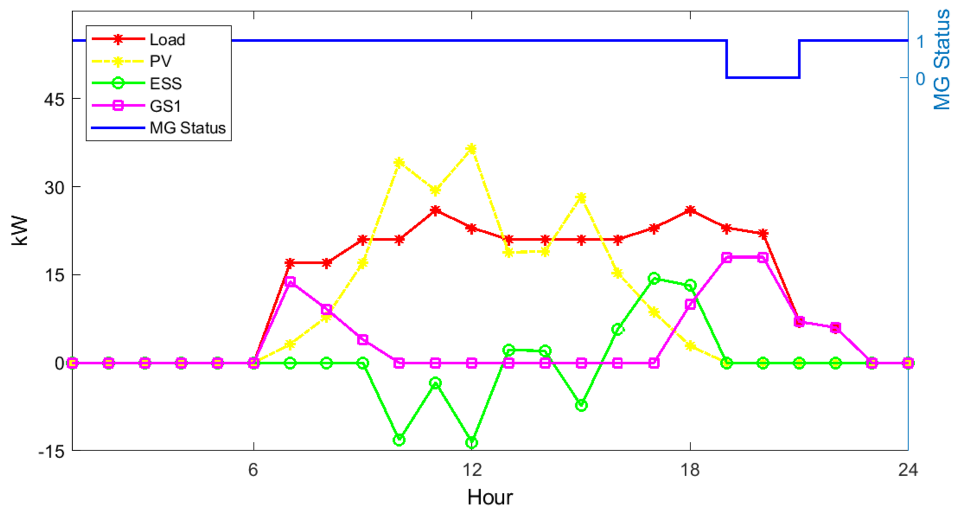

Figure 6.4 PV+ESS+GS contingencty scenario

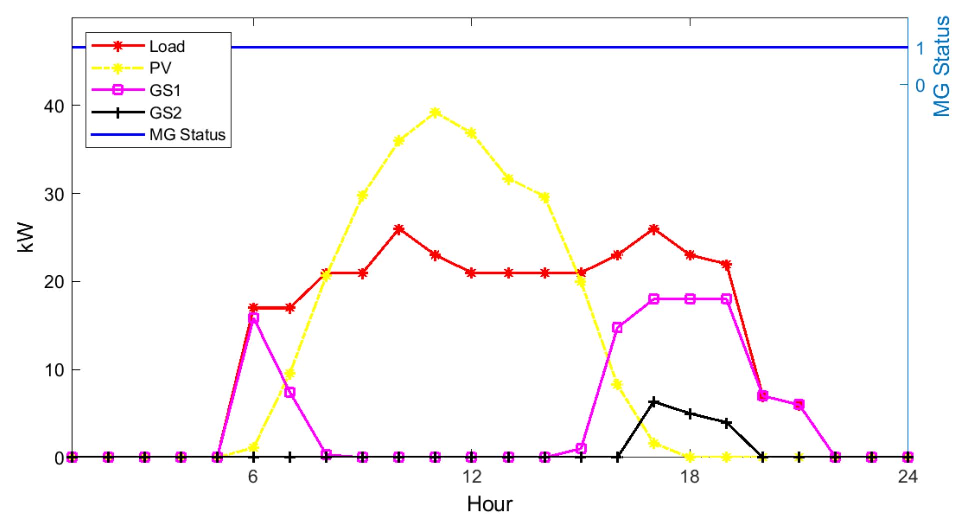

Figure 6.5 PV+2GS normal operation example

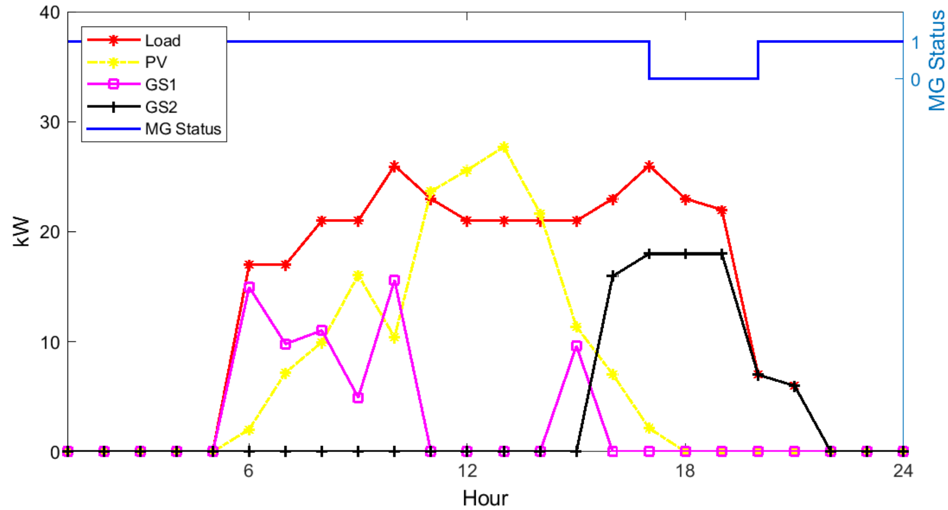

Figure 6.6 PV+2GS contingency scenario

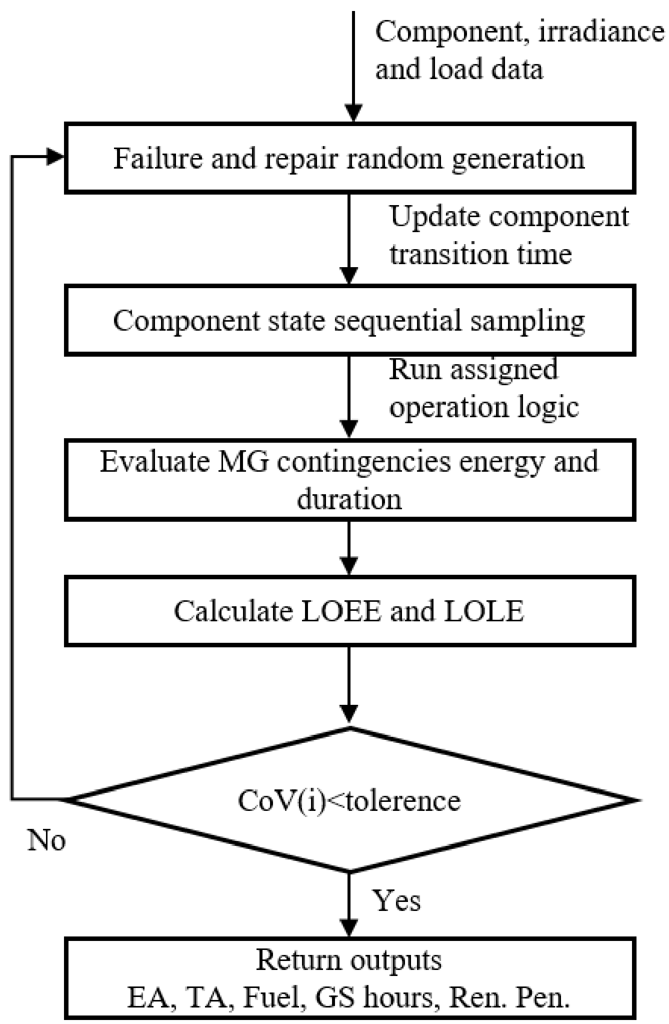

Figure 6.7 Reliability assessment flow chart

6.4 Particle swarm optimization

Particle swarm optimization is utilized to recalibrate the employed particles at every iteration sweeping the search area to narrow down the best system location in the search space. PSO allows implementing non-linear constraints that require long-term simulations to be estimated. Despite starting with a randomly generated population, it reaches the optimal configuration after several runs. Fig. 6.8 shows the optimization algorithm steps, while also representing the optimizerś communication with the reliability assessment simulation and the cost estimator. The required computational effort is minimized through parameters' calibration and a customized search agent for each run.

The initial population is generated using Eq. 6.7,

$$P_{i,j} = LL + rand(s,n) \times (UL - LL) \tag{6.7}$$

where $P_{i,j}$ is the population at iteration i of run j is initialized at each run using the population size s ,the number of variables n, representing the used technologies and components, and the boundaries LL and UL.The lower boundaries are set to zero, and the upper boundaries are selected based on the available surface area. The number of particles is selected empirically to represent the least number of systems that achieve the performance requirements. To improve the efficiency of the search process, the search space is broken into several segments. These search segments are distributed between the runs to cut down the execution time. The final best configuration is determined by comparing the best configurations in all the runs.

The chart in Fig. 6.8 illustrates an optimization algorithm that takes into account the optimizer's interaction with the reliability assessment and the cost function models. The algorithm starts with generating a certain number of random configurations together called a population. Each MG configuration (particle) is evaluated by the reliability assessment and the cost estimator to indicate particle fitness and cost-effectiveness. At each iteration, the most cost-effective particle is tagged as the global best *gbest* of the run. The position of particles is then updated based on the velocity v, as in Eq. 6.8,

$$\begin{aligned} v =& w \times v_{i-1} + c1 \times r\,\mathrm{cond}(s,n) \times (\mathrm{pbest} - p) \\ &+ c2 \times \mathrm{rand}(s,n) \times (\mathrm{gbest} - p) \end{aligned} \tag{6.8}$$

where v is the velocity of each particle, where w is the inertial weight of the current iteration, v_{i-1} is the previous iteration velocity, $mlipbest$ is the particle personal best so far and *gbest* is the run global best. $C1$ and $C2$ are the acceleration factors governing $mlipbest$ and *gbest* weights, influence, to update the population as in Eq. 6.9,

$$P_{i,j} = \begin{cases} LL & P_{i-1,j} + v < LL \\ P_{i-1,j} + v & LL < P_{i-1,j} + v < UL \\ UL & P_{i-1,j} + v > UL \end{cases} \tag{6.9}$$

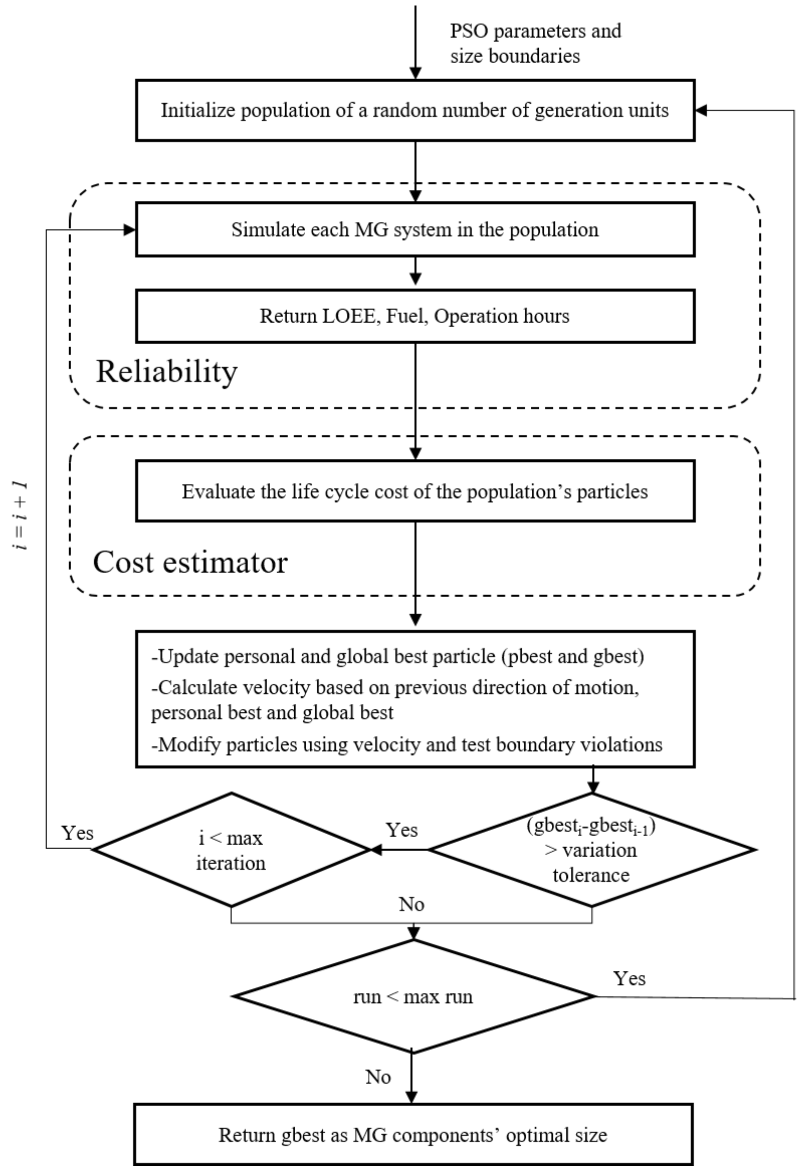

Figure 6.8 PSO optimizer flow chart

where the particles are updated by adding the current iteration associated velocity and maintaining the assigned boundaries for each component. This population position is moved for a number of iterations before the tolerance level is met. The run is concluded to determine the most cost-effective configuration for the run. To maximize accuracy, the described process is repeated for a number of runs to scan different areas of the search space. Finally, the best particle in all runs is proposed as the optimal power mix. To evaluate the model performance, the results are compared to different alternatives based on their net present cost. The criterion of choosing the optimizerś parameters is based on achieving an acceptable accuracy using the least computational time.

6.5 Methodology steps demonstration

The steps of the proposed framework are further illustrated by employing the methodology to find the optimal mix that meets a set of requirements. In this section, the selection of the optimal system is driven by the cost-effectiveness objective. The demonstrative example is utilized in Section VI as a base case to apply further analyses, where the influence of the major driving costs and implementing precise targets are presented.

6.5.1 Case study initialization

A small commercial load, with a poor-reliability interconnection to the utility grid, is tested in the reference example. The demand is characterized by a 26kW peak load and an average daily consumption of 316 kWh. Due to the grid status at the studied location, the MG system is designed to operate in islanded mode and meet the load demand year-round. The designed system is intended to meet the load using the available solar resources and battery system, before needing to start the primary genset unit. A secondary unit is considered to provide a redundancy approach for high-reliability purposes. To estimate the project costs, the economic assumptions in Table 6.1 are considered for the analysis. Component failure and repair data are based on assessments in [19, 23, 26, 27].

Table 6.1 Base case economic inputs

Duration	**Interest rate**	**Adequacy target**	**PV price**	**ESS price**	**GS price**	**PV O&M**
20 years	6%	100%	\$2200/kW	\$600/kW	\$500/kW	\$55/kW-y
GS O&M	**Fuel cost**	**MTTF$_{PV}$**	**MTTF$_{ESS}$**	**MTTF$_{GS}$**	**MTTR**	**Dist**
\$0.02/kW-h	\$3.3/gal	35,040h	26,200h	4,043h	100h	Expo.

The average yearly value for the PV O&M cost is set as \$ 55/kW-yr. Generators O&M is set to be \$ 0.02/kW-hr, where the total GS O&M is determined based on the hour of operation and the loading. Replacement cost for the generators is based on the hour of operation with a maximum of 10,000 hours before replacement. For renewable resources, the PV system and the energy storage system are replaced after 25 and 10 years, respectively. The unit steps for the PV, ESS, and GS are 5kW, 5kW (2.8h), and 18kW with search boundaries between 0:25, 0:20, and 0:2 respectively. Unit steps are calculated based on the unit cost of each component to achieve near equal-cost increments. The search process is initialized by generating a random population of thirty mixed generation systems,

$P_{0,1}$, where the rows represent thirty candidate MG systems and each column indicates the size of its component as in Table 6.2

Table 6.2 Initial population

Particle	**PV (5kW)**	**ESS (5kW)**	**GS1 (18kW)**	**GS2 (18kW)**
1	12	4	2	1
2	14	0	1	1
3	2	1	2	2
4	14	0	2	2
5	9	0	2	2
6	1	4	2	1
7	4	3	2	2
8	8	2	1	1
9	14	5	1	1
10	14	0	1	1
11	2	2	2	1
12	15	2	1	2
13	14	4	2	1
14	7	4	1	2
15	12	1	2	1
16	2	2	1	2
17	6	2	1	1
18	14	3	1	2
19	12	4	2	2
20	14	4	1	2
21	10	1	1	1
22	1	3	2	1
23	13	3	2	1
24	14	1	2	2
25	10	1	2	1
26	11	2	1	2
27	11	5	2	2
28	6	2	2	2
29	10	3	1	1
30	3	1	2	1

6.5.2 Candidate systems reliability assessment

As shown in Fig. 6.1, the random population is directly called by the reliability assessment function in the first iteration. For every particle, the operation of the system is simulated for the adequate number of trials to evaluate their capability to meet the demand and estimate the system's annual environmental and economic measures. Particle 19, in P0, consists of a 60kW PV capacity, 20kW ESS, and two 36kW GSs. Particle 19 reliability assessment resulted in a *LOEE* of 0 kWh/y and *LOLE* of 0h/y.

The simulation first random failure generation resulted in a minimum time to failure of 4240h, associated with the primary GS. By using Eq. 5.4, Eq. 5.5, Eq. 5.6 and Eq. 5.7, the simulation time is advanced. The operation, between the simulation time t0 and t1, is assessed by evaluating the system states. Components states are used to estimate the available power at each hour, and the battery logic is applied to utilize available capacities efficiently. Component's scheduled power and the required demand are compared to evaluate the microgrid reliability. Load curtailment events are recorded with details for the *ENS* and *LLD* values to be averaged on an annual basis and recorded as *LOEE* and *LOLE*.

The next simulation trial starts using the updated times, where a new failure event is randomly generated for the primary GS, and the time to the next transition is updated for the rest of the components. The same steps, to estimate *LOEE* and *LOLE*, are repeated. To prevent an early termination, the convergence criteria, *CoV* for *LOEE* and *LOLE*, are initially evaluated after l00 simulation trials. At each trial, *LOEE* and *LOLE* is calculated from the beginning of the simulation, t_0, to the end of the trial period, t_N.

Once the simulation meets the convergence criteria, availability and energy adequacy are estimated using Eq. 5.12 and Eq. 5.13. Moreover, the GS operation is evaluated based on the simulation results, for each unit, to estimate their annual performances. Fuel consumption, the number of operation hours, and the loading values are annually estimated. Subsequently, the renewable penetration is calculated by comparing the GSs total generated power to the annual demand as in Eq. 5.14. For this first optimization trial, the best system achieves a renewable percentage of 65% by consuming 4,974 gallons of fuel annually. The GSs expected annual operation hours are 2988h and 188h

6.5.3 Optimizer search process

After assessing the population reliability and estimating the required indices, the cost of each system in the population is evaluated using LCC function shown in Eq. 6.1, Eq. 6.2 and Eq. 6.3. Particle 19 attains the minimum LCC, as shown in Table 6.3.

By showing the initial population performance, it is observed that the estimated *LCC* varies significantly. The extremely high-cost value, in Particles 1 and 30, is a result of the large penalty assigned for violating the objectives. However, these values will disappear when the optimizer learns, through imposing high inertial velocities, to avoid the associated system structures. To progress to the next iteration, the velocity is calculated using Eq. 6.8, where the initial values for the velocity, pbest and gbest are set as 0.1P0, P0, and P0(15), respectively. The population is then updated using the calculated velocity and applying search boundaries as in Eq. 6.9. The population is again called by the reliability assessment function, followed by the cost estimation procedure

Table 6.3 Cost function for initial population

Part. #	LLC ($K)
1	293530
2	549690
3	640
4	500
5	540
6	443590
7	640
8	554100
9	534450
10	549690
11	766780
12	245460
13	291820
14	255220
15	298340
16	734570
17	573580
18	246570
19	490
20	271610
21	550140
22	443580
23	294430
24	500
25	298720
26	280350
27	510
28	620
29	548240
30	526310

using the assessment results along with the population size. At the sixth iteration of the second run, the optimizer terminates with Particle 18, achieving the overall best result, as shown in Table 6.4. It is also shown that the cost estimates converge to reasonable values with smaller differences, indicating no violations. Table 6.5 shows the transitions for the optimal candidate system. The final system consists of a 105kW PV system, a 65kW storage system, and two 18 kW GSs.

Table 6.4 Final population

Part. #	**PV (5kW)**	**ESS (5kW)**	**GS1 (18kW)**	**GS2 (18kW)**	**LLC ($K)**
1	21	14	1	1	459
2	22	10	1	1	471
3	20	19	1	1	508
4	22	15	1	1	481
5	21	15	1	1	470
6	20	20	1	1	520
7	22	20	0	1	68883
8	23	15	1	1	493
9	21	15	1	1	470
10	21	12	1	1	456
11	20	16	1	1	472
12	21	12	1	1	456
13	22	16	1	0	81089
14	21	12	1	1	456
15	21	13	1	1	454
16	23	16	0	1	70402
17	21	12	1	1	456
18	21	13	1	1	454
19	25	18	1	0	68461
20	23	15	1	1	493
21	21	11	1	1	458
22	22	20	0	1	68883
23	20	19	1	1	508
24	22	18	1	1	518
25	24	20	0	1	68465
26	21	15	1	1	470
27	22	13	1	1	462
28	24	18	1	0	68463
29	24	18	1	0	68463
30	21	13	1	1	454

Table 6.5 Candidate system evolution through a full search process

run	Iteration	Part. #	PV (kW)	ESS (kW)	GS1 (kW)	GS2 (kW)	LLC ($K)	EA (%)	Ren. (%)
1	1	19	60	20	36	36	490	100	64.51
1	2	4	70	25	36	36	488	100	68.97
2	1	21	100	75	18	18	461	100	98.31
2	6	15	105	65	18	18	454	100	97.57

6.6 Further sensitivity analysis

The presented analyses show a practical methodology to analyze the major driving costs and the economic trade-offs influencing the value of a microgrid system. By applying variations on unit prices, the trade-off between initial investments spent on renewable systems and operation cost mainly associated with fuel consumption is assessed. Besides, the ESS size impact on the avoided operating cost is presented. Also, the benefits of assigning reliability and renewable objectives are presented, by evaluating the design economics for high levels of reliability and renewables. Availability and adequacy targets are implemented and the candidate systems fitness, by comparing the SMC assessment results to the imposed targets. Finally, renewable targets are tested at various reliability levels, and the resulting systems are discussed.

6.6.1 investment and running cost trade-off

The size of initial investments, on renewables, has a significant impact on the operating cost during the system service period. In this subsection, the impact of renewables' unit prices, including ESS, on the total life cycle cost is studied. In addition, the effect of renewable expansion on the economic and environmental returns is shown by fixing a technology size while finding the optimal system.

6.6.1.1 Renewables investment capital

Despite the relative maturity of PV technology, variability in system unit price is expected while developing solar projects. The uncertainty is not only associated with panels and balance of system varying prices, but with renewable policies and incentives, such as investment tax credits (ITC), as well. This analysis would allow a solar developer to estimate the impact of future forecasted incentives and the maximum PV price that guarantee viability for a given location. Energy storage system's price is expected to fall with the continuous development of technology and manufacturing capability. The Cost-effectiveness of energy storage systems depends on various economic and engineering factors. Moreover, the growth of manufacturing volumes of specific technologies, such as lithium-ion batteries, promotes the reduction of the unit price [55, 56]. Thus, it is necessary to analyze the impact of the anticipated ESS cost on a MG system configuration and total cost. Fig.

6.9 and 6.10 show the results for PV and ESS prices between $1.7-5.2/W and $200-1000/kWh. The impact of varying these prices on the LCC and the renewable penetration is shown, where a major change in the penetration represents a change in the system structure.

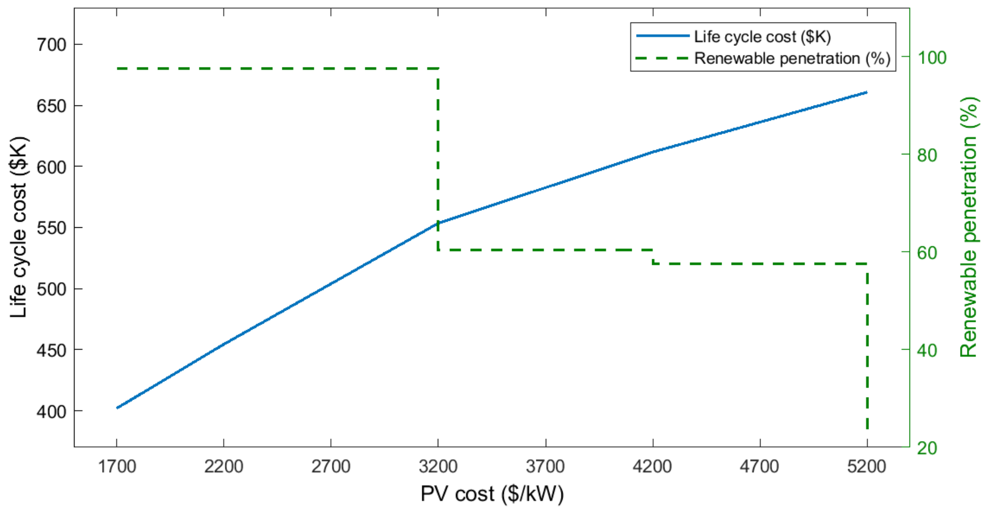

Figure 6.9 PV unit price vs. total cost/renewable penetration

The results show the pattern of upgrading the GS sizes at a given PV price, $3.2/W. This behavior is expressed in Fig. 6.9 by a major drop in renewable percentage. At this price point, the solar PV component transitions from a large primary power system to a small capacity with a fuel reduction objective. As shown in Table 6.6, the LCC rate of change is reduced while increasing the PV unit price beyond $3.2/W, which is due to the significant reduction of the PV system size at these high prices.

Table 6.6 Microgrid systems for various PV prices

Case	PV price ($/W)	PV (kW)	ESS (kW)	GS1 (kW)	GS2 (kW)	LLC ($K)	Δ LLC (%)
1.1	1.7	105	65	18	18	454	-11.55
1.2	2.2	105	65	18	18	454	0
1.3	3.2	60	15	36	36	554	21.8
1.4	4.2	55	15	36	36	612	34.61
1.5	5.2	20	0	36	36	661	45.4

Fig. 6.10 shows that decreasing the ESS price below the base price results in a major LCC reduc-

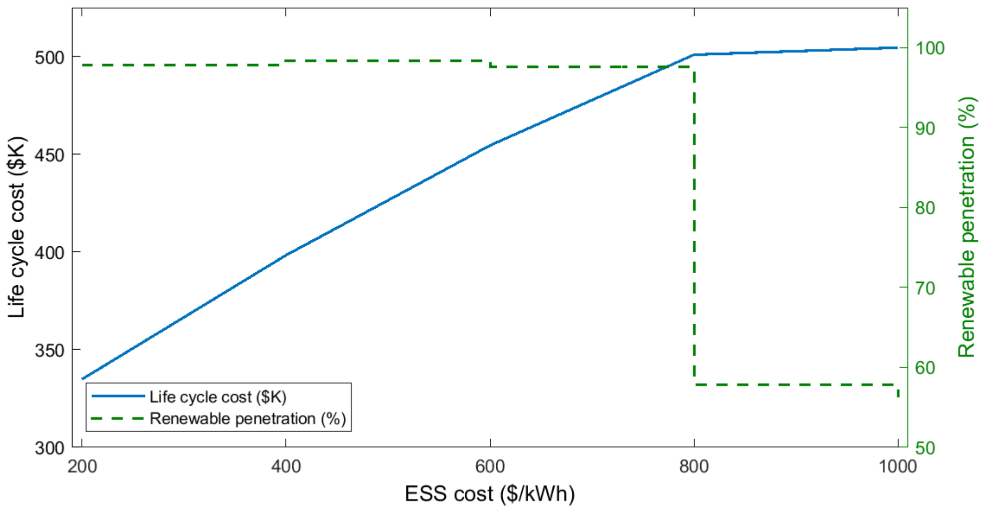

Figure 6.10 ESS unit price vs. total cost/renewable penetration

tion. However, increasing the ESS price leads to a minimum renewable percentage of 50% since a large PV system is still a viable choice. Table 6.7 shows that reducing ESS unit price $200/kWh results in eliminating one-quarter of the project cost. The influence of ESS size on the total and the operating cost is investigated to help determine the ESS viable range of sizes.

Table 6.7 Microgrid systems for various ESS prices

Case	ESS price ($/kWh)	PV (kW)	ESS (kW)	GS1 (kW)	GS2 (kW)	LLC ($K)	Δ LLC (%)
2.1	200	95	85	18	18	335	-26.32
2.2	400	100	75	18	18	398	-12.36
2.3	600	105	65	18	18	454	0
2.4	800	65	5	36	36	501	10.22
2.5	1000	70	0	36	36	505	11.01

Fig. 6.11 shows an expansion analysis for energy storage. Using the base case parameters, the size of ESS is set to a fixed value while searching for the optimal MG system. The high operating cost, caused by fuel consumption, is significantly reduced by upgrading ESS size to 50-75kW. This reduction plateaus beyond this size range. Assuming a DC-coupled system, the solar-battery ratio of the described range is 2.1-1.33.

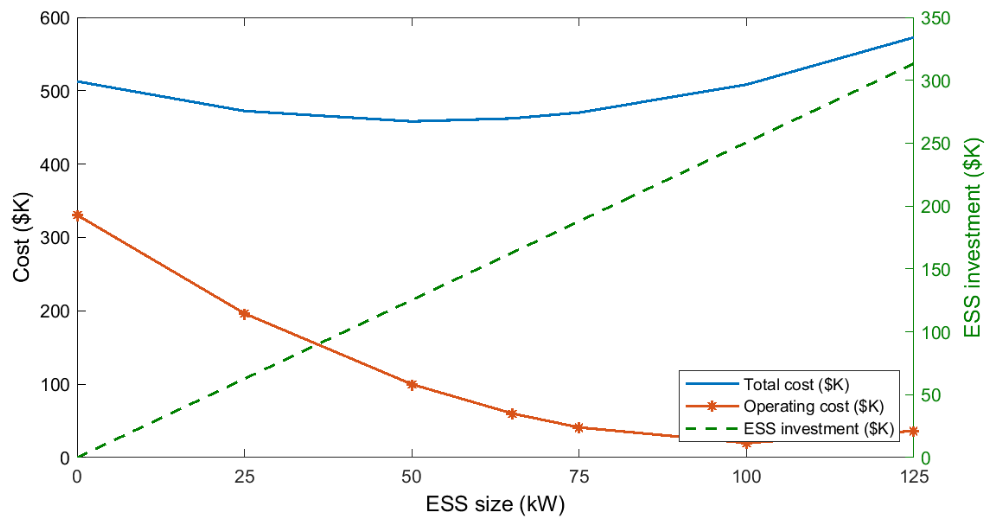

Figure 6.11 ESS size vs. project costs

6.6.1.2 Fuel cost

Fuel consumption typically represents the largest proportion of a MG operating cost. Thus, it is found essential to assess the impact of the fuel price variations on LCC. Based on the availability and the technology preference, the type of fuel is indicated. The fuel price is then estimated for the case study location. In this analysis, the base case price of diesel, \$3/gal, is varied by ±\$2.

Table 6.8 Microgrid systems for various fuel prices

Case	Fuel price (\$/gal)	PV (kW)	ESS (kW)	GS1 (kW)	GS2(kW)	LLC (\$K)	Δ LLC (%)
3.1	1	5	0	36	36	349	-23.21
3.2	1.5	60	5	36	36	391	-13.92
3.3	2	105	5	36	36	427	-6.1
3.4	3	100	65	18	18	454	0
3.5	5	100	75	18	18	466	2.57

It is shown in Table 6.8 that low fuel prices promote GSs based systems. Since fuel consumption is the main contributor in the operating cost, the total cost reduction can be significant, considering a high fuel accessibility precursor. On the other hand, it is shown that increasing the fuel price above \$3/gal leads to an insignificant change in LCC, given that the GSs operation is already restricted at the base price. Fig. 6.12 illustrates the minimum fuel price required to promote high renewable systems for a given case.

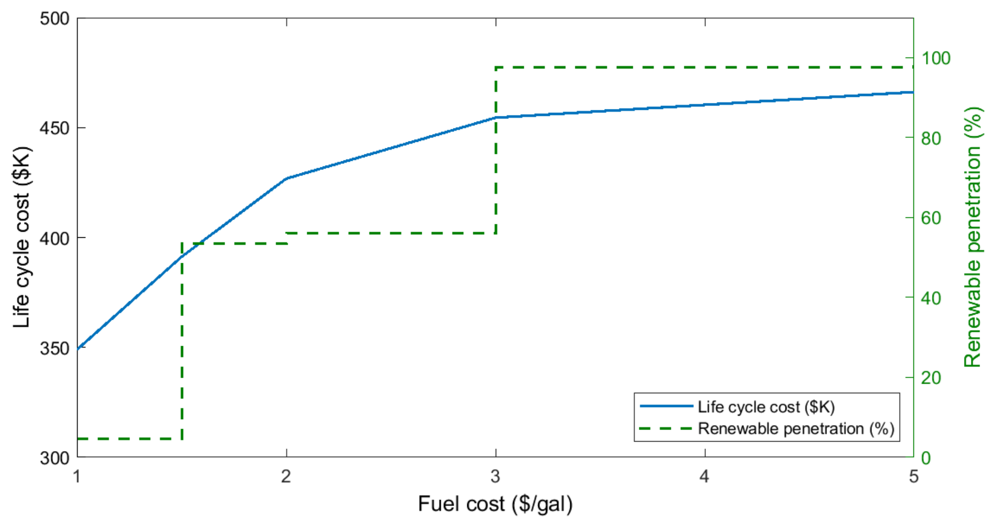

Figure 6.12 Fuel unit price vs. total cost/renewable penetration

6.6.2 Reliability targets and total cost trade-off

A Microgrid system can be designed to achieve high-reliability numbers. While designing the system, it is found beneficial to estimate the cost associated with various high-reliability levels. The objective to achieve six nines, 99.9999%, reliability leads to oversized and redundant components. In this subsection, the proposed method is utilized to investigate different reliability targets for the base case. Through performing an economic analysis for various system availability and energy adequacy levels, the algorithm provides a group of candidate solutions. The time and energy metrics estimated by the SMC assessment provides a dual perspective for the developers and the customers, helping in making planning decisions. Table 6.9 shows the outage minutes representing various system availability annual percentage.

Table 6.9 Availability outage time

Availability (%h)	Outage time (min)
99	5256
99.5	2628
99.9	525
99.99	52.5
99.999	5.2
99.9999	0.5
100	0

6.6.2.1 System availability

In the proposed methodology, the reliability constraint can be specifically indicated. In this section, availability targets, between 95-99.999%, are imposed. Table 6.10 proposes a group of solutions for the user, where MG is designed to achieve various reliability levels. Results show that LCC decreases by 12% when the target is reduced to 95%. However, a high-reliability target such as 99.5% reduces the cost by 6%. This analysis enables for exploring more cost-effective solutions for cases where a reasonable number of load curtailment events is acceptable.

Table 6.10 Optimal designs for various availability targets

Case	Availability target (%h)	PV (kW)	ESS (kW)	GS1 (kW)	GS2(kW)	TA (%h)	Δ LLC (%)
4.1	95	75	40	18	0	95.478	-11.66
4.2	97	80	45	18	0	97.496	-9.46
4.3	99	70	25	18	18	99.141	-7.23
4.4	99.5	75	40	18	18	99.677	-6.27
4.5	99.9	85	55	18	18	99.937	-4.47
4.6	99.99	95	60	18	18	99.992	-2.79
4.7	99.999	105	65	18	18	100	0

The main objective of the sensitivity analysis is to rank the model inputs by the required level of precision to obtain the most accurate outcomes. The analyzed inputs in this section are the discount rate, project duration, fuel cost, unreliability cost, PV unit cost, ESS unit cost, GS unit cost, and the required reliability target. The base case input values, in Table 6.1, are used for the rest of the inputs while assessing each input.

Fig. 6.13 shows a comparison between designs with different reliability levels with respect to influence on LCC and renewable percentage. The fluctuation in renewable percentage occurs due to the higher viability of increasing the renewable capacity compared to upgrading and operating GSs until a GS upgrade is required to meet the reliability target. The proposed reliability analysis shows renewable penetration for the most cost-effective solutions at various reliability levels, which can help in making renewable-reliability trade-off decisions

6.6.2.2 Energy adequacy

The next step is assessing the impact of varying energy adequacy targets on the optimal configuration and project economics. The system reliability is evaluated based on the served energy proportion of the total load. The trend is shown in Fig. 6.14 and Table 6.11 is similar to the previous analysis with a few more solutions to explore. The pattern of a high LCC elevation associated with levels over 99%

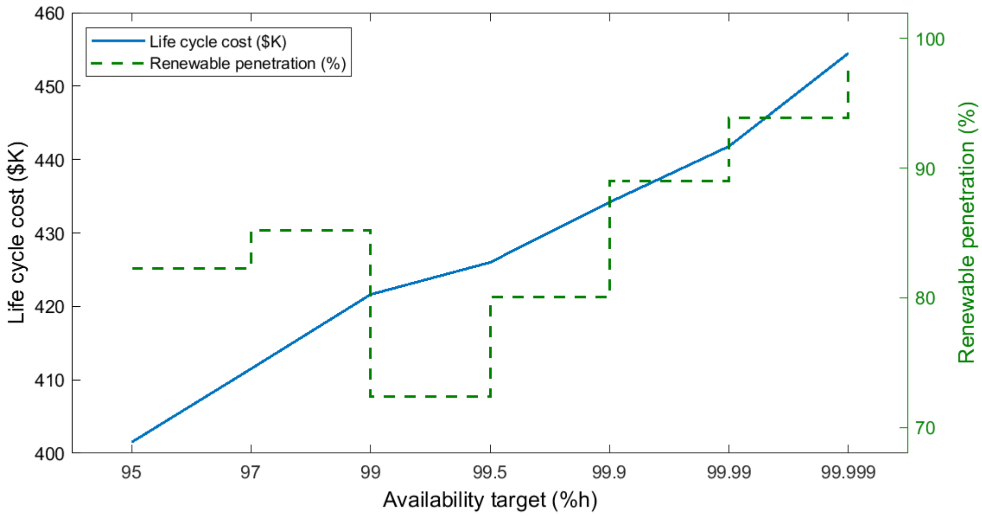

Figure 6.13 System availability vs. total cost

is repeated. Fig. 6.15 illustrates the changes in system structure, such as adding a secondary GS at 99.5% target.

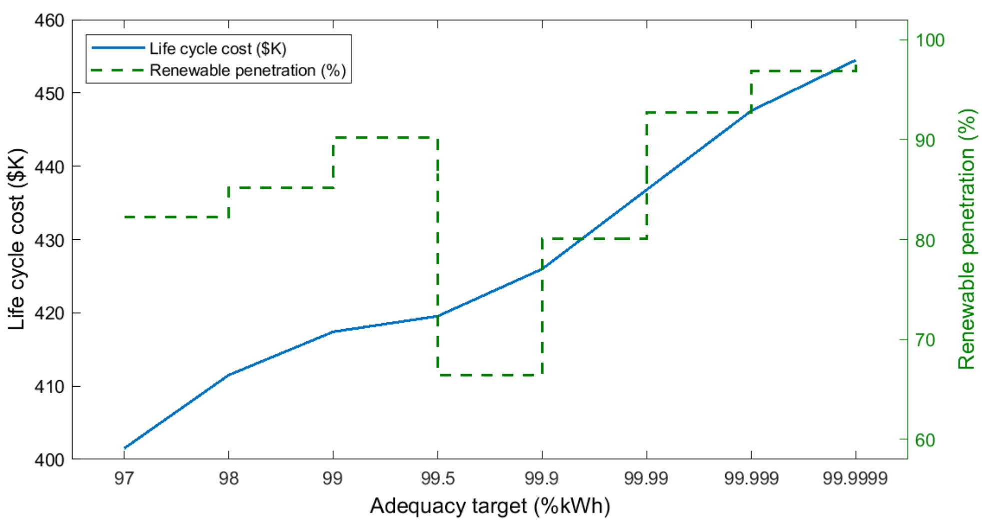

Figure 6.14 Energy Adequacy vs. total cost

6.6.3 Renewable penetration target

In this subsection, renewable penetration levels are investigated to determine the achievable levels at a given reliability target. Renewable penetration is calculated as a percentage of the average

Table 6.11 Optimal designs for various adequacy targets

Case	Adequacy target (%h)	PV (kW)	ESS (kW)	GS1 (kW)	GS2 (kW)	EA (%h)	Δ LLC (%)
5.1	97	75	40	18	0	97.997	-11.66
5.2	98	80	45	0	18	98.82	-9.46
5.3	99	85	55	18	0	99.13	-8.16
5.4	99.5	65	15	18	18	99.618	-7.69
5.5	99.9	75	40	18	18	99.917	-6.27
5.6	99.99	90	60	18	18	99.994	-3.89
5.7	99.999	100	65	18	18	99.9992	-1.52
5.8	99.9999	105	65	18	18	100	0.00

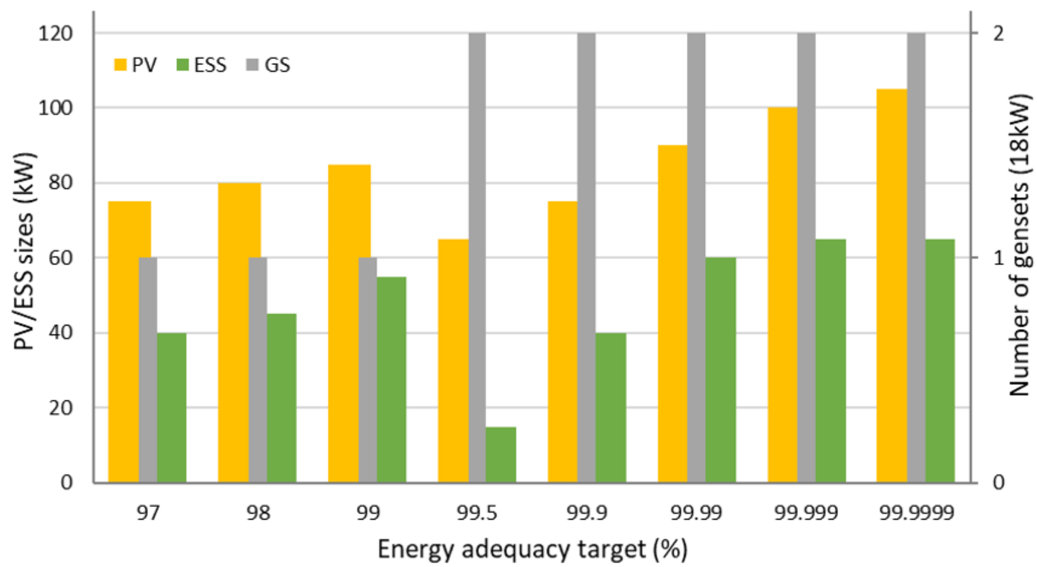

Figure 6.15 System availability vs. total cost

annual consumption, to represent the proportion of the load met by renewable resources as shown in Fig. 6.16 and Fig. 6.17. Fig. 6.18 shows the best renewable solution, for every reliability level, considering imposed targets between 60-100%. It is shown that a 100% renewable target cannot be achieved for adequacy levels higher than 99%. Moreover, LCC exponentially increases for targets higher than 90%.

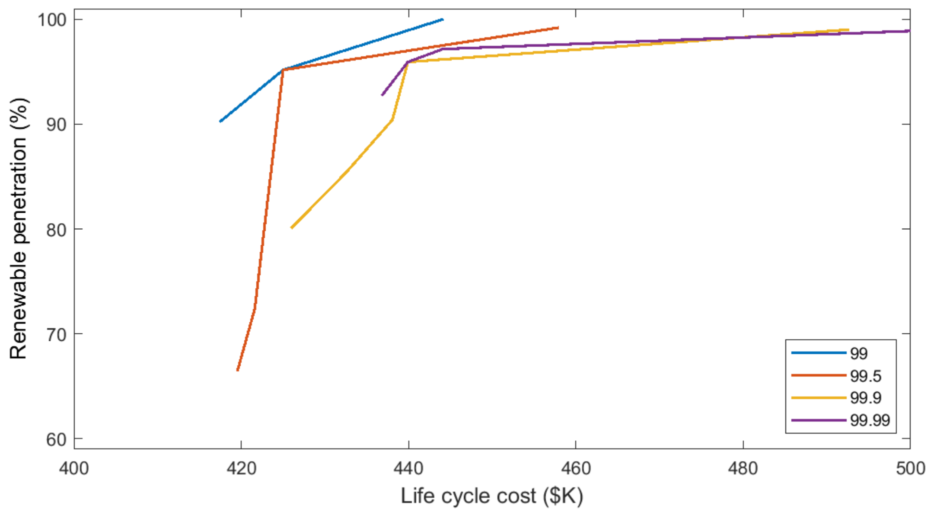

Figure 6.16 Renewable penetration target cost for %99-99.99

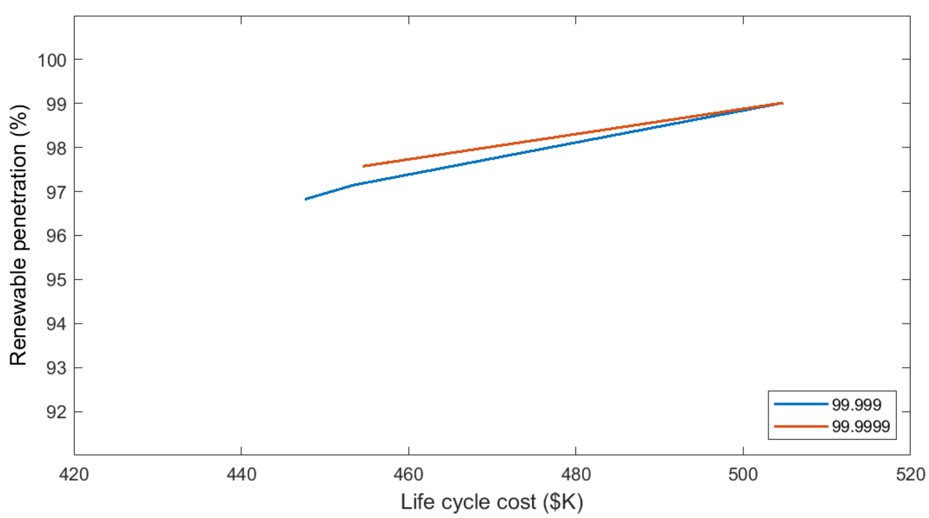

Figure 6.17 Renewable penetration target cost for %99.999-99.9999

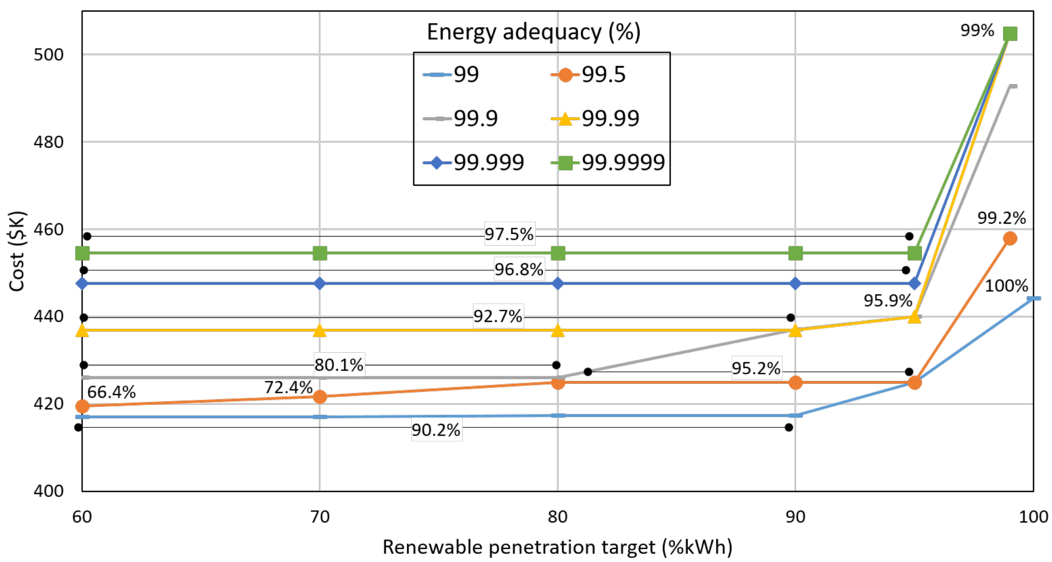

Figure 6.18 Achievable renewable penetration for various reliability targets

6.7 Conclusions

Results in Fig. 6.19 show the LCC sensitivity to the performed analysis. It should be noted that the results shown are majorly affected by the long project duration, 20 years, favoring large PV capacities with long life expectancy and minimal operating costs. However, the optimal configuration was turned into a fuel-based generation system by implementing a 7-year period for the same example. Similarly, the available surface area highly affects the results, since the area mainly limits the PV capacity. Therefore, the renewable percentage is reduced by 28% when the available area was reduced by 25%.

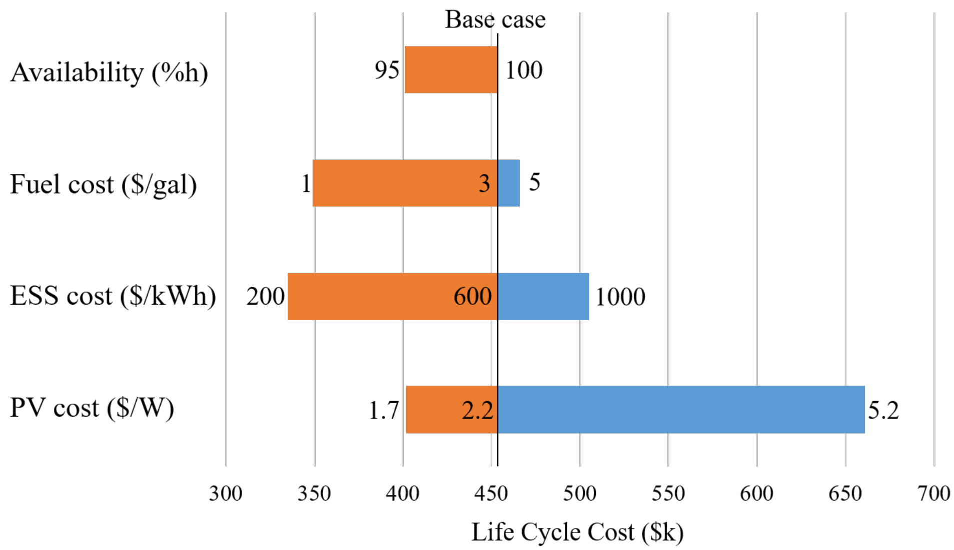

Figure 6.19 Sensitivity analysis results

CHAPTER

7

MICROGRID MAINTENANCE PLANNING USING REINFORCEMENT LEARNING

7.1 Introduction to maintenance planning

According to the BSI standards [57], maintenance can be defined as the "combination of all technical, administrative, and managerial actions during the life cycle of an item intended to retain it in, or restore it to, a state in which it can perform the required function". Maintenance definitions in [58], is oriented to divide the process into methods. Maintenance action, maintenance policy, maintenance concept, and maintenance support are the parts of an implemented maintenance method as defined in [58, 59]. During the life cycle of the component, the operation is evaluated and characterized by its up and downtime. A maintenance action is performed to slow down the component deterioration. This process is evaluated with an assumption of components' ability to be retained, also known as maintainability. Maintainability is the ability of a component or a system under specific operation conditions, to be retained or restored to its state through which it can perform the required function when maintenance action is taken place with specific procedures and resources. Maintenance is a complex field that includes many disciplines within a system, such as operations, information technologies, economics, power security, and analytics [59].

Maintenance activities are versatile and sophisticated that require planning and management to optimize the process [7]. Planning of a maintenance action aims to improve component reliability. The downtime during maintenance is controlled and efficient, unlike a repair action that can lead to more extended downtime. On the other hand, management of maintenance is more concerned about optimizing the plan to reach a particular objective. This optimization process can be either based on the importance of the component for the integrated system to perform a function, or based on a priority list approach when the managed components belong to various systems. The strategy is influenced by the importance of the component for the system reliability, the components monitoring results, and a schedule to be followed that was built to optimize the operation and maintenance process. Maintenance planning and management are very important due to their prospect to reduce downtime while using the same resources used in reactive repairing.

This chapter is developed based on the results of the reliability assessment tool. It is seen in Chapter 4 that the reliability indices characterized by a widely spread distributions. After investigating the reasons behind the challenge, it is concluded that the consideration of random repair duration causes the wide distributions. The randomly-generated duration resulted in very long repair actions in some cases leading to a few bad results that can be seen in the estimated in the reliability indices. This phenomenon is the main driver to write this chapter and show the importance of smart planning of microgrid maintenance. Moreover, the scheduling of maintenance can be one way to utilize the measurements taken in the field to improve system performance.

The rest of the chapter is organized as follows. Section 2 describes the different maintenance strategies for power systems and discusses the maintenance problem in the sector. Section 3 presents background on reinforcement learning for time-series analysis. Section 4 introduces the proposed methodology and case study. Section 5 shows how the methodology can be applied to the reliability assessment model.

7.2 Maintenance strategies for power systems

Maintenance orders and tasks will be initiated by the maintenance policy assigned. Maintenance planning is usually driven by predesignated key performance indicators, which measure the success of the planning process. Those indicators are the objectives the maintenance is intended to achieve. Examples of those objectives are reliability improvement, cost reduction or improved plant performance. A maintenance policy can be described as a set of rules to explain the triggering mechanisms for various actions. These actions can be either corrective or preventive based on studying the operating system[59].

7.2.1 Failure-based maintenance

Maintenance actions take place only after a failure event. This strategy is entirely reactive. Therefore, there is no space for improvement. Even though there is no planning for the actions, a spare parts policy is required.

7.2.2 Time-based maintenance (TBM)

A preventive objective drives a time-based policy. Maintenance is planned periodically to prevent or minimize the occurrence of failures. This routine maintenance is usually suitable for irreparable sub-components, such as air filters. The action intervals are usually constantly planned based on the asset type. A warranty usually accompanies this maintenance strategy, and the component manufacturer recommends the intervals.

7.2.3 Condition-centered maintenance (CCM)

This method is purely based on predictive actions. Unlike TBM, the planning is based on the probability of failure for the assets and the sub-components. Through monitoring tools and measurements, CCM can identify problems at the beginning of deterioration, as shown in [60, 61]. CCM is also aimed to reduce costs by only taking the necessary actions.

7.2.4 Reliability-centered maintenance (RCM)

As the name suggests, RCM is built around the reliability of the system. The sequence of maintenance or replacement tasks is planned by assessing various failure modes for the assets. The consequences of failure are identified through studying the functional dependency and impact of the failed component on the reliability of the whole system.

7.2.5 Applying a reliability-centered policy

Reliability-based maintenance can be defined as the policy that structures the maintenance strategy by determining the maintenance, testing, and inspection required to achieve the reliability of the system and the components where they can succeed to operate as planned. In [62], RCM is applied in nuclear power plants to optimize the operation and the maintenance of the plant. Principally, RCM is supposed to focus on the function of the system and the consequences of failures. To formulate the principles of RCM the report suggested, a set of questions similar to the following one was asked

1. *What are the standards of the microgrid performance?*
2. *In what ways does the microgrid fail to fulfill its functions?*
3. *What is the status of the microgrid when every failure occurs?*
4. *In what way does each failure matter?*
5. *What can be done to predict or prevent failures?*.

RBM was studied to be implemented in hydropower organizations in the work of [63]. Due to mainly managerial obstacles and sometimes technical ones, it was difficult for several plants to utilize an RBM Policy. The RBM introductory work of [64] was suggested to prolong the normal 3-5 years of heavy maintenance interval to 6-8 years. The efficiency of the power supply was suggested to rise by 50%. The basic tasks to introduce RBM is illustrated in [2],

1. *Comparing maintenance alternatives*
2. *Lowest-risk maintenance scheduling*

3. *Predictive vs. corrective maintenance*

4. *Ranking components' importance*

7.2.6 Background on distributed energy systems maintenance

7.2.6.1 PV Systems

Periodic maintenance activities for PV system components are suggested in [65]. It is stated that once a year, a maintenance team should be on-site conducting a general inspection of the PV site. Several activities are suggested, including; checking for corrosion and erosion, checking the cleanliness of the panels, and ensuring electrical wiring and connections are safe and in good condition.

The nature of the PV system installation location is the origin of several system issues. Common malfunctions can be basic equipment failure, damage to electric circuits by animals or accidents, installation, and mounting damage, which are many times caused by inadequate maintenance actions [66]. In [67], the importance of considering the PV in maintenance planning is stated emphatically to avoid the misconception of the PV system being a low maintenance system. To minimize the cost of O&M, essential maintenance tasks such as panel cleaning, inverter strategies, and warranty enforcement were stressed.

7.2.6.2 Energy storage systems

Energy storage is the newest technology in the distributed energy field. The maintenance of those systems has been under experimentation to find the most appropriate planning that can minimize system degradation. As in [55], the planning can be divided into a fixed operation and maintenance component and warranty maintenance based on the performance of the system to ensure the contracted state of charge. New flexible warranties are being considered nowadays to accommodate the possible change in the application and the cycling strategy from the manufacturer's point of view.

7.2.6.3 Diesel generators

The nature of the operation for a diesel generator plays a vital role in the process of maintenance planning. System dynamics methods were investigated in the works of [68]. The costs in the study included not only the operation cost but also the cost of maintenance and downtime. Generator maintenance was categorized by the sub-components that needed to be checked, fixed or changed. Those items are fuel pump, water separator, pressure-time pump, injector, and oil pump. Other non-repairable components were scheduled to be replaced after specific hours, i.e., calendar-based.

A combined technique of fuzzy logic and genetic algorithms (GA) was presented in [69]. The combination was used to handle a multi-objective function of a cost minimization and reliability indices consideration. The proposed method validation was performed on a real power system in Korea. Results show improvement at the 24th generation of the GA. An online sensor-driven approach is taken in the works of [70]. Generators were diagnosed to optimize the process of maintenance.

Reliability-centered maintenance method was used in [71], where RBM is utilized to construct a maintenance schedule for a maritime vessel. The operation of the vessel was taken into consideration. The maintenance program designed was suggested to be effective for similar equipment, and it can be a part of a maintenance strategy to diesel systems.

7.2.7 Expected impact of maintenance scheduling

In Chapter 4, it is shown that the time to repair impacts the reliability evaluation values. The randomness of repair duration can be seen in the probability distributions for the reliability and adequacy indices. Even though the expected values results showed an excellent performance for the case study, it is still clear that by having more control over the repair time, there will be an improvement in the probability distributions resulted from the base case simulation.

Improving the maintenance schedule is a crucial step in reliability engineering. Following the likelihood of failure estimated from the model, the maintenance timing and duration can be more precise. This helps in achieving high-reliability systems without overdoing the maintenance actions in the strategy. It is essential to introduce a suitable maintenance strategy to achieve excellent performance while minimizing maintenance costs.

7.3 Reinforcement learning for time-series analysis

Reinforcement learning (RL) is an area of machine learning algorithms based on the psychological concept of reinforcement, where the prospect of a particular behavior is increased by applying a reward when it happens. In the machine learning terms, reinforcement learning works with maximizing long term rewards followed by a sequence of right actions. The learner interacts with the environment to know how to map situations or actions [72]. It is widely used for games where a group of steps is given to move forward, where some of the steps will lead to facing obstacles, and some will be rewarded with the main objective to reach the terminal state. A deep RL algorithm is developed to play Atari in [73]. These groups of machine learning algorithms are also handy tools to plan or schedule actions based on time-series analysis. In [74], airfare price data is mined to make a buying decision based on minimizing the cost. A trading game framework is developed for univariate and bivariate in [75] to plan buying and selling actions in order to maximize the profit for the trader. It is shown in the literature that RL is a useful tool for scheduling given the availability of statistical data. The methodology is applied for the maintenance scheduling problem at various domains such as aircraft, military trucks, distributed computers, and power systems' maintenance [76–83]. In particular, reinforcement learning is used to optimize the operation and maintenance of power grids in [84].

7.3.1 Markov decision process

RL focuses on how an object might act in a certain environment to maximize a reward. The algorithm is built to study the system behavior in its environment and learn to optimize its action. The RL problem can be structured through a Markov Decision Process. MDP is a discrete-time stochastic process suitable to formulate a sequence of decisions. At each time step, the decision-maker, usually referred to as an **agent**, interacts with the operating **environment** in the form of sequential events overtime. Using this formalization the agent selects an **action** from a group to receive a **reward** based on the selection and its time. The agent then transitions to a new state. This process is repeated over several episodes for several time steps leading to a trajectory that represents a sequence of action, state pairs. The main goal of the process is to maximize the cumulative reward over time, leading the agent always to have to choose between an immediate regular reward or waiting to maximize the cumulative reward.

The notations usually used to describe MDP is given below:

1. ***S***: The set of states an agent can exist in.
2. ***A***: The available set of actions for the agent to make.
3. ***R***: The set of rewards an agent can receive based on the action-state pair.
4. ***t***: The time step the game will be played at.

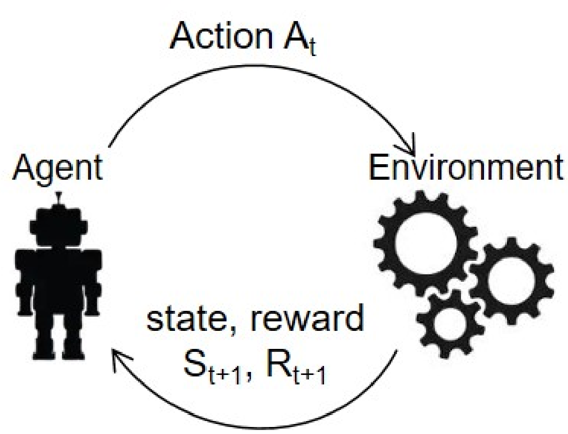

Figure 7.1 Agent, Environment interaction

The agent receives the environment state S_t at each time step t, where it selects an action A_t. The state-action pair (S_t, A_t) is then recorded and the process advances the next step $t+1$. As shown in Fig. 7.1, the agent receives a reward R_{t+1} based on the state it transitioned to at the same time step. Hence, the agent has no information about how the states are related to rewards. It can only observe the consequences of time $t+1$ for the action it has taken at time t. States and rewards can be expressed as random variables with a probability distribution. For instance, the next state being s' and the corresponding reward being r can be defined by a conditional probability based on the state, action a pair of the previous time step as follows

$$p\left(s', r|s, a\right) = \Pr\left\{S_t = s', R_t = r|S_{t-1} = s, A_{t-1} = a\right\}. \tag{7.1}$$

7.3.2 Policy

The policy is a mapping function to describe the probability of each action in a given state. Policy is usually denoted by π. When an agent follows policy π at time t, the probability of taking action a at time t is given by $\pi(A_t = a|S_t = s)$.

7.3.3 Value functions

The value functions are used to evaluate a state-action pair and help the agent to decide which action to take. These estimates can be done for a state value function or a state-action value function. In a state value function, the agent is assisted by information about how valuable to be in a given state, and the goodness of performing an action is estimated based the current state from the state-action value function. The algorithm estimates the value function to find the most rewarding route for the agent to take.

The value or the quality of a state or a state action pair is measured by the expected return or the previously described reward. Expected return is what an agent expects to get by taking an action in a given state. The state value and the state action value functions are estimated for a given policy as,

$$\begin{aligned} v_\pi(s) &= E_\pi\left[G_t|S_t = s\right] \\ &= E_\pi\left[\sum_{k=0}^{\infty} \gamma^k R_{t+k+1}|S_t = s\right]. \end{aligned} \tag{7.2}$$

$$\begin{aligned} q_\pi(s, a) &= E_\pi\left[G_t|S_t = s, A_t = a\right] \\ &= E_\pi\left[\sum_{k=0}^{\infty} \gamma^k R_{t+k+1}|S_t = s, A_t = a\right] \end{aligned} \tag{7.3}$$

Equation Eq. 7.2 and Eq. 7.2 describe the value of a given state or a state action pair while applying a policy π. We will be using the state-action case from now on since it is the function used in the rest of the work. $q_\pi(s, a)$ defines the value of taking action a at state s, applying policy π. Therefore, it describes the value of an action under a specific policy. The function shown in Eq. 7.3 is also referred to as $Q-$*function*. Since Q stands for *Quality*, the quality of a state-action pair is referred to as $Q-$ *value*.

7.3.4 Optimal policy

The reinforcement learning algorithm is developed with an object to find the optimal policy that yields the highest amount of rewards. Hence, a $\pi_1 > \pi_2$ if $q_{\pi 1}(s,a) > q_{\pi 2}(s,a)$ for all s,a pairs where $s \in S$ and $a \in A$. Hence, the optimal policy is given by

$$q_*(s,a) = \max_{\pi} q_\pi(s,a) \tag{7.4}$$

Following Richard Bellman's work, the expected return of the optimal policy is defined by

$$q_*(s,a) = E\left[R_{t+1} + \gamma \max_{a'} q_*\left(s',a'\right)\right] \tag{7.5}$$

where at time t, the expected return from taking action a at state s is represented by the expected reward of the state-action pair (s,a), R_{t+1}, in addition to the maximum return for any available action at next state s', discounted by a given factor γ.

7.3.5 Q-Learning

Q-learning is an Off-Policy algorithm. Off-policy methods learn versatile policies for strategy and estimation. The policy for the strategy is usually soft which means that it will always have an element of exploration. The value functions are updated based on experience and can separate exploration from control. Q-learning is developed to find the optimal policy where the expected total reward over a certain number of steps is the maximum achievable reward. Using a value iteration process, Q-learning updates the Q-values for all the state action pairs until convergence is achieved, when the optimal Q-function is found.

An episode can be defined by the agent reaching the terminal state or after a maximum number of time steps. Each episode starts by the agent choosing an action at the starting state based on the last updated Q-values in the table. The agent will take action with the highest value, consider a certain degree of exploration. Hence, the action chooses an action considering a *exploration-exploitation* trade-off. Exploration is based on taking action randomly, hence, exploring the environment and continue learning.

Exploitation is mainly using the learned information so far to maximize the total return. The exploration elements help the agent to investigate larger rewards and returns that it already knows about, letting the agent avoid missing out on bigger opportunities in the future. However, the balance of exploration and exploitation needs to be achieved. A Q-learning algorithm usually starts with a 100% exploration rate, given as $\epsilon = 1$. ϵ is the probability that the agent will take an exploratory action, starting with 1 and decaying at each new episode. This exploration-exploitation technique is called Epsilon greedy, which indicates that the agent will get "greedy" in the sense of exploiting the information after it had an adequate amount of exploration.

Q-values are updated at each time step of each episode. The new values are calculated considering temporal difference. TD is used to estimate the value function considering a final reward estimate.

At each time step, the final reward estimate is calculated and used to update every state-action pair as follows,

$$Q(s_t, a_t) \leftarrow Q(s_t, a_t) + \alpha \Big(r_{t+1} + \gamma \max_a Q(s_{t+1}, a) - Q(s_t, a_t) \Big) \tag{7.6}$$

where r is the reward the agent receives due to reaching a state at $t+1$, γ the discount factor applied to the estimated future rewards and α is the learning rate. The update iteratively occurs by calculating the loss between the current and the optimal Q-value in order to converge to the optimal Q, q_*. Learning rate is between 0 and 1 and it governs how fast the learning process is. If $\alpha = 0$ the Q-value will never be updated and no learning will take place. It is not necessary to keep overwriting the values so to ensure convergence learning rate can day based on the number of times the state-action pair is visited as shown,

$$\alpha(s, a) = \frac{1}{n(s, a)} \tag{7.7}$$

where n is the number of time a pair has been visited.

7.4 Microgrid maintenance scheduling algorithm

The presented algorithm is designed to interact with the simulated operation of the single component or the microgrid system. The algorithm learns about the best action to be taken at each state for several episodes. The learning process converges to the optimal Q-values. Q-table is then tested by running validation mode where no learning or updating is taken place.

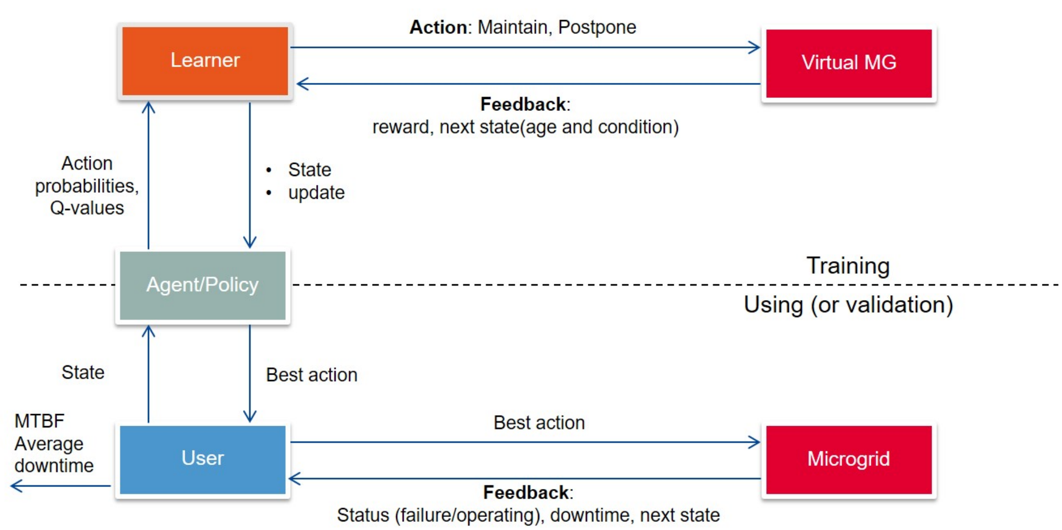

Figure 7.2 Verification framework

The framework in Fig. 7.2 describes the process of learning from the real life data where the agent takes the best maintenance action for the system and send back the status of the system. The status helps estimating the appropriate action probabilities and Q values. The Q value results from training the model are validated and evaluated using system reliability metrics.

7.4.1 Problem formulation

The algorithm takes an action of postponing the maintenance *Action 1: Hold* or maintaining the system *Action 2: Maintain*. Then, it received feedback based on the consequence of the action on the system environment. Feedback info is the resulting *reward* expressed as the downtime in the form of outage hours for overhauling, failure, or normal operation (which is equal to zero). The *next state* is also given in the form of the component age. The interaction illustrated in Fig. 7.3 is repeated at each time step of the running episode.

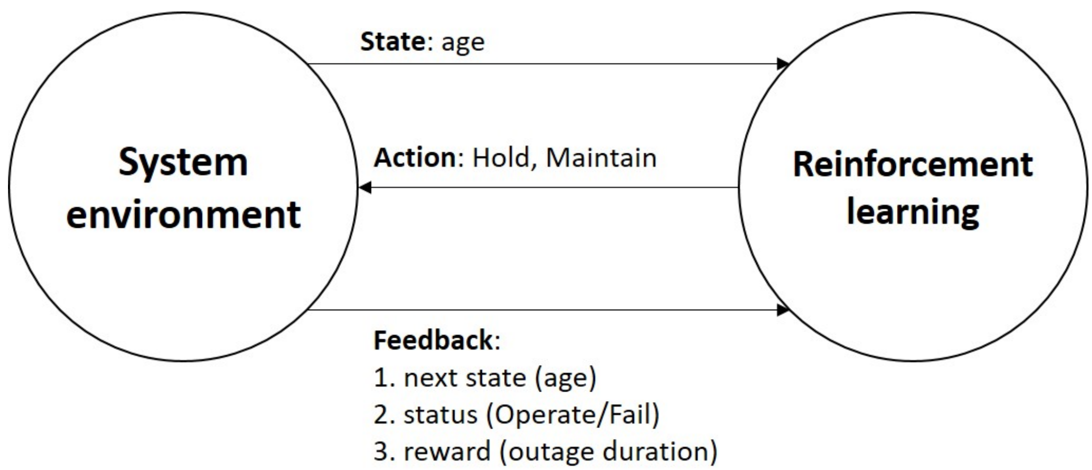

Figure 7.3 Problem formulation

If maintenance is performed, there will be no failure, but the overhaul duration is counted. Overhaul duration represents an immediate small reward. If maintenance is not performed, a failure is randomly generated based on a probability distribution. If the generated failure is less than the decision-making time, a fail is considered, and long random repair duration is recorded. If the system did not fail, the system claims the highest reward of zero outage hours.

7.4.2 Algorithm steps

1. ***Inputs***: The QL parameters is passed as the algorithm inputs. Parameters are the exploration rate ϵ, the discount factor γ, the decision making epoch, the life expectancy of the component, the number of episodes, the number of steps in an episode and in validation mode.

2. ***Initialize***: The variables used for the Q-values, n, average reward, and expected number of failures for both Q-learning and no planning case are initialized.

3. ***Running the episode***: As each episode starts, the environment is reset to its starting state, and the exploration rate is set to the selected value. The episode runs to find the optimal q-function, and the episode terminates when the steps is completed or when the expected life is reached. The next episode starts using the previous q-values. The process in detail is expressed in Algorithm 3.

4. ***Validation mode***: Validation mode is run at the end of each episode to calculate the expected reward using the achieved Q-values so far. Hence, there is no learning or updating of Q at validation mode. Steps are explained in Algorithm 4.

5. ***Reactive maintenance mode***: Reactive maintenance mode is also run after each episode to calculate the expected reward for the case of no planning. This mode has only one action Hold, where repair takes place when a failure occurs. This mode is run for comparison reasons, as shown in Algorithm 5.

Algorithm 3 Q-Learning algorithm

Input:
 ϵ, γ, $\mathrm{N}_{decision}$, $\mathrm{N}_{episodes}$, Age_{max}, N_{steps}, $\mathrm{N}_{validation}$
Initialize:
 Q, n, $\mathrm{AReward}_{RL}$, ENF_{RL}, $\mathrm{AReward}_{RM}$, ENF_{RM}
for $i = 1$ to $\mathrm{N}_{episodes}$ **do**
  Initialize:
  Episode parameters: $State = 0$, $\epsilon = 0.1$
  for $t = 1$ to N_{steps} **do**
   With ϵ and Q, create action policy and generate action probabilities
   Take a new random action using action probabilities
   Given a_t, environment emulator returns reward, status and next state S_{t+1}
   if $S_{t+1} == \mathrm{Age}_{max}$ **then** Terminate episode
   end if
   Update n and calculate the learning rate α
   Calculate Temporal difference TD
   Update Q using temporal difference and update *state* to *next state*
  end for
  Call validation mode function to calculated expected reward
  Call reactive maintenance function to to compare expected reward and measure improvement
end for
Calculate average reward $AReward$ and expected number of failures ENF for both cases
Measure percentage of improvement between predictive maintenance using Q-learning and reactive maintenance.

Algorithm 4 Validation mode

Initialize:

Validation parameters:$State = 0$, $\epsilon = 0$, $reward = 0$, $failure = 0$, $Q_{valid} = Q$

Call current episode action policy

for $v = 1$ to $\mathrm{N}_{validation}$ **do**

With ϵ and current Q, create a 100% exploitative policy

Take an action based on policy (Always the action with the maximum Q value)

Given a_t, environment emulator Returns *reward, status* and next state S_{t+1}

Increment *reward* and *failure* using *reward* and *status*

Update *state* to *next state*

end for

Store(reward / $\mathrm{N}_{validation}$) in $\mathrm{AReward}_{RL}$

Store(failure / $\mathrm{N}_{validation}$) in ENF_{RL}

Algorithm 5 Reactive maintenance mode (No planning)

Initialize:

Validation parameters: $State = 0$, $reward = 0$, $failure = 0$

for $o = 1$ to $\mathrm{N}_{validation}$ **do**

Action is always *Hold*

Given a_t, environment emulator Returns *reward, status* and next state S_{t+1}

Increment *reward* and *failure* using *reward* and *status*

Update *state* to *next state*

end for

Store(reward / $\mathrm{N}_{validation}$) in $\mathrm{AReward}_{RM}$

Store(failure / $\mathrm{N}_{validation}$) in ENF_{RM}

7.4.2.1 Environment emulator

The environment is simulated at each time step such that the reward is calculated. In the environment function, the state and the selected action are passed as inputs. The function returns the reward received, the status of the component and the next state. This function is based on failure and health scenarios. If the action is Hold, a failure time is generated using the Weibull parameters of the component. The time-to-failure, in hours, is scaled up to the decision epoch unit (monthly) and compared to the current state expressing the current operation month of the service period. If the time-to-failure is lower than the operation time, a failure is recorded, and the state of the component is set to the starting state, given that a repair or replacement has taken place. The repair duration is randomly generated. If time-to-failure is higher than the age, then the component is healthy at the current operation time and advances to the following state. If the action was to maintain, then no failure occurs, and the overhaul duration is recorded as deterministic value, and the operation time is set to the starting state. The repair duration is returned as the reward, the status is returned as failure or operation as well as the next state.

7.5 Case study

The generator failure data previously presented in Chapter 3 is used to estimate Weibull parameters and test the algorithm. Using *Python* statistical library *Scipy*, a Frechet right random variable is used to fit the data using Weibull distribution as in Fig. 7.4. The scale α and shape β parameters are estimated as,

$$\alpha = 59974$$
$$\beta = 2.0258$$

Parameters are implemented in the environment emulator to be used in drawing a time-to-failure at each time step. Repair duration is drawn from a normal distribution with a normal value of 5 days, where the maintenance overhaul was set to only one day, given the planning. The number of episodes and the exploration rate was found to be the most effective parameters on the convergence process and are selected empirically as,

$$N_{episodes} = 600$$
$$\epsilon = 0.1$$

The decision epoch is set to be monthly. The states are the years of operation since the last maintenance. The maximum number of steps at each episode is the service period in month unit. The validation trials are 50 times the number of steps in the episode. Fig. 7.5 shows the Q-values for the two actions, hold and maintain. It is observed that the quality of the action Hold is higher than Maintain until a certain period of operation (approx 2.5 years), which indicates that a maintenance action after 2 and a half years would maximize the average reward, which can be expressed as minimizing the outage hours.

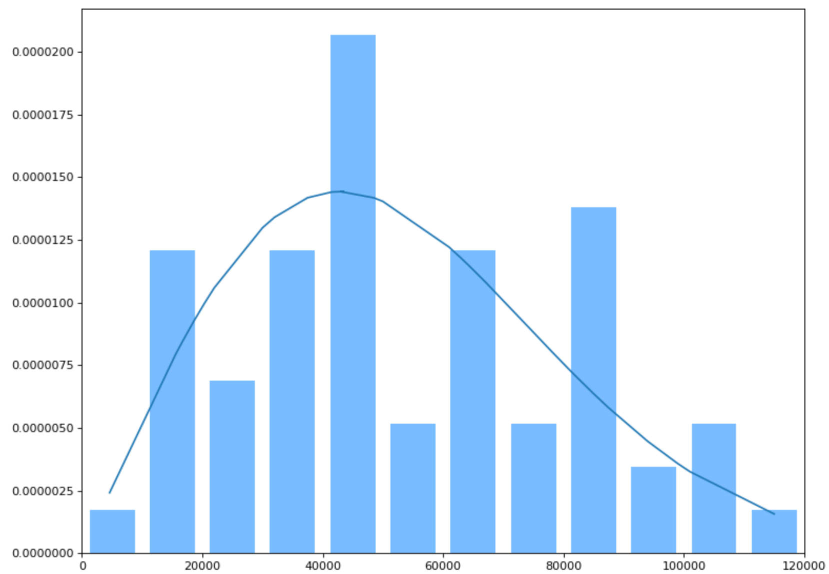

Figure 7.4 Weibull fitting distribution

Fig. 7.6 and 7.7 show the propagation of the average expected reward in the case of Q-learning with comparison to reactive maintenance. The planning Q-learning algorithm is shown to decrease the outage duration by 21% and the expected number of failures by 28%.

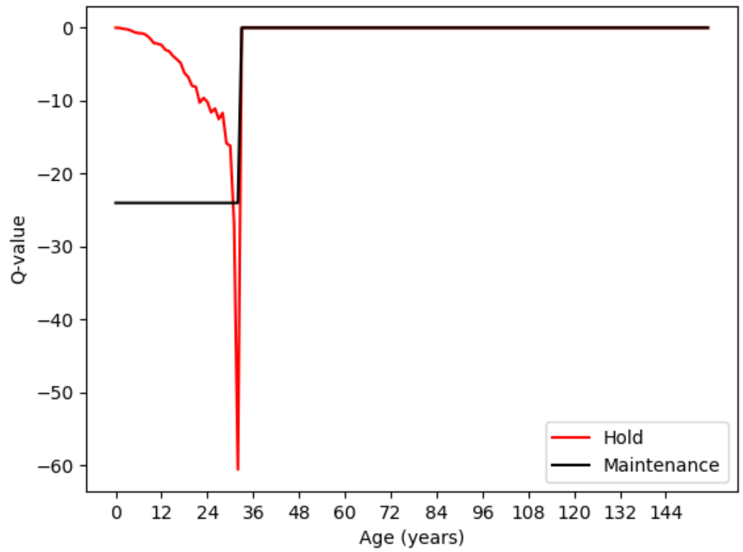

Figure 7.5 Q values

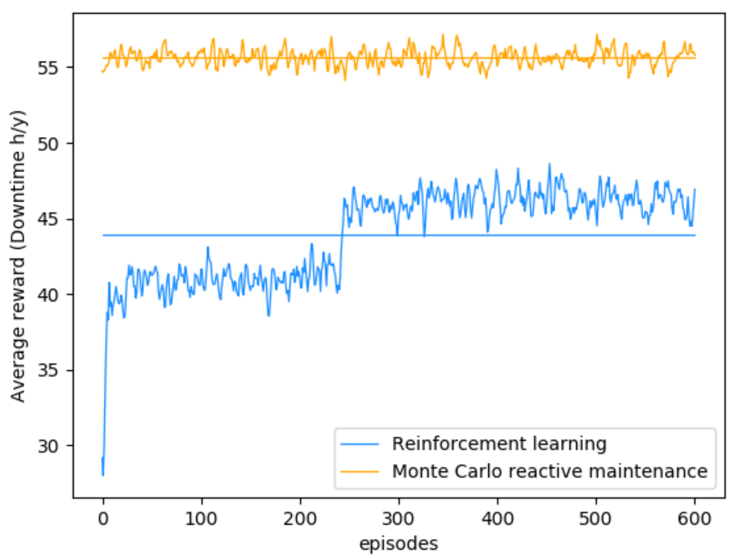

Figure 7.6 Expected average reward for Q-learning and reactive maintenance

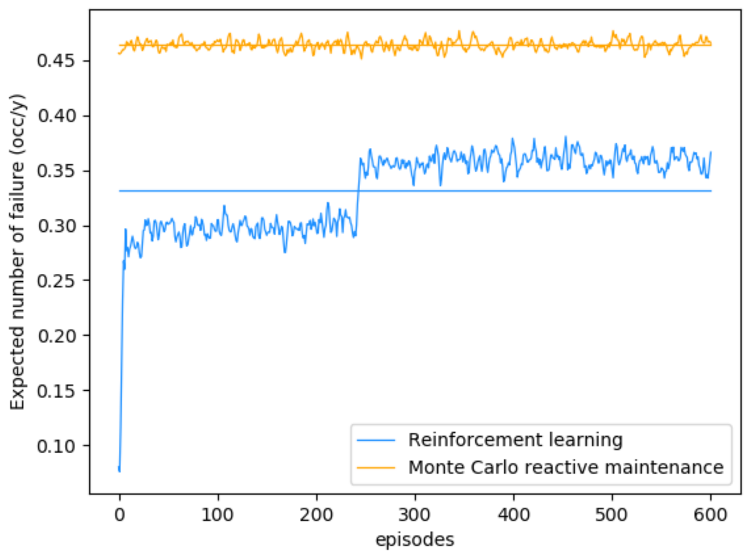

Figure 7.7 Expected number of failure for Q-learning and reactive maintenance

7.6 Conclusions

The presented reinforcement learning is designed to plan the maintenance of the component based on the failure probability and the component aging. The algorithm is intended to be a part of the microgrid component maintenance strategy. The results show that predictive planning improves the reliability metrics of the system. Metrics are tested using components' failure data. The schedule shown in the results is expected to improve a diesel generator failure rate.

CHAPTER

8

CONCLUSION

8.1 Conclusions

This thesis has presented a methodology for a microgrid-sizing framework, shown in Fig. 8.1, with the capability of evaluating reliability and renewable penetration levels. Reliability and renewable metrics are estimated for the investigated system using an assessment based on sequential Monte Carlo method. In addition, the assessment evaluates the annual operation of the dispatchable units, where operation hours, loading and fuel consumption are calculated and implemented in the cost function. A new search technique, based on particle swarm optimization, is developed to find the most cost-effective hybrid system in the search space. At each iteration, a group of candidate systems undergoes an economic-reliability assessment estimating their fitness to meet targets and reflecting the findings on the cost function. The optimizer parameters are selected empirically to achieve an accuracy higher than 99% and minimizing the execution time.

The methodology is applied on a typical example for a small commercial load and the results are evaluated through an extensive sensitivity analysis. The study shows that system total cost is reduced by about 25% when the base case prices of storage or fuel are reduced to \$200/kWh and \$1/gal respectively. On the other hand, ESS unit costs greater than \$700/kWh leads to PV and GS only systems. Most of the proposed solutions include two generators; nonetheless, they operate for only 367 and 52 hours annually. The presented methodology is developed to estimate an optimal mixed generation for a given demand, while factoring in technical and economic requirements. In addition, a detailed analysis is created to propose alternative systems and predict impact of future variations in the energy sector.

The last chapter shows the prospect of applying reinforcement learning to provide a predictive

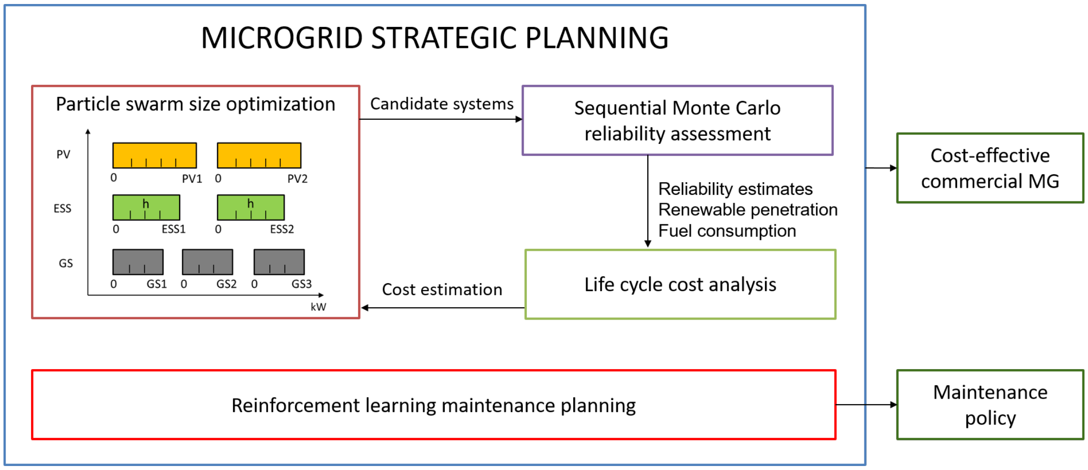

Figure 8.1 Final microgrid planning framework

planning strategy while utilizing historical failure data of the components. Compared to reactive maintenance, the planning showed a reduction in the annual number of outages and the total duration.

8.2 Future work

Computational time is always a discussed issue when simulation methods are proposed. The proposed reliability assessment was designed to extremely reduce the computational requirement for multi-component systems. Future interesting development would be to test the methodology for a fleet of distributed generation systems and include several types of failures for each component in order to measure the performance for larger and more complex systems.

The optimizer parameters worked with a 99% accuracy for various 100kW-range cases. It will be useful to test the same parameters for planning MW-scale systems and quantify the required change in parameters. Moreover, the presented reinforcement learning approach shown to improve the planning of a microgrid component and the integration of the method in the reliability assessment will surely present insightful findings. Fig. 8.2 shows the most interesting future work. Commercialization of the research work can be either done through developing a new design tool or incorporation of the methodology in an existing tool. Moreover, a data management platform is expected to enhance the capability to run and manage a fleet of microgrid systems.

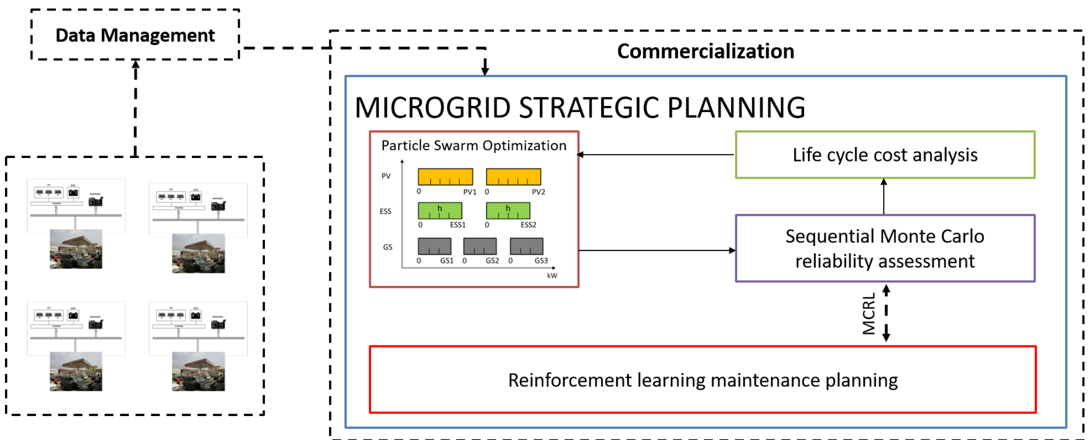

Figure 8.2 Future work

BIBLIOGRAPHY

[1] Billinton, R. & Allan, R. N. "Basic power system reliability concepts". *Reliability Engineering and System Safety* **27**.3 (1990), pp. 365–384.

[2] Li, W. *Risk assessment of power systems*. Second. Piscataway, NJ: WILEY, 2014.

[3] Billinton, R. & Sankarakrishnan, A. "A system state transition sampling technique for reliability evaluation". *Reliability Engineering and System Safety* **44**.2 (1994), pp. 131–134.

[4] Mello, J. et al. "Reliability worth assessment based on Monte Carlo simulation". *Proc. 1993 11th Power System Computation Conference*, pp. 47–53.

[5] Saraiva, J. et al. "Generation / transmission power system reliability evaluation by monte-carlo simulation". *Proc. 1995 Power Industry Computer Applications Conf.* Pp. 554–559.

[6] Billinton, R & Sankarakrishnan, A. "A comparison of Monte Carlo simulation techniques for composite power system reliability assessment". *Proc. IEEE WESCANEX 95. Communications, Power, and Computing Conference*. Winnipeg, 1995, pp. 145–150.

[7] Manzini, R. et al. *Maintenance for Industrial Systems*. 2010.

[8] Easton, V. & McColl, J. *Statistics Glossary*. 1997.

[9] Pham, H. *System Software Reliability*. 2008, p. 442.

[10] Romeu, J. L. *Practical Reliability Engineering*. Vol. 45. 2. 2003, pp. 173–173.

[11] Verma, A. K. et al. *Reliability and Safety Engineering*. Ed. by Pham, H. Second. Piscataway, NJ: Springer, 2015, pp. 311–337.

[12] Lucijanic, M. & Petrovecki, M. "Analysis of censored data Lessons in biostatistics". *Biochemia Medica* **22**.2 (2012), pp. 151–5.

[13] Ebeling, C. *An Introduction to Reliability and Maintainability Engineering*. Ed. by Grove, L. III. Vol. 14. 4. Waveland Press, 2010.

[14] Lewis, E. *Introduction to reliability engineering*. New York: Wiley, 1987.

[15] Mobley, R. K. *Plant Engineer's Handbook*. Butterwort. 2001.

[16] Alsina, E. F. et al. "On the use of machine learning methods to predict component reliability from data-driven industrial case studies". *International Journal of Advanced Manufacturing Technology* **94**.5-8 (2018), pp. 2419–2433.

[17] Hsieh, K. L. "Applying neural networks approach to achieve the parameter optimization for censored data". *WSEAS Transactions on Computers* **6**.5 (2007), pp. 858–863.

[18] Zhou, X. & Wang, J. "A genetic method of LAD estimation for models with censored data". *Computational Statistics and Data Analysis* **48**.3 (2005), pp. 451–466.

[19] Huang, H. et al. "Performance and Availability Analyses of PV Generation Systems in Taiwan". *International Journal of Electrical, Computer, Energetic, Electronic and Communication Engineering* **5**.1 (2011), pp. 524–528.

[20] Abdi, B. et al. "Reliability of MPPT Converter in Different Operating Modes". *International Journal of Machine Learning and Computing* **3**.3 (2013), pp. 274–278.

[21] Defense, D. of. *MILITARY HANDBOOK RELIABILITY PREDICTION OF ELECTRONIC EQUIPMENT*. Washington: Department of Defense, 1991.

[22] Obeidat, F. & Shuttleworth, R. "PV Inverters Reliability Prediction". *World Applied Sciences Journal* **35**.2 (2017), pp. 275–287.

[23] Brocken, E. M. "Improving The Reliability Of Ship Machinery: A Step Towards Unmanned Shipping". PhD thesis. TU Delft, 2016, pp. 227–230.

[24] Root, M. "Battery reliability and safety" (2013).

[25] Eom, S. W. et al. "Life prediction and reliability assessment of lithium secondary batteries". *Journal of Power Sources* **174**.2 (2007), pp. 954–958.

[26] Harris, S. et al. "Failure statistics for commercial lithium ion batteries: A study of 24 pouch cells". *Journal of Power Sources* **342**.2 (2017), pp. 589–597.

[27] Liu, T. Y. et al. "Cycle Life Prediction of Lithium-Ion Cells Under Complex Temperature Profiles". *Eksploatacja I Niezawodnosc-Maintenance and Reliability* **18**.1 (2016), pp. 25–31.

[28] Ganjeizadeh, F. et al. "Predicting Reliability of Lithium Ion Batteries". *International Journal of Engineering Research & Technology* **3**.8 (2014), p. 2014.

[29] Wittwer, J. "Monte Carlo Simulation Basics". *Vertex42.com* (2004), pp. 18–20.

[30] Hoffman, P. *The man who loved only numbers : the story of Paul Erdos and the search for mathematical truth*. 1st ed. New York, 1998.

[31] Bo, H. S. "Estimation of Reliability by Monte Carlo Simulations: Combined with Optimized Parametric Models". PhD thesis. 2014.

[32] Ton, D. T. & Smith, M. A. "The U.S. Department of Energy's Microgrid Initiative". *Electricity Journal* (2012).

[33] Billinton, R. & Jonnavithula, A. "Application of sequential Monte Carlo simulation to evaluation of distributions of composite system indices". *IEE Proceedings - Generation, Transmission and Distribution* **144**.2 (1997), p. 87.

[34] Ghahderijani, M. M. et al. "Reliability evaluation of stand-alone hybrid microgrid using Sequential Monte Carlo Simulation". *Proc. 2012 Iranian Conference on Renewable Energy and Distributed Generation*, pp. 33–38.

[35] Johansen, A. M. “SMCTC : Sequential Monte Carlo in C ++”. *Journal of Statistical Software* **30**.6 (2009), pp. 1–41.

[36] Da Silva, A. M. et al. “Chronological Monte Carlo-based assessment of distribution system reliability”. *2006 9th International Conference on Probabilistic Methods Applied to Power Systems, PMAPS* (2006).

[37] Abdelsamad, A. & Lubkeman, D. “Reliability Analysis for a Hybrid Microgrid based on Chronological Monte Carlo Simulation with Markov Switching Modeling”. *IEEE Innovative Smart Grid Conference*. Washington, DC, 2019.

[38] Naesseth, C. A. et al. “Elements of Sequential Monte Carlo” (2019). arXiv: 1903.04797.

[39] Abd Ellah, A. H. “Bayesian and Non-Bayesian Estimation of the Inverse Weibull Model Based on Generalized Order Statistics”. *Intelligent Information Management* **04**.02 (2012), pp. 23–31.

[40] Billinton, R. & Li, W. *Reliability assessment of electric power systems using Monte Carlo methods*. New York: Plenum Press, 1994.

[41] Shaaban, M. F. et al. “DG allocation for benefit maximization in distribution networks”. *IEEE Transactions on Power Systems* **28**.2 (2013), pp. 939–949.

[42] Kahrobaee, S. et al. “Optimum renewable generation capacities in a microgrid using generation adequacy study”. *2014 IEEE PES T&D Conference and Exposition* (2014), pp. 1–5.

[43] Kubba, S. “Economics of Green Design”. *LEED Practices, Certification, and Accreditation Handbook*. 4th ed. Oxford, UK: Elsevier, 2009. Chap. 10, pp. 379–415.

[44] Arefifar, S. A. & Mohamed, Y. A. R. I. “DG mix, reactive sources and energy storage units for optimizing microgrid reliability and supply security”. *IEEE Transactions on Smart Grid* **5**.4 (2014), pp. 1835–1844.

[45] Heleno, M. et al. “Optimal sizing and placement of distributed generation: MILP vs PSO comparison in a real microgrid application”. *19th International Conference on Intelligent System Application to Power Systems*. 2017.

[46] Bahramirad, S. et al. “Reliability-constrained optimal sizing of energy storage system in a microgrid”. *IEEE Transactions on Smart Grid* **3**.4 (2012), pp. 2056–2062.

[47] Shahidehpour, M. “Security-constrained unit commitment with stochastic constraints”. *Proc. IEEE Power Engineering Society General Meeting*. 2007, pp. 7–9.

[48] Georgilakis, P. S. & Hatziargyriou, N. D. “Optimal distributed generation placement in power distribution networks: Models, methods, and future research”. *IEEE Transactions on Power Systems* **28**.3 (2013), pp. 3420–3428.

[49] Eberhart, R. & Kennedy, J. “A new optimizer using particle swarm theory”. *Proc. of the Sixth International Symposium on Micro Machine and Human Science*. Nagoya, 1995, pp. 39–43. arXiv: 9780201398298.

[50] Yuan, C. & Illindala, M. S. “Economic sizing of distributed energy resources for reliable community microgrids”. *Proc. IEEE Power and Energy Society General Meeting*. 4. 2018, pp. 1–5.

[51] Tooryan, F. & Collins, E. R. “Optimum size and placement of distributed generators in microgrid based on reliability concept”. *Proc. IEEE Power and Energy Conference*. IEEE, 2018, pp. 1–6.

[52] Nasser, A. & Reji, P. “Optimal planning approach for a cost effective and reliable microgrid”. *Proc. International Conference on Cogeneration, Small Power Plants and District Energy*. Asian Institute of Technology, 2016, pp. 1–6.

[53] Nikmehr, N. & Najafi-Ravadanegh, S. “Reliability evaluation in multi-microgrids under probabilistic optimum operation using heuristic algorithm”. *Smart Grid Conference, SGC 2015* Sgc (2017), pp. 92–98.

[54] Jacobi, J. & Starkweather, R. *Solar Photovoltaic Plant Operation and Maintenance costs*. Tech. rep. Atlanta: Scott Madden, 2010.

[55] North Carolina State University. *Energy storage options for North Carolina*. Tech. rep. Raleigh, NC: North Carolina State University, 2018, p. 254.

[56] Lazard. *Levelized cost of storage analysis — version 12.0*. Tech. rep. November. 2018, pp. 0–19.

[57] British Standards Institution. *BSI Standards Publication Maintenance — Maintenance terminology*. Tech. rep. British Standard, 2010, p. 36.

[58] Standard, I. *International Standard IEC 60300-3-14*. Tech. rep. Geneva: INTERNATIONAL STANDARD, 2006.

[59] Mehairjan, R. et al. *International Council on Large Electric Systems (CIGRE) Study Committee B3: Substations*. 2019, pp. 997–1009.

[60] Medeiros, R. “Assessment of Operating Condition Dependent Reliability Indices in Microgrids”. PhD thesis. Clemson University, 2016, p. 70.

[61] Ahmad, R. & Kamaruddin, S. *An overview of time-based and condition-based maintenance in industrial application*. 2012.

[62] IAEA. *Application of Reliability Centred Maintenance to Optimize Operation and Maintenance in Nuclear Power Plants*. Tech. rep. Vienna: IAEA, 2007.

[63] Backlund, F. “Managing the Introduction of Reliability-Centred Maintenance , RCM - RCM as a Method of Working within Hydropower Organisations”. PhD thesis. Lulea University of Technology, 2003, p. 317.

[64] Yu, J. & Zhao, H. “Maintenance plan based on RCM”. *Proceedings of the IEEE Power Engineering Society Transmission and Distribution Conference* **2005** (2005), pp. 1–4.

[65] Haney, J. & Burstein, A. *PV System Operations and Maintenance Fundamentals*. Tech. rep. Solar America Board for Codes and Standards, 2013, pp. 1–46.

[66] Nikolaos, P. *Photovoltaic System Maintenance*. Tech. rep. Irvine: Helios Lab.

[67] Shapiro, D. et al. *Solar PV Operation & Maintenance Issues*. Tech. rep. Desert Research Institute, 2014, pp. 1–13.

[68] Widarto, H. "Maintenance Scheduling for Diesel Generator Support System of Container Crane Using System Dynamic Modeling" (2014), pp. 188–193.

[69] Oh, T. et al. "Generators maintenance scheduling using combined fuzzy set theory and GA". *2011 IEEE 54th International Midwest Symposium on Circuits and Systems (MWSCAS)* 1 (2011), pp. 1–4.

[70] Yildirim, M. et al. "Sensor-Driven Condition-Based Generator Maintenance Scheduling — Part II : Incorporating Operations". **31**.6 (2016), pp. 4263–4271.

[71] Wabakken, I. "Application of RCM to Construct a Maintenance Program for a Maritime Vessel". June (2015), p. 111.

[72] Richard S., S. & Barto, A. G. *Reinforcement Learing - An Introduction*. 2018, pp. 1–548.

[73] Mnih, V. et al. "Playing Atari with Deep Reinforcement Learning" (2013), pp. 1–9. arXiv: 1312.5602.

[74] Etzioni, O. et al. "To buy or not to buy: Mining airfare data to minimize ticket purchase price". *Proceedings of the ACM SIGKDD International Conference on Knowledge Discovery and Data Mining* (2003), pp. 119–128.

[75] Gao, X. "Deep reinforcement learning for time series: playing idealized trading games" (2018), pp. 1–8. arXiv: 1803.03916.

[76] Hussin, M. et al. *Improving reliability in resource management through adaptive reinforcement learning for distributed systems*. 2015.

[77] Ling, Z. et al. "Reinforcement Learning-Based Maintenance Scheduling for Resource Constrained Flow Line System". *2018 IEEE 4th International Conference on Control Science and Systems Engineering (ICCSSE)* (2018), pp. 364–369.

[78] Koprinkova-Hristova, P. "Reinforcement Learning for Predictive Maintenance of Industrial Plants". *Information Technologies and Control* **11**.1 (2014), pp. 21–28.

[79] Verbert, K. et al. "Timely condition-based maintenance planning for multi-component systems". *Reliability Engineering and System Safety* **159**.October 2016 (2017), pp. 310–321.

[80] Compare, M. et al. "A reinforcement learning approach to optimal part flow management for gas turbine maintenance". *Proceedings of the Institution of Mechanical Engineers, Part O: Journal of Risk and Reliability* August (2019), p. 1748006X1986975.

[81] Compare, M. et al. “Reinforcement learning-based flow management of gas turbine parts under stochastic failures”. *International Journal of Advanced Manufacturing Technology* **99**.9-12 (2018), pp. 2981–2992.

[82] Barde, S. R. et al. “Optimal preventive maintenance policy based on reinforcement learning of a fleet of military trucks”. *Journal of Intelligent Manufacturing* **30**.1 (2019), pp. 147–161.

[83] Mattila, V. & Virtanen, K. “Scheduling fighter aircraft maintenance with reinforcement learning”. *Winter simulation conference* (2011), pp. 2540–2551.

[84] Rocchetta, R. et al. “A reinforcement learning framework for optimal operation and maintenance of power grids”. *Applied Energy* March (2019), pp. 291–301.